*Electronic Supplementary Information (ESI) to accompany:*

# Diffusion in Porous Crystalline Materials

**Rajamani Krishna**

Van 't Hoff Institute for Molecular Sciences, University of Amsterdam, Science Park 904,

1098 XH Amsterdam, The Netherlands

Tel +31 20 6270990

email: r.krishna@uva.nl

# Additional References to Published Literature

All the simulation and experimental data on diffusion presented or cited in the Tutorial review are from published works. A more comprehensive set of references that will serve as further background reading material is given below for the various subject areas covered in the review.

Published reviews on diffusion in zeolites, and MOFs: [1-22]

Maxwell-Stefan, Onsager and Fick diffusion theories: [1, 16, 17, 23-30]

CBMC simulation methodologies, along with force fields: [1, 12, 13, 31-46]

MD simulation methodologies: [1, 10, 13, 19, 20, 31, 47-51]

Influence of extra-framework cations on adsorption and diffusion: [40, 44, 52]

Kinetic Monte Carlo simulations: [53-62]

MD simulation data: [63-109]

Segregation effects: [75, 110-112]

Molecular clustering and hydrogen bonding: [87, 113-148]

Influence of framework flexibility, and structural transformations: [149-159]

Mesopore diffusion, and validity of the Knudsen formula: [1, 160-172]

Catatytic processes: [173-178]

Experimental data on diffusion: [1, 3, 4, 6, 135, 179-227]

Pressure swing adsorption: [17, 228-235]

Membrane Permeation: [236-284]

$CO_2$ capture processes [231, 233, 235, 238, 285-288]

# Structural Details and Simulation Methodology

For convenience the structural information on zeolites, MOFs, and ZIFs are summarized in the accompanying Tables. The accompanying Figures provide the pore landscapes.

## 1. Zeolite Structures

### 1.1. All-silica zeolites

Tables 1 and 2 gives salient information on the variety of all-silica zeolite structures discussed in the Tutorial review. The crystallographic data are available on the zeolite atlas website of the International Zeolite Association (IZA) [289]. The unit cell dimensions, and pore volumes are summarized in Tables 3 and 4.

### 1.2. Zeolite structures with cations present

Simulations were performed to determine the adsorption selectivity for $CO_2/CH_4$ mixtures in cation exchanged zeolites. The following structures were investigated

NaX (106 Si, 86 Al, 86 $Na^+$, Si/Al=1.23),

NaY (144 Si, 48 Al, 48 $Na^+$, Si/Al=3),

LTA-5A (96 Si, 96 Al, 32 $Na^+$, 32 $Ca^{++}$, Si/Al=1)

LTA-4A (96 Si, 96 Al, 96 $Na^+$, Si/Al=1)

The structural details, including pore volume data, are given in Table 5.

## 2. MOFs and ZIFs

The structural information for the metal organic frameworks (MOFs) and ZIFs (zeolitic imidazolate frameworks) have been taken from various publications.

For IRMOF-1 (= MOF 5 = $Zn_4O(BDC)_3$ with $BDC^{2-}$ = 1-4 benzenedicarboxylate), we used the structural data published by Dubbeldam et al. [38, 290].

The structural information for CuBTC (= $Cu_3(BTC)_2$ with BTC = 1,3,5-benzenetricarboxylate) have been taken from Chui et al. [291] and Yang and Zhong [292]. The crystal structure of Chui et al. [291] includes axial oxygen atoms weakly bonded to the Cu atoms, which correspond to water ligands. Our simulations have been performed on the dry CuBTC with these oxygen atoms removed.

The structural information for Zn(bdc)dabco is from Bárcia et al.[293] and Lee et al. [294].

MIL-47 structural data was taken from Alaerts et al. [295], Finsy et al. [296], and Barthelet et al. [297].

The structural data for MIL-53 (Cr) = $Cr(OH)(O_2C\text{-}C_6H_4\text{-}CO_2)$ was taken from Coombes et al [298] (the simulations were carried out with the large-pore (-lp) structure).

The ZIF-8 = Zn(methylimidazole)$_2$ structure was constructed on the basis of the structural data from Banerjee et al.[299]. The original structural data files (cif file) contain solvent molecules; these were removed and the solvent-free structures were considered.

The structural information on MgMOF-74 ( = $Mg_2$(dobdc) = Mg\(dobdc) with dobdc = ($dobdc^{4-}$ = 1,4-dioxido-2,5-benzenedicarboxylate)), ZnMOF-74 (= $Zn_2$(dobdc) = Zn\(dobdc)), CoMOF-74 = ($Co_2$(dobdc) = Co\(dobdc)), NiMOF-74 = ($Ni_2$(dobdc) = Ni\(dobdc)), were obtained from a variety of references [300-305].

The structural information on FeMOF-74 ( = $Fe_2$(dobdc) = Fe\(dobdc) with dobdc = ($dobdc^{4-}$ = 1,4-dioxido-2,5-benzenedicarboxylate)) is from Bloch et al.[306]

The structural information for MOF-177 (= $Zn_4O(BTB)_2$ with ($BTB^{3-}$ = 1,3,5-benzenetribenzoate)) is provided by Chae et al.[307].

The structural information for Co(BDP) with ($BDP^{2-}$ = 1,4-benzenedipyrazolate) is from Choi et al. [308] and Salles et al. [309].

The structural information for BeBTB = $Be_{12}(OH)_{12}(BTB)_4$ with ($BTB^{3-}$ = 1,3,5-benzenetribenzoate) is from Sumida et al. [310].

The structural information for CuBTT is from Demessence et al. [311]

The salient information on MOF and ZIF structures are summarized in Table 7.

Table 8 gives information on the unit cell dimensions, and pore volumes.

## 3. Simulations for diffusion in 3.4 nm pores of BTP-COF

The crystallographic structural information for the covalent organic framework BTP-COF was obtained from the paper of Dogru et al.[312]. The original structure is monoclinic structure $\alpha = \beta = 90^o$, $\gamma = 120^o$. For convenience in simulations this monoclinic structure was transformed to the orthogonal form for simulation purposes. The transformed orthogonal structure has twice the number of framework atoms. The unit cell dimensions of the transformed orthogonal structure are $a$ = 43.65 Å; $b$ = 75.604 Å; $c$ = 3.52 Å, with angles $\alpha = \beta = \gamma = 90^o$. The paper by Dogru et al.[312] quotes the pore diameter as being 4 nm; this is a "nominal" value. We determined the actual pore diameter following the method of Delaunay triangulation, described in the work by Foster et al.[313] The value obtained is 3.4 nm, and this represents maximum hard-sphere diameter that can pass through the 1D channels; this value was used in the calculations for the Knudsen diffusivity. All simulations were performed with 1×1×7 unit cells. The details of the force fields used for the BTP-COF framework are given in our earlier publication [168].

## 4. Data on pore volume

The pore volume data are included in Table 4 (all-silca zeolites), Tables 6 (zeolites with cations), and Table 8 (MOFs and ZIFs).

## 5. Data on surface area

The surface area of various structures were determined using the method described by Düren et al.[314]. The information is summarized in Tables 9, and 10.

# 6. Foster diameters obtained using Delaunay triangulation

In many cases, the characteristic size of the channels or windows of microporous structures are referred to. These data are obtained following the method of Delaunay triangulation, described in the work by Foster et al.[313] These values represent the maximum hard-sphere diameter that can pass through the structure.The values quoted are obtained by substracting the Lennard-Jones sigma parameter of the framework atom. The information is summarized in Tables 9, and 10.

# 7. Surface area vs pore dimension

Additionally, the accompanying Figures present plots of surface area vs pore dimensions, using a combination of the procedures of Düren et al.[314], and the Delaunay triangulation described in the work by Foster et al.[313]. The computational details will be provided in a forthcoming publication.

# 8. MD simulation methodology

Diffusion is simulated using Newton's equations of motion until the system properties, on average, no longer change in time. The Verlet algorithm is used for time integration. A time step of 1 fs was used in all simulations. For each simulation, *initializing* CBMC moves are used to place the molecules in the domain, minimizing the energy. Next, follows an *equilibration* stage. These are essentially the same as the production cycles, only the statistics are not yet taken into account. This removes any initial large disturbances in the system that do not affect statistics on molecular displacements. After a fixed number of initialization and equilibrium steps, the MD simulation *production* cycles start. For every cycle, the statistics for determining the mean square displacements (MSDs) are updated. The MSDs are determined for time intervals ranging from 2 fs to 1 ns. In order to do this, an order-*N* algorithm, as detailed in Chapter 4 of Frenkel and Smit [31] is implemented. The Nosé-Hoover thermostat is applied to all the diffusing particles.

For all the MD simulation results presented in this Tutorial Review, the DLPOLY code [315] was used along with the force field implementation as described in the previous section. DL_POLY is a

molecular dynamics simulation package written by W. Smith, T.R. Forester and I.T. Todorov and has been obtained from CCLRCs Daresbury Laboratory via the website.[315]

The self-diffusivities $D_{i,self}$ for each species in binary mixtures are computed from MD simulations by analyzing the mean square displacement of each species $i$ for each coordinate direction

$$D_{i,self} = \frac{1}{2n_i} \lim_{\Delta t \to \infty} \frac{1}{\Delta t} \left\langle \left( \sum_{l=1}^{n_i} \left( \mathbf{r}_{l,i}(t+\Delta t) - \mathbf{r}_{l,i}(t) \right)^2 \right) \right\rangle \quad (1)$$

For three-dimensional pore networks (e.g. MFI, BOG, FAU, NaX, NaY, BEA, LTA, TSC, ERI, LTA-5A, LTA-4A, CHA, ISV, IRMOF-1, CuBTC, ZIF-8, MOF-177, BeBTB, CuBTT) the arithmetic average of the diffusivities in the three coordinate directions were used in further analysis and reported. For one-dimensional pore structures (AFI, MTW, TON, LTL, MIL-47, MIL-53(Cr), MgMOF-74, ZnMOF-74, NiMOF-74, CoMOF-74, Co(BDP)) the diffusivities along the direction of diffusion are reported and analyzed. For DDR the reported diffusivities are the averages in x- and y- directions.

The Maxwell-Stefan (M-S) equations for binary mixture diffusion can be written as

$$-\phi \frac{c_i}{RT} \nabla \mu_i = \sum_{\substack{j=1 \\ j \neq i}}^{2} \frac{x_j N_i - x_i N_j}{Đ_{ij}} + \frac{N_i}{Đ_i}; \quad i = 1,2 \quad (2)$$

In equation (2) the $Đ_i$ are the M-S diffusivities of species 1 and 2, respectively, portraying the interaction between component $i$ in the mixture with the surface, or wall of the structure. The fluxes $N_i$ defined in equation (2) are expressed in terms of the number of moles of species $i$ transported per $m^2$ of *membrane cross sectional area* per second. The $Đ_{ij}$ are M-S exchange coefficients representing interaction between component $i$ with component j. The $c_i$ are the loadings, defined in terms of moles per $m^3$ of *accessible* pore volume, within the pore and $x_i$ represent the component mole fractions

$$x_i = c_i / (c_1 + c_2 + \ldots . c_n); \quad i = 1, n \quad (3)$$

$\phi$ represents the fractional pore volume of the microporous crystalline material. It is to be noted that the $\phi$ appears in the M-S equations because the $c_i$ are defined in terms of pore volume and not the total volume of the crystals. The Onsager reciprocal relations require

$$Đ_{ij} = Đ_{ji} \tag{4}$$

For binary mixtures we can define a square 2×2 matrix [$B$]

$$-\phi \frac{c_i}{RT} \nabla \mu_i = \sum_{j=1}^{2} B_{ij} N_j ; \quad i = 1,2 \tag{5}$$

The four elements of the matrix [$B$] are given explicitly by

$$B_{11} = \frac{1}{Đ_1} + \frac{x_2}{Đ_{12}} \tag{6}$$

$$B_{22} = \frac{1}{Đ_2} + \frac{x_1}{Đ_{12}} \tag{7}$$

$$B_{12} = -\frac{x_1}{Đ_{12}} \tag{8}$$

$$B_{21} = -\frac{x_2}{Đ_{12}} \tag{9}$$

Furthermore, we define a matrix [Δ] as the inverse of [$B$]

$$[\Delta] \equiv [B]^{-1} = \begin{bmatrix} \frac{1}{Đ_1} + \frac{x_2}{Đ_{12}} & -\frac{x_1}{Đ_{12}} \\ -\frac{x_2}{Đ_{12}} & \frac{1}{Đ_2} + \frac{x_1}{Đ_{12}} \end{bmatrix}^{-1} \tag{10}$$

The inversion can be carried out explicitly to give the following expressions

$$\Delta_{11} = \frac{Đ_1 \left( 1 + \frac{x_1 Đ_2}{Đ_{12}} \right)}{1 + \frac{x_1 Đ_2 + x_2 Đ_1}{Đ_{12}}} \tag{11}$$

$$\Delta_{22} = \frac{Đ_2\left(1+\frac{x_2 Đ_1}{Đ_{12}}\right)}{1+\frac{x_2 Đ_1 + x_1 Đ_2}{Đ_{12}}} \tag{12}$$

$$\Delta_{12} = \frac{Đ_1 \frac{x_1 Đ_2}{Đ_{12}}}{1+\frac{x_1 Đ_2 + x_2 Đ_1}{Đ_{12}}} \tag{13}$$

$$\Delta_{21} = \frac{x_2}{x_1}\Delta_{12} = \frac{Đ_2 \frac{x_2 Đ_1}{Đ_{12}}}{1+\frac{x_1 Đ_2 + x_2 Đ_1}{Đ_{12}}} \tag{14}$$

The elements $\Delta_{ij}$ can be determined from MD simulations in each of the three coordinate directions using the formula

$$\Delta_{ij} = \frac{1}{2}\lim_{\Delta t\to\infty}\frac{1}{n_j}\frac{1}{\Delta t}\left\langle\left(\sum_{l=1}^{n_i}\left(\mathbf{r}_{l,i}(t+\Delta t)-\mathbf{r}_{l,i}(t)\right)\right)\bullet\left(\sum_{k=1}^{n_j}\left(\mathbf{r}_{k,j}(t+\Delta t)-\mathbf{r}_{k,j}(t)\right)\right)\right\rangle \tag{15}$$

In this expression $n_i$ and $n_j$ represent the number of molecules of species $i$ and $j$ respectively, and $\mathbf{r}_{l,i}(t)$ is the position of molecule $l$ of species $i$ at any time $t$. For unary systems eq (15) yields the M-S diffusivity $Đ_i$.

The Onsager reciprocal relations (4) translate to

$$\Delta_{ij} c_j = \Delta_{ji} c_i \tag{16}$$

# 9. Notation

| | |
|---|---|
| $[B]$ | matrix of inverse Maxwell-Stefan coefficients, $m^{-2}$ s |
| $c_i$ | concentration of species $i$, mol $m^{-3}$ |
| $c_t$ | total concentration in mixture, mol $m^{-3}$ |
| $D_{i,self}$ | self-diffusivity of species $i$ within pore, $m^2$ $s^{-1}$ |
| $Đ_{ii}$ | self-exchange diffusivity, $m^2$ $s^{-1}$ |
| $Đ_i$ | M-S diffusivity of species $i$, $m^2$ $s^{-1}$ |
| $Đ_{ij}$ | M-S exchange coefficient, $m^2$ $s^{-1}$ |
| $f_i$ | fugacity of species $i$, Pa |
| $f_t$ | total bulk fluid phase fugacity of mixture, Pa |
| $k_B$ | Boltzmann constant, $1.38\times10^{-23}$ J $molecule^{-1}$ $K^{-1}$ |
| $N_i$ | molar flux of species $i$, based on membrane area, mol $m^{-2}$ $s^{-1}$ |
| $n_i$ | number of molecules of species $i$ in simulation box, dimensionless |
| $n$ | number of species in mixture, dimensionless |
| $q_i$ | component molar loading of species $i$, mol $kg^{-1}$ |
| $\mathbf{r}_{l,i}(t)$ | position vector for molecule $l$ of species $i$ at any time $t$, m |
| $R$ | gas constant, 8.314 J $mol^{-1}$ $K^{-1}$ |
| $S_{ads}$ | adsorption selectivity, dimensionless |
| $S_{diff}$ | diffusion selectivity, dimensionless |
| $S_{perm}$ | permeation selectivity, dimensionless |
| $t$ | time, s |
| $T$ | absolute temperature, K |
| $V_p$ | accessible pore volume, $m^3$ $kg^{-1}$ |
| $x_i$ | mole fraction of species $i$ based on loading within pore, dimensionless |

***Greek letters***

| | |
|---|---|
| $\varepsilon$ | Lennard-Jones interaction energy parameter, J molecule$^{-1}$ |
| $[\Gamma]$ | matrix of thermodynamic factors, dimensionless |
| $\Gamma_{ij}$ | thermodynamic factors, dimensionless |
| $[\Delta]$ | matrix of Maxwell-Stefan diffusivities, m$^2$ s$^{-1}$ |
| $\phi$ | fractional pore volume, dimensionless |
| $\theta_i$ | fractional occupancy of component *i*, dimensionless |
| $\mu_i$ | molar chemical potential, J mol$^{-1}$ |
| $\phi$ | fractional pore volume, dimensionless |
| $\rho$ | framework density, kg m$^{-3}$ |
| $\sigma$ | Lennard-Jones size parameter, m |

***Subscripts***

| | |
|---|---|
| i | referring to component *i* |
| p | referring to pore |
| t | referring to total mixture |

***Vector and Matrix Notation***

| | |
|---|---|
| $\nabla$ | gradient operator |

# 10. References

[1] J. Kärger, D.M. Ruthven, D.N. Theodorou, Diffusion in Zeolites and Other Nanoporous Materials, Wiley - VCH, Weinheim, 2012.
[2] R.M. Barrer, Zeolites and Clay minerals as Sorbents and Molecular sieves, Academic Press, London, 1978.
[3] J. Kärger, D.M. Ruthven, Diffusion in zeolites and other microporous solids, John Wiley, New York, 1992.
[4] J. Kärger, S. Vasenkov, S.M. Auerbach, Diffusion in zeolites, Chapter 10, in S.M. Auerbach, K.A. Carrado and P.K. Dutta (Ed.), Handbook of Zeolite Science and Technology, Vol. pp. 341-422, Marcel Dekker, New York, 2003.
[5] F.J. Keil, R. Krishna, M.O. Coppens, Modeling of diffusion in zeolites, Rev. Chem. Eng. 16 (2000) 71-197.
[6] C. Chmelik, J. Kärger, In situ study on molecular diffusion phenomena in nanoporous catalytic solids, Chem. Soc. Rev. 39 (2010) 4864-4884.
[7] S.M. Auerbach, Theory and simulation of jump dynamics, diffusion and phase equilibrium in nanopores, Int. Rev. Phys. Chem. 19 (2000) 155-198.
[8] S.M. Auerbach, Theory and simulation of cohesive diffusion in nanopores: Transport in subcritical and supercritical regimes, Abstr. Pap. Am. Chem. Soc. 220 (2000) 147-COMP.
[9] S.M. Auerbach, K.A. Carrado, P.K. Dutta, Handbook of Zeolite Science and Technology, Marcel Dekker, New York, 2003.
[10] D. Dubbeldam, R.Q. Snurr, Recent developments in the molecular modeling of diffusion in nanoporous materials, Mol. Simulation 33 (2007) 15-30.
[11] R.Q. Snurr, A.Ö. Yazaydın, D. Dubbeldam, H. Frost, Molecular modeling of adsorption and diffusion in metal-organic frameworks, Chapter 11, in L.R. MacGillivray (Ed.), Metal-Organic Frameworks: Design and Application, Vol. pp. 313-339, John Wiley & Sons, Hoboken, N.J., 2010.
[12] B. Smit, T.L.M. Maesen, Towards a molecular understanding of shape selectivity, Nature 451 (2008) 671-678.
[13] B. Smit, T.L.M. Maesen, Molecular Simulations of Zeolites: Adsorption, Diffusion, and Shape Selectivity, Chem. Rev. 108 (2008) 4125-4184.
[14] B. Smit, R. Krishna, Molecular simulations in zeolitic process design, Chem. Eng. Sci. 58 (2003) 557-568.
[15] J. Jiang, R. Babarao, Z. Hu, Molecular simulations for energy, environmental and pharmaceutical applications of nanoporous materials: from zeolites, metal–organic frameworks to protein crystals, Chem. Soc. Rev. 40 (2011) 3599-3612.
[16] R. Krishna, Describing the diffusion of guest molecules inside porous structures, J. Phys. Chem. C 113 (2009) 19756-19781.
[17] R. Krishna, R. Baur, Modelling issues in zeolite based separation processes, Sep. Purif. Technol. 33 (2003) 213-254.
[18] D.N. Theodorou, Principles of Molecular Simulation of Gas Transport in Polymers, in Y. Yampolskii, I. Pinnau and B.D. Freeman (Ed.), Materials Science of Membranes for Gas and Vapor Separation, Vol. pp. 49-94, John Wiley & Sons, New York, 2006.
[19] D.N. Theodorou, R.Q. Snurr, A.T. Bell, Molecular dynamics and diffusion in microporous materials, in G. Alberti and T. Bein (Ed.), Comprehensive Supramolecular Chemistry, Vol. 7, pp. 507-548, Pergamon Press, Oxford, 1996.

[20] A.T. Bell, E.J. Maginn, D.N. Theodorou, Molecular simulation of adsorption and diffusion in zeolites, in G. Ertl, H. Knözinger and J. Weitkamp (Ed.), Handbook of Heterogeneous Catalysis, Vol. 3, pp. 1165-1188, VCH, Weinheim, 1997.
[21] T. Düren, Y.S. Bae, R.Q. Snurr, Using molecular simulation to characterise metal–organic frameworks for adsorption applications, Chem. Soc. Rev. 38 (2009) 1237-1247.
[22] S. Keskin, J. Liu, R.B. Rankin, J.K. Johnson, D.S. Sholl, Progress, Opportunities, and Challenges for Applying Atomically Detailed Modeling to Molecular Adsorption and Transport in Metal-Organic Framework Materials, Ind. Eng. Chem. Res. 48 (2009) 2355-2371.
[23] R. Krishna, A Unified Theory of Separation Processes Based on Irreversible Thermodynamics, Chem. Eng. Commun. 59 (1987) 33-64.
[24] R. Krishna, Multicomponent surface diffusion of adsorbed species - A description based on the generalized Maxwell-Stefan equations, Chem. Eng. Sci. 45 (1990) 1779-1791.
[25] R. Krishna, A unified approach to the modelling of intraparticle diffusion in adsorption processes, Gas Sep. & Purif. 7 (1993) 91-104.
[26] R. Krishna, Problems and Pitfalls in the Use of the Fick Formulation for Intraparticle Diffusion, Chem. Eng. Sci. 48 (1993) 845-861.
[27] F. Kapteijn, J.A. Moulijn, R. Krishna, The generalized Maxwell-Stefan model for diffusion in zeolites: sorbate molecules with different saturation loadings, Chem. Eng. Sci. 55 (2000) 2923-2930.
[28] R. Krishna, J.M. van Baten, Onsager coefficients for binary mixture diffusion in nanopores, Chem. Eng. Sci. 63 (2008) 3120-3140.
[29] R. Krishna, J.A. Wesselingh, The Maxwell-Stefan approach to mass transfer, Chem. Eng. Sci. 52 (1997) 861-911.
[30] X. Liu, A. Bardow, T.J.H. Vlugt, Multicomponent Maxwell-Stefan Diffusivities at Infinite Dilution, Ind. Eng. Chem. Res. 50 (2011) 4776-4782.
[31] D. Frenkel, B. Smit, Understanding molecular simulations: from algorithms to applications, Academic Press, 2nd Edition, San Diego, 2002.
[32] T.J.H. Vlugt, BIGMAC, University of Amsterdam, http://molsim.chem.uva.nl/bigmac/, 1 November 2000.
[33] T.J.H. Vlugt, R. Krishna, B. Smit, Molecular simulations of adsorption isotherms for linear and branched alkanes and their mixtures in silicalite, J. Phys. Chem. B 103 (1999) 1102-1118.
[34] T.J.H. Vlugt, M.G. Martin, B. Smit, J.I. Siepmann, R. Krishna, Improving the efficiency of the configurational-bias Monte Carlo algorithm, Mol. Phys. 94 (1998) 727-733.
[35] T.J.H. Vlugt, J.P.J.M. Van der Eerden, M. Dijkstra, B. Smit, D. Frenkel, Introduction to Molecular Simulation and Statistical Thermodynamics, Universiteit Utrecht, http://www.phys.uu.nl/~vlugt/imsst/, 1 January 2008.
[36] D. Dubbeldam, S. Calero, T.J.H. Vlugt, R. Krishna, T.L.M. Maesen, E. Beerdsen, B. Smit, Force Field Parametrization through Fitting on Inflection Points in Isotherms, Phys. Rev. Lett. 93 (2004) 088302.
[37] D. Dubbeldam, S. Calero, T.J.H. Vlugt, R. Krishna, T.L.M. Maesen, B. Smit, United Atom Forcefield for Alkanes in Nanoporous Materials, J. Phys. Chem. B 108 (2004) 12301-12313.
[38] D. Dubbeldam, H. Frost, K.S. Walton, R.Q. Snurr, Molecular simulation of adsorption sites of light gases in the metal-organic framework IRMOF-1, Fluid Phase Equilib. 261 (2007) 152-161.
[39] S. Calero, Modelling of Transport and Accessibility in Zeolites, Chapter 12, in J. Cejka, A. Corma and S. Jones (Ed.), Zeolites and Catalysts., Vol. 2, pp. 335-360, Wiley-VCH, Weinheim, 2010.
[40] S. Calero, D. Dubbeldam, R. Krishna, B. Smit, T.J.H. Vlugt, J.F.M. Denayer, J.A. Martens, T.L.M. Maesen, Understanding the role of sodium during adsorption. A force field for alkanes in sodium exchanged faujasites, J. Am. Chem. Soc. 126 (2004) 11377-11386.
[41] S. Calero, B. Smit, R. Krishna, Configurational entropy effects during sorption of hexane isomers in silicalite, J. Catal. 202 (2001) 395-401.

[42] S. Calero, B. Smit, R. Krishna, Separation of linear, mono-methyl and di-methyl alkanes in the 5-7 carbon atom range by exploiting configurational entropy effects during sorption on silicalite-1, Phys. Chem. Chem. Phys. 3 (2001) 4390-4398.

[43] E. García-Pérez, J.B. Parra, C.O. Ania, A. García-Sánchez, J.M. Van Baten, R. Krishna, D. Dubbeldam, S. Calero, A computational study of $CO_2$, $N_2$ and $CH_4$ adsorption in zeolites, Adsorption 13 (2007) 469-476.

[44] A. García-Sánchez, C.O. Ania, J.B. Parra, D. Dubbeldam, T.J.H. Vlugt, R. Krishna, S. Calero, Development of a Transferable Force Field for Carbon Dioxide Adsorption in Zeolites, J. Phys. Chem. C 113 (2009) 8814-8820.

[45] S. Ban, A. van Laak, P.E. de Jongh, J.P.J.M. van der Eerden, T.J.H. Vlugt, Adsorption Selectivity of Benzene and Propene Mixtures for Various Zeolites, J. Phys. Chem. C 111 (2007) 17241-17248.

[46] K. Makrodimitris, G.K. Papadopoulos, D.N. Theodorou, Prediction of permeation properties of $CO_2$ and $N_2$ through silicalite via molecular simulations, J. Phys. Chem. B 105 (2001) 777-788.

[47] E. Beerdsen, D. Dubbeldam, B. Smit, Molecular Understanding of Diffusion in Confinment, Phys. Rev. Lett. 95 (2005) 164505.

[48] E. Beerdsen, D. Dubbeldam, B. Smit, Molecular Simulation of Loading Dependent Slow Diffusion in Confined Systems, Phys. Rev. Lett. 93 (2005) 248301.

[49] E. Beerdsen, D. Dubbeldam, B. Smit, Understanding Diffusion in Nanoporous Materials, Phys. Rev. Lett. 96 (2006) 044501.

[50] E. Beerdsen, D. Dubbeldam, B. Smit, Loading Dependence of the Diffusion Coefficient of Methane in Nanoporous Materials, J Phys Chem B 110 (2006) 22754-22772.

[51] E. Beerdsen, B. Smit, Diffusion in Confinement: Agreement between Experiments Better than Expected, J. Phys. Chem. B 110 (2006) 14529-14530.

[52] A. García-Sánchez, E. García-Pérez, D. Dubbeldam, R. Krishna, S. Calero, A Simulation Study of Alkanes in Linde Type A Zeolites, Adsorpt. Sci. Technol. 25 (2007) 417-427.

[53] D. Paschek, R. Krishna, Monte Carlo simulations of self- and transport-diffusivities of 2-methylhexane in silicalite, Phys. Chem. Chem. Phys. 2 (2000) 2389-2394.

[54] D. Paschek, R. Krishna, Diffusion of binary mixtures in zeolites: Kinetic Monte Carlo versus molecular dynamics simulations, Langmuir 17 (2001) 247-254.

[55] D. Paschek, R. Krishna, Inter-relation between self- and jump-diffusivities in zeolites, Chem. Phys. Lett. 333 (2001) 278-284.

[56] D. Paschek, R. Krishna, Monte Carlo simulations of sorption and diffusion of isobutane in silicalite, Chem. Phys. Lett. 342 (2001) 148-154.

[57] D. Paschek, R. Krishna, Kinetic Monte Carlo simulations of transport diffusivities of binary mixtures in zeolites, Phys. Chem. Chem. Phys. 3 (2001) 3185-3191.

[58] R. Krishna, J.M. van Baten, D. Dubbeldam, On the Inflection in the Concentration Dependence of the Maxwell-Stefan diffusivity of $CF_4$ in MFI zeolite, J. Phys. Chem. B 108 (2004) 14820-14822.

[59] R. Krishna, J.M. van Baten, Kinetic Monte Carlo simulations of the loading dependence of diffusion in zeolites, Chem. Eng. Technol. 28 (2005) 160-167.

[60] R. Krishna, D. Paschek, R. Baur, Modelling the occupancy dependence of diffusivities in zeolites, Microporous Mesoporous Mater. 76 (2004) 233-246.

[61] M.O. Coppens, A.T. Bell, A.K. Chakraborty, Dynamic Monte-Carlo and mean-field study of the effect of strong adsorption sites on self-diffusion in zeolites, Chem. Eng. Sci. 54 (1999) 3455-3463.

[62] L.J.P. van den Broeke, S.A. Nijhuis, R. Krishna, Monte-Carlo Simulations of Diffusion in Zeolites and Comparison with the Generalized Maxwell-Stefan Theory, J. Catal. 136 (1992) 463-477.

[63] R.L. June, A.T. Bell, D.N. Theodorou, Transition-State Studies of Xenon and SF6 Diffusion in Silicalite, J. Phys. Chem. 95 (1991) 8866-8878.

[64] R.L. June, A.T. Bell, D.N. Theodorou, Molecular-Dynamics Studies of Butane and Hexane in Silicalite, J. Phys. Chem. 96 (1992) 1051-1060.
[65] R.L. June, A.T. Bell, D.N. Theodorou, Molecular-Dynamics Study of Methane and Xenon in Silicalite, J. Phys. Chem. 94 (1990) 8232-8240.
[66] R. Krishna, J.M. van Baten, The Darken relation for multicomponent diffusion in liquid mixtures of linear alkanes. An investigation using Molecular Dynamics (MD) simulations, Ind. Eng. Chem. Res. 44 (2005) 6939-6947.
[67] R. Krishna, J.M. van Baten, Influence of isotherm inflection on the diffusivities of C5-C8 linear alkanes in MFI zeolite, Chem. Phys. Lett. 407 (2005) 159-165.
[68] R. Krishna, J.M. van Baten, Diffusion of alkane mixtures in zeolites. Validating the Maxwell-Stefan formulation using MD simulations, J. Phys. Chem. B 109 (2005) 6386-6396.
[69] R. Krishna, J.M. van Baten, Validating the Darken relation for diffusivities in fluid mixtures of varying densities by use of MD simulations, Chem Eng Technol 29 (2006) 761-765.
[70] R. Krishna, J.M. van Baten, MD simulations of diffusivities in methanol – n-hexane mixtures near the liquid-liquid phase splitting region, Chem Eng Technol 29 (2006) 516-519.
[71] R. Krishna, J.M. van Baten, A Molecular Dynamics investigation of diffusion of methane-ethane and methane-propane mixtures in zeolites, Chem. Eng. Technol. 29 (2006) 1429-1437.
[72] R. Krishna, J.M. van Baten, Describing binary mixture diffusion in carbon nanotubes with the Maxwell-Stefan equations. An investigation using molecular dynamics simulations, Ind. Eng. Chem. Res. 45 (2006) 2084-2093.
[73] R. Krishna, J.M. van Baten, Linking the loading dependence of the Maxwell-Stefan diffusivity of linear alkanes in zeolites with the thermodynamic correction factor, Chem. Phys. Lett. 420 (2006) 545-549.
[74] R. Krishna, J.M. van Baten, Loading dependence of self-diffusivities of gases in zeolites, Chem. Eng. Technol. 30 (2007) 1235-1241.
[75] R. Krishna, J.M. van Baten, Influence of segregated adsorption on mixture diffusion in DDR zeolite, Chem. Phys. Lett. 446 (2007) 344-349.
[76] R. Krishna, J.M. van Baten, Using molecular simulations for screening of zeolites for separation of $CO_2/CH_4$ mixtures, Chem. Eng. J. 133 (2007) 121-131.
[77] R. Krishna, J.M. van Baten, Screening of zeolite adsorbents for separation of hexane isomers: A molecular simulation study, Sep. Purif. Technol. 55 (2007) 246-255.
[78] R. Krishna, J.M. van Baten, Diffusion of hydrocarbon mixtures in MFI zeolite: Influence of intersection blocking, Chem. Eng. J. 140 (2008) 614-620.
[79] R. Krishna, J.M. van Baten, Insights into diffusion of gases in zeolites gained from molecular dynamics simulations, Microporous Mesoporous Mater. 109 (2008) 91-108.
[80] R. Krishna, J.M. van Baten, Diffusion of alkane mixtures in MFI zeolite, Microporous Mesoporous Mater. 107 (2008) 296-298.
[81] R. Krishna, J.M. van Baten, Unified Maxwell-Stefan description of binary mixture diffusion in micro- and meso- porous materials, Chem. Eng. Sci. 64 (2009) 3159-3178.
[82] R. Krishna, J.M. van Baten, A molecular simulation study of commensurate – incommensurate adsorption of n-alkanes in cobalt formate frameworks, Mol. Simulation 35 (2009) 1098-1104.
[83] R. Krishna, J.M. van Baten, A molecular dynamics investigation of a variety of influences of temperature on diffusion in zeolites, Microporous Mesoporous Mater. 125 (2009) 126-134.
[84] R. Krishna, J.M. van Baten, An investigation of the characteristics of Maxwell-Stefan diffusivities of binary mixtures in silica nanopores, Chem. Eng. Sci. 64 (2009) 870-882.
[85] R. Krishna, J.M. van Baten, Letter to the Editor, A.I.Ch.E.J. 56 (2010) 3288-3289.
[86] R. Krishna, J.M. van Baten, Comment on "Modeling Adsorption and Self-Diffusion of Methane in LTA Zeolites: The Influence of Framework Flexibility", J. Phys. Chem. C 114 (2010) 18017-18021.
[87] R. Krishna, J.M. van Baten, Mutual slowing-down effects in mixture diffusion in zeolites, J. Phys. Chem. C 114 (2010) 13154-13156.

[88] R. Krishna, J.M. van Baten, A molecular dynamics investigation of the unusual concentration dependencies of Fick diffusivities in silica mesopores, Microporous Mesoporous Mater. 138 (2011) 228-234.
[89] R. Krishna, J.M. van Baten, A molecular dynamics investigation of the diffusion characteristics of cavity-type zeolites with 8-ring windows, Microporous Mesoporous Mater. 137 (2011) 83-91.
[90] R. Babarao, J. Jiang, Molecular screening of metal-organic frameworks for $CO_2$ storage, Langmuir 24 (2008) 6270-6278.
[91] R. Babarao, J. Jiang, Diffusion and Separation of $CO_2$ and $CH_4$ in Silicalite, $C_{168}$ Schwarzite, and IRMOF-1: A Comparative Study from Molecular Dynamics Simulation, Langmuir 24 (2008) 5474-5484.
[92] R. Babarao, J. Jiang, Exceptionally high $CO_2$ storage in covalent-organic frameworks: Atomistic simulation study, Energy Environ. Sci. 1 (2008) 139-143.
[93] R. Babarao, J. Jiang, Upgrade of natural gas in *rho* zeolite-like metal–organic framework and effect of water: a computational study, Energy& Environ. Sci. 2 (2009) 1088-1093.
[94] R. Babarao, J. Jiang, Unprecedentedly High Selective Adsorption of Gas Mixtures in rho Zeolite-like Metal-Organic Framework: A Molecular Simulation Study, J. Am. Chem. Soc. 131 (2009) 11417-11425.
[95] R. Babarao, J. Jiang, S.I. Sandler, Molecular simulations for adsorptive separations of $CO_2$ / $CH_4$ mixture in metal-exposed, catenated, and charged metal-organic frameworks, Langmuir 25 (2009) 5239-5247.
[96] R. Babarao, Y.H. Tong, J. Jiang, Molecular Insight into Adsorption and Diffusion of Alkane Isomer Mixtures in Metal-Organic Frameworks, J. Phys. Chem. B 113 (2009) 9129-9136.
[97] R. Krishna, B. Smit, Exploiting entropy to separate alkane isomers, Chem. Innov. 31(1) (2001) 27-33.
[98] R. Krishna, B. Smit, S. Calero, Entropy effects during sorption of alkanes in zeolites, Chem. Soc. Rev. 31 (2002) 185-194.
[99] D. Dubbeldam, B. Smit, Computer simulation of incommensurate diffusion in zeolites: Understanding window effects, J. Phys. Chem. B 107 (2003) 12138-12152.
[100] D. Dubbeldam, S. Calero, T.L.M. Maesen, B. Smit, Incommensurate diffusion in confined systems, Phys. Rev. Lett. 90 (24) Art. No. 245901 (2003)
[101] S. Chempath, R. Krishna, R.Q. Snurr, Nonequilibrium MD simulations of difusion of binary mixtures containing short n-alkanes in faujasite, J. Phys. Chem. B 108 (2004) 13481-13491.
[102] L.N. Gergidis, D.N. Theodorou, Molecular dynamics simulation of n-butane-methane mixtures in silicalite, J. Phys. Chem. B 103 (1999) 3380-3390.
[103] L.N. Gergidis, D.N. Theodorou, H. Jobic, Dynamics of n-butane-methane mixtures in silicalite, using quasielastic neutron scattering and molecular dynamics simulations, J. Phys. Chem. B 104 (2000) 5541-5552.
[104] L.N. Gergidis, D.N. Theodorou, H. Jobic, Dynamics of alkane mixtures in silicalite pores, J. Phys. IV 10 (2000) 143-146.
[105] S. Jakobtorweihen, M.G. Verbeek, C.P. Lowe, F.J. Keil, B. Smit, Understanding the Loading Dependence of Self-Diffusion in Carbon Nanotubes, Phys. Rev. Lett. 95 (2005) 044501.
[106] E.J. Maginn, A.T. Bell, D.N. Theodorou, Transport Diffusivity of Methane in Silicalite from Equilibrium and Nonequilibrium Simulations, J. Phys. Chem. 97 (1993) 4173-4181.
[107] M.J. Sanborn, R.Q. Snurr, Diffusion of binary mixtures of $CF_4$ and n-alkanes in faujasite, Sep. Purif. Technol. 20 (2000) 1-13.
[108] M.J. Sanborn, R.Q. Snurr, Predicting membrane flux of $CH_4$ and $CF_4$ mixtures in faujasite from molecular simulations, A.I.Ch.E.J. 47 (2001) 2032-2041.
[109] A.I. Skoulidas, D.S. Sholl, R. Krishna, Correlation effects in diffusion of $CH_4$/$CF_4$ mixtures in MFI zeolite. A study linking MD simulations with the Maxwell-Stefan formulation, Langmuir 19 (2003) 7977-7988.
[110] L.A. Clark, A. Gupta, R.Q. Snurr, Siting and segregation effects of simple molecules in zeolites MFI, MOR, and BOG, J. Phys. Chem. B 102 (1998) 6720-6731.

[111] A. Gupta, L.A. Clark, R.Q. Snurr, Grand canonical Monte Carlo simulations of nonrigid molecules: Siting and segregation in silicalite zeolite, Langmuir 16 (2000) 3910-3919.
[112] R. Krishna, J.M. van Baten, Segregation effects in adsorption of $CO_2$ containing mixtures and their consequences for separation selectivities in cage-type zeolites, Sep. Purif. Technol. 61 (2008) 414-423.
[113] B.L. Newalkar, R.V. Jasra, V. Kamath, S.G.T. Bhat, Sorption of water in aluminophosphate molecular sieve $AlPO_4$-5, Microporous Mesoporous Mater. 20 (1998) 129-137.
[114] I. Halasz, S. Kim, B. Marcus, Uncommon Adsorption Isotherm of Methanol on a Hydrophobic Y-zeolite, J. Phys. Chem. B 105 (2001) 10788-10796.
[115] C. Bussai, S. Fritzsche, R. Haberlandt, S. Hannongbua, Formation of Low-Density Water Clusters in the Silicalite-1 Cage: A Molecular Dynamics Study, J. Phys. Chem. B 107 (2003) 12444-12450.
[116] P. Demontis, G. Stara, G.B. Suffritti, Behavior of Water in the Hydrophobic Zeolite Silicalite at Different Temperatures. A Molecular Dynamics Study, J. Phys. Chem. B 107 (2003) 4426-4436.
[117] P. Demontis, J. Gulin-González, H. Jobic, M. Masia, R. Sale, G.B. Suffritti, Dynamical Properties of Confined Water Nanoclusters: Simulation Study of Hydrated Zeolite NaA: Structural and Vibrational Properties, ACS Nano 2 (2008) 1603-1614.
[118] P. Demontis, H. Jobic, M.A. Gonzalez, G.B. Suffritti, Diffusion of Water in Zeolites NaX and NaY Studied by Quasi-Elastic Neutron Scattering and Computer Simulation, J. Phys. Chem. C 113 (2009) 12373-12379.
[119] M.U. Ari, M.G. Ahunbay, M. Yurtsever, A. Erdem-Senatalar, Molecular Dynamics Simulation of Water Diffusion in MFI-Type Zeolites, J. Phys. Chem. B 113 (2009) 8073-8079.
[120] D.F. Plant, G. Maurin, R.G. Bell, Modeling the Concentration Dependence of the Methanol Self-Diffusivity in Faujasite Systems: Comparison with the Liquid Phase, J. Phys. Chem. B 110 (2006) 15926-15931.
[121] J.Z. Yang, Q.L. Liu, H.T. Wang, Analyzing adsorption and diffusion behaviors of ethanol/water through silicalite membranes by molecular simulation, J. Membr. Sci. 291 (2007) 1-7.
[122] J.Z. Yang, Y. Chen, A.M. Zhu, Q.L. Liu, J.Y. Wu, Analyzing diffusion behaviors of methanol/water through MFI membranes by molecular simulation, J. Membr. Sci. 318 (2008) 327-333.
[123] M. Fleys, R.W. Thompson, J.C. MacDonald, Comparison of the Behavior of Water in Silicalite and Dealuminated Zeolite Y at Different Temperatures by Molecular Dynamic Simulations, J. Phys. Chem. B 108 (2004) 12197-12203.
[124] M. Fleys, R.W. Thompson, Monte Carlo Simulations of Water Adsorption Isotherms in Silicalite and Dealuminated Zeolite Y, J. Chem. Theory Comput. 1 (2005) 453-458.
[125] A. Di Lella, N. Desbiens, A. Boutin, I. Demachy, U. P., J.P. Bellat, A.H. Fuchs, Molecular simulation studies of water physisorption in zeolites, Phys. Chem. Chem. Phys. 8 (2006) 5396-5406.
[126] J.Y. Wu, Q.L. Liu, Y. Xiong, A.M. Zhu, Y. Chen, Molecular Simulation of Water/Alcohol Mixtures' Adsorption and Diffusion in Zeolite 4A Membranes, J. Phys. Chem. B 113 (2009) 4267-4274.
[127] S. Konduri, H.M. Tong, S. Chempath, S. Nair, Water in Single-Walled Aluminosilicate Nanotubes: Diffusion and Adsorption Properties, J. Phys. Chem. C 112 (2008) 15367-15374.
[128] A.Ö. Yazaydın, R.W. Thompson, Molecular simulation of water adsorption in silicalite: Effect of silanol groups and different cations, Microporous Mesoporous Mater. 123 (2009) 169-176.
[129] L. Narasimhan, P. Boulet, B. Kuchta, O. Schaef, R. Denoyel, P. Brunet, Molecular Simulations of Water and Paracresol in MFI Zeolite - A Monte Carlo Study, Langmuir 25 (2009) 11598-11607.
[130] T. Nanok, S. Vasenkov, F. Keil, S. Fritzsche, Molecular dynamics simulation study of the concentration dependence of the self-diffusivity of methanol in NaX zeolite, Microporous Mesoporous Mater. 127 (2010) 176-181.

[131] R.S. Pillai, R.V. Jasra, Computational Study for Water Sorption in AlPO4-5 and AlPO4-11Molecular Sieves, Langmuir 26 (2010) 1755-1764.
[132] L. Lu, Q. Shao, L. Huang, X. Lu, Simulation of adsorption and separation of ethanol–water mixture with zeolite and carbon nanotube, Fluid Phase Equilib. 261 (2007) 191-198.
[133] J. Puibasset, R.J.M. Pellenq, Grand Canonical Monte Carlo Simulation Study of Water Adsorption in Silicalite at 300 K, J. Phys. Chem. B 112 (2008) 6390-6397.
[134] H. Nasiri, A. Aroujalian, A Novel Model Based on Cluster Formation for Pervaporation Separation of Polar Components from Aqueous Solutions, Sep. Purif. Technol. 72 (2010) 13-21.
[135] C. Chmelik, H. Bux, J. Caro, L. Heinke, F. Hibbe, T. Titze, J. Kärger, Mass transfer in a nanoscale material enhanced by an opposing flux, Phys. Rev. Lett. 104 (2010) 085902.
[136] J. Zang, S. Konduri, S. Nair, D.S. Sholl, Self-Diffusion of Water and Simple Alcohols in Single-Walled Aluminosilicate Nanotubes, ACS Nano 3 (2010) 1548-1556.
[137] J. Zang, S. Chempath, S. Konduri, S. Nair, D.S. Sholl, Flexibility of Ordered Surface Hydroxyls Influences the Adsorption of Molecules in Single-Walled Aluminosilicate Nanotubes, J. Phys. Chem. Letters 1 (2010) 1235-1240.
[138] R. Krishna, J.M. van Baten, Investigating cluster formation in adsorption of $CO_2$, $CH_4$, and Ar in zeolites and metal organic frameworks at sub-critical temperatures, Langmuir 26 (2010) 3981-3992.
[139] R. Krishna, J.M. van Baten, Highlighting a variety of unusual characteristics of adsorption and diffusion in microporous materials induced by clustering of guest molecules, Langmuir 26 (2010) 8450-8463.
[140] R. Krishna, J.M. van Baten, Hydrogen bonding effects in adsorption of water-alcohol mixtures in zeolites and the consequences for the characteristics of the Maxwell-Stefan diffusivities, Langmuir 26 (2010) 10854-10867.
[141] R. Krishna, J.M. van Baten, Highlighting Pitfalls in the Maxwell-Stefan Modeling of Water-Alcohol Mixture Permeation across Pervaporation Membranes, J. Membr. Sci. 360 (2010) 476-482.
[142] R. Krishna, J.M. van Baten, A rationalization of the Type IV loading dependence in the Kärger-Pfeifer classification of self-diffusivities, Microporous Mesoporous Mater. 142 (2011) 745-748.
[143] T. Maris, T.J.H. Vlugt, B. Smit, Simulation of alkane adsorption in the aluminophosphate molecular sieve $AlPO_4$-5, J. Phys. Chem. B 102 (1998) 7183-7189.
[144] S. Samios, A.K. Stubos, G.K. Papadopoulos, N.K. Kanellopoulos, F. Rigas, The Structure of Adsorbed CO2 in Slitlike Micropores at Low and High Temperature and the Resulting Micropore Size Distribution Based on GCMC Simulations, J. Colloid Interface Sci. 224 (2000) 272-290.
[145] Q. Yang, C. Zhong, Molecular Simulation Study of the Stepped Behaviors of Gas Adsorption in Two-Dimensional Covalent Organic Frameworks, Langmuir 25 (2009) 2302-2308.
[146] Y.B. Melnichenko, G.D. Wignall, D.R. Cole, H. Frielinghaus, L.A. Bulavin, Liquid–gas critical phenomena under confinement: small-angle neutron scattering studies of $CO_2$ in aerogel, J. Mol. Liq. 120 (2005) 7-9.
[147] T.A. Steriotis, K.L. Stefanopoulos, N.K. Kanellopoulos, M. A.Ch., Structural studies of supercritical carbon dioxide in confined space, Appl. Phys. A. 74 (2002) S1333-S1335.
[148] T.A. Steriotis, K.L. Stefanopoulos, N.K. Kanellopoulos, M. A.Ch., The structure of adsorbed $CO_2$ in carbon nanopores: a neutron diffraction study, Colloids Surf., A 241 (2004) 239-244.
[149] S. Fritzsche, M. Wolfsberg, R. Haberlandt, P. Demontis, G.B. Suffritti, A. Tilocca, About the influence of lattice vibrations on the diffusion of methane in a cation-free LTA zeolite, Chem. Phys. Lett. 296 (1998) 253-258.
[150] P. Demontis, G.B. Suffritti, A comment on the flexibility of framework in molecular dynamics simulations of zeolites, Microporous Mesoporous Mater. 125 (2009) 160-168.
[151] S. Amirjalayer, M. Tafipolsky, R. Schmid, Molecular Dynamics Simulation of Benzene Diffusion in MOF-5: Importance of Lattice Dynamics, Angew. Chem. Int. Ed. 46 (2007) 463-466.

[152] A.F. Combariza, G. Sastre, A. Corma, Propane/Propylene Diffusion in Zeolites: Framework Dynamics, J. Phys. Chem. C 113 (2009) 11246-11253.
[153] K. Seehamart, C. Chmelik, R. Krishna, S. Fritzsche, Molecular dynamics investigation of the self-diffusion of binary mixture diffusion in the metal-organic framework Zn(tbip) accounting for framework flexibility, Microporous Mesoporous Mater. 143 (2011) 125-131.
[154] K. Seehamart, T. Nanok, J. Kärger, C. Chmelik, R. Krishna, S. Fritzsche, Investigating the reasons for the significant influence of lattice flexibility on self-diffusivity of ethane in Zn(tbip), Microporous Mesoporous Mater. 130 (2010) 92-96.
[155] K. Seehamart, T. Nanok, R. Krishna, J.M. van Baten, T. Remsungnen, S. Fritzsche, A Molecular Dynamics investigation of the influence of framework flexibility on self-diffusivity of ethane in Zn(tbip) frameworks, Microporous Mesoporous Mater. 125 (2009) 97-100.
[156] A. García-Sánchez, D. Dubbeldam, S. Calero, Modeling Adsorption and Self-Diffusion of Methane in LTA Zeolites: the Influence of Framework Flexibility, J. Phys. Chem. C 114 (2010) 15068-15074.
[157] C. Gücüyener, J. van den Bergh, J. Gascon, F. Kapteijn, Ethane/Ethene Separation Turned on Its Head: Selective Ethane Adsorption on the Metal-Organic Framework ZIF-7 through a Gate-Opening Mechanism, J. Am. Chem. Soc. 132 (2010) 17704-17706.
[158] S. Jakobtorweihen, C.P. Lowe, F.J. Keil, B. Smit, Diffusion of chain molecules and mixtures in carbon nanotubes: The effect of host lattice flexibility and theory of diffusion in the Knudsen regime, J. Chem. Phys. 127 (2007) 024904.
[159] D.I. Kopelevich, H.C. Chang, Does lattice vibration drive diffusion in zeolites? J. Chem. Phys. 114 (2001) 3776-3789.
[160] S.K. Bhatia, Influence of Adsorbate Interaction on Transport in Confined Spaces, Adsorpt. Sci. Technol. 24 (2006) 101-116.
[161] S.K. Bhatia, Modeling Pure Gas Permeation in Nanoporous Materials and Membranes, Langmuir 26 (2010) 8373-8385.
[162] S.K. Bhatia, O. Jepps, D. Nicholson, Tractable molecular theory of transport of Lennard-Jones fluids in nanopores, J. Chem. Phys. 120 (2004) 4472-4485.
[163] S.K. Bhatia, D. Nicholson, Transport of Simple Fluids in Nanopores: Theory and Simulation, A.I.Ch.E.J. 52 (2006) 29-38.
[164] S.K. Bhatia, D. Nicholson, Comments on ‘‘Diffusion in a mesoporous silica membrane: Validity of the Knudsen diffusion model’, Chem. Eng. Sci. 65 (2010) 4519-4520.
[165] S.K. Bhatia, D. Nicholson, Some Pitfalls in the use of the Knudsen Equation in Modelling Diffusion in Nanoporous Materials, Chem. Eng. Sci. 66 (2011) 284-293.
[166] D.M. Ruthven, W. DeSisto, S. Higgins, Diffusion in a mesoporous silica membrane:Validity of the Knudsen diffusion model, Chem. Eng. Sci. 64 (2009) 3201-3203.
[167] D.M. Ruthven, Letter to the Editor. Response to Comments from S.K. Bhatia and D. Nicholson, Chem. Eng. Sci. 65 (2010) 4521-4522.
[168] R. Krishna, J.M. van Baten, Investigating the validity of the Knudsen prescription for diffusivities in a mesoporous covalent organic framework, Ind. Eng. Chem. Res. 50 (2011) 7083-7087.
[169] R. Krishna, J.M. van Baten, Influence of adsorption on the diffusion selectivity for mixture permeation across mesoporous membranes, J. Membr. Sci. 369 (2011) 545-549.
[170] S. Gruener, P. Huber, Knudsen diffusion in silicon nanochannels, Phys. Rev. Lett. 100 (2008) 064502.
[171] R. Krishna, J.M. van Baten, Investigating the validity of the Bosanquet formula for estimation of diffusivities in mesopores, Chem. Eng. Sci. XX (2012) XXX-XXX. (http://dx.doi.org/10.1016/j.ces.2011.11.026)
[172] S.K. Bhatia, M.R. Bonilla, D. Nicholson, Molecular transport in nanopores: a theoretical perspective, Phys. Chem. Chem. Phys. 13 (2011) 15350-15383.
[173] G.F. Froment, K.B. Bischoff, Chemical Reactor - Analysis and Design, John Wiley & Sons, New York, 1979.

[174] R. Baur, R. Krishna, Effectiveness factor for zeolite catalysed isomerization reactions, Chem. Eng. J. 99 (2004) 105-116.
[175] R. Baur, R. Krishna, A moving bed reactor concept for alkane isomerization, Chem. Eng. J. 109 (2005) 107-113.
[176] R. Baur, R. Krishna, The effectiveness factor for zeolite catalysed reactions, Catal. Today 105 (2005) 173-179.
[177] N. Hansen, R. Krishna, J.M. van Baten, A.T. Bell, F.J. Keil, Analysis of Diffusion Limitation in the Alkylation of Benzene over H-ZSM-5 by Combining Quantum Chemical Calculations, Molecular Simulations, and a Continuum Approach, J. Phys. Chem. C 113 (2009) 235-246.
[178] N. Hansen, R. Krishna, J.M. van Baten, A.T. Bell, F.J. Keil, Reactor simulation of benzene ethylation and ethane dehydrogenation catalyzed by ZSM-5: A multiscale approach, Chem. Eng. Sci. 65 (2010) 2472-2480.
[179] C. Chmelik, D. Enke, P. Galvosas, O.C. Gobin, A. Jentys, H. Jobic, J. Kärger, C.B. Krause, J. Kullman, J. Lercher, S. Naumov, D.M. Ruthven, T. Titze, Nanoporous Glass as a Model System for a Consistency Check of the Different Techniques of Diffusion Measurement, ChemPhysChem 12 (2011) 1130-1134.
[180] C. Chmelik, L. Heinke, J. Kärger, D.B. Shah, W. Schmidt, J.M. van Baten, R. Krishna, Inflection in the loading dependence of the Maxwell-Stefan diffusivity of iso-butane in MFI zeolite, Chem. Phys. Lett. 459 (2008) 141-145.
[181] C. Chmelik, L. Heinke, J.M. van Baten, R. Krishna, Diffusion of *n*-butane/*iso*-butane mixtures in silicalite-1 investigated using infrared (IR) microscopy, Microporous Mesoporous Mater. 125 (2009) 11-16.
[182] C. Chmelik, J. Kärger, M. Wiebcke, J. Caro, J.M. van Baten, R. Krishna, Adsorption and diffusion of alkanes in CuBTC crystals investigated using infrared microscopy and molecular simulations, Microporous Mesoporous Mater. 117 (2009) 22-32.
[183] C. Chmelik, A. Varma, L. Heinke, D.B. Shah, J. Kärger, F. Kremer, U. Wilczok, W. Schmidt, Effect of Surface Modification on Uptake Rates of Isobutane in MFI Crystals: An Infrared Microscopy Study, Chem. Mater. 19 (2007) 6012-6019.
[184] M. Fernandez, J. Kärger, D. Freude, A. Pampel, J.M. van Baten, R. Krishna, Mixture diffusion in zeolites studied by MAS PFG NMR and molecular simulation, Microporous Mesoporous Mater. 105 (2007) 124-131.
[185] Z. Bao, S. Alnemrat, I. Vasiliev, Q. Ren, L. Yu, X. Lu, S. Deng, Adsorption of Ethane, Ethylene, Propane and Propylene on a Magnesium-Based Metal-Organic Framework, Langmuir 27 (2011) 13554-13562.
[186] Z. Bao, L. Yu, Q. Ren, X. Lu, S. Deng, Adsorption of $CO_2$ and $CH_4$ on a magnesium-based metal organic framework, J. Colloid Interface Sci. 353 (2011) 549-556.
[187] S. Brandani, D.M. Ruthven, J. Kärger, Concentration-Dependence of Self-Diffusivity of Methanol in NaX Zeolite Crystals, Zeolites 15 (1995) 494-495.
[188] D.V. Cao, R.J. Mohr, M.B. Rao, S. Sircar, Self-diffusivities of $N_2$, $CH_4$, and Kr on 4A zeolite pellets by isotope exchange technique, J. Phys. Chem. B 104 (2000) 10498-10501.
[189] I. Déroche, G. Maurin, B.J. Borah, H. Jobic, S. Yashonath, Diffusion of pure $CH_4$ and its binary mixture with $CO_2$ in Faujasite NaY: A combination of neutron scattering experiments and Molecular Dynamics simulations, J. Phys. Chem. C 114 (2010) 5027-5034.
[190] I. Déroche, S. Rives, T. Trung, Q. Yang, A. Ghoufi, N.A. Ramsahye, P. Trens, F.D. Fajula, T., C. Serre, G. Férey, H. Jobic, G. Maurin, Exploration of the Long-Chain N-Alkanes Adsorption and Diffusion in the MOF-Type MIL-47 (V) Material by Combining Experimental and Molecular Simulation Tools, J. Phys. Chem. C 115 (2011) 13868-13876.
[191] D.R. Garg, D.M. Ruthven, Effect of the concentration dependence of diffusivity on zeolitic sorption curves, Chem. Eng. Sci. 27 (1972) 417-423.
[192] N. Hedin, G.J. DeMartin, W.J. Roth, K.G. Strohmaier, S.C. Reyes, PFG NMR self-diffusion of small hydrocarbons in high silica DDR, CHA and LTA structures, Microporous Mesoporous Mater. 109 (2008) 327-334.

[193] N. Hedin, G.J. DeMartin, K.G. Strohmaier, S.C. Reyes, PFG NMR self-diffusion of propylene in ITQ-29, CaA and NaCaA: Window size and cation effects, Microporous Mesoporous Mater. 98 (2007) 182-188.
[194] W. Heink, J. Kärger, S. Ernst, J. Weitkamp, P.F.G. N.M.R. study of the influence of the exchangeable cations on the self-diffusion of hydrocarbons in zeolites, Zeolites 14 (1994) 320-325.
[195] W. Heink, J. Kärger, H. Pfeifer, K.P. Datema, A.K. Nowak, High-temperature pulsed field gradient Nuclear-Magnetic-Resonance self-diffusion measurements of n-alkanes in MFI-type zeolites, J. Chem. Soc., Faraday Trans. 88 (1992) 3505-3509.
[196] W. Heink, J. Kärger, H. Pfeifer, P. Salverda, K.P. Datema, A.K. Nowak, Self-diffusion measurements of n-alkanes in zeolite NaCaA by pulsed-field gradient Nuclear Magnetic Resonance, J. Chem. Soc., Faraday Trans. 88 (1992) 515-519.
[197] L. Heinke, C. Chmelik, P. Kortunov, D.M. Ruthven, D.B. Shah, S. Vasenkov, J. Kärger, Application of Interference Microscopy and IR Microscopy for Characterizing and Investigating Mass Transport in Nanoporous Materials, Chem. Eng. Technol. 30 (2007) 995-1002.
[198] L. Heinke, J. Kärger, Assessing one-dimensional diffusion in nanoporous materials from transient concentration profiles, New Journal of Physics 10 (2008) 023035.
[199] L. Heinke, D. Tzoulaki, C. Chmelik, F. Hibbe, J.M. van Baten, H. Lim, J. Li, R. Krishna, J. Kärger, Assessing guest diffusivities in porous hosts from transient concentration profiles, Phys. Rev. Lett. 102 (2009) 065901.
[200] M. Jiang, M. Eic, S. Miachon, J.A. Dalmon, M. Kocirik, Diffusion of n-butane, isobutane and ethane in a MFI-zeolite membrane investigated by gas permeation and ZLC measurements, Sep. Purif. Technol. 25 (2001) 287-295.
[201] H. Jobic, Diffusion of linear and branched alkanes in ZSM-5. A quasi-elastic neutron scattering study, J. Mol. Catal. A: Chem. 158 (2000) 135-142.
[202] H. Jobic, M. Bee, J. Caro, M. Bulow, J. Kärger, Molecular Self-Diffusion of Methane in Zeolite ZSM-5 by Quasi- Elastic Neutron-Scattering and Nuclear Magnetic-Resonance Pulsed Field Gradient Technique, 85 (1989) 4201-4209.
[203] H. Jobic, M. Bee, J. Kärger, H. Pfeifer, J. Caro, On the Translational Mobility of Benzene Adsorbed on Nax-Type Zeolites, J. Chem. Soc.-Chem. Commun. (1990) 341-342.
[204] H. Jobic, M. Bee, J. Kärger, R.S. Vartapetian, C. Balzer, A. Julbe, Mobility of Cyclohexane in a Microporous Silica Sample - a Quasi-Elastic Neutron-Scattering and Nmr Pulsed-Field Gradient Technique Study, J. Membr. Sci. 108 (1995) 71-78.
[205] H. Jobic, H. Ernst, W. Heink, J. Kärger, A. Tuel, M. Bee, Diffusion of ammonia in silicalite studied by QENS and PFG NMR, Microporous Mesoporous Mat. 26 (1998) 67-75.
[206] H. Jobic, K. Hahn, J. Kärger, M. Bee, A. Tuel, M. Noack, I. Girnus, G.J. Kearley, Unidirectional and single-file diffusion of molecules in one- dimensional channel systems. A quasi-elastic neutron scattering study, J. Phys. Chem. B 101 (1997) 5834-5841.
[207] H. Jobic, J. Kärger, M. Bée, Simultaneous measurement of self- and transport diffusivities in zeolites, Phys. Rev. Lett. 82 (1999) 4260-4263.
[208] H. Jobic, J. Kärger, C. Krause, S. Brandani, A. Gunadi, A. Methivier, G. Ehlers, B. Farago, W. Haeussler, D.M. Ruthven, Diffusivities of n-Alkanes in 5A Zeolite Measured by Neutron Spin Echo, Pulsed-Field Gradient NMR, and Zero Length Column Techniques, Adsorption 11 (2005) 403-407.
[209] H. Jobic, C. Laloué, C. Laroche, J.M. van Baten, R. Krishna, Influence of isotherm inflection on the loading dependence of the diffusivities of n-hexane and n-heptane in MFI zeolite. Quasi-Elastic Neutron Scattering experiments supplemented by molecular simulations, J. Phys. Chem. B 110 (2006) 2195-2201.
[210] H. Jobic, A. Methivier, G. Ehlers, B. Farago, W. Haeussler, Accelerated diffusion of long-chain alkanes between nanosized cavities, Angew. Chem.-Int. Edit. 43 (2004) 364-366.

[211] H. Jobic, N. Rosenbach, A. Ghoufi, D.I. Kolokolov, P.G. Yot, T. Devic, C. Serre, G. Férey, G. Maurin, Unusual Chain-Length Dependence of the Diffusion of n-Alkanes in the Metal–Organic Framework MIL-47(V): The Blowgun Effect, Chem. Eur. J. 16 (2010) 10337-10341.
[212] H. Jobic, W. Schmidt, C.B. Krause, J. Kärger, PFG NMR and QENS diffusion study of n-alkane homologues in MFI-type zeolites, Microporous Mesoporous Mater. 90 (2006) 299-306.
[213] H. Jobic, A.I. Skoulidas, D.S. Sholl, Determination of Concentration Dependent Transport Diffusivity of CF4 in Silicalite by Neutron Scattering Experiments and Molecular Dynamics, J. Phys. Chem. B 108 (2004) 10613-10616.
[214] H. Jobic, D.N. Theodorou, Quasi-elastic neutron scattering and molecular dynamics simulation as complementary techniques for studying diffusion in zeolites, Microporous Mesoporous Mater. 102 (2006) 21-50.
[215] A.O. Koriabkina, A.M. de Jong, D. Schuring, J. van Grondelle, R.A. van Santen, Influence of the acid sites on the intracrystalline diffusion of hexanes and their mixtures within MFI-zeolites, J. Phys. Chem. B 106 (2002) 9559-9566.
[216] A.O. Koriabkina, D. Schuring, A.M. de Jong, R.A. van Santen, Positron Emission Profiling study of the diffusion of 3-methylpentane in silicalite-1, Top. Catal. 24 (2003) 103-113.
[217] F. Leroy, H. Jobic, Influence of extra-framework cations on the diffusion of alkanes in silicalite: Comparison between quasi-elastic neutron scattering and molecular simulations, Chem. Phys. Lett. 406 (2005) 375-380.
[218] B. Millot, A. Méthivier, H. Jobic, Adsorption of n-alkanes on silicalite crystals. A temperature-programmed desorption study, J. Phys. Chem. B 102 (1998) 3210-3215.
[219] B. Millot, A. Méthivier, H. Jobic, I. Clemencon, B. Rebours, Adsorption of branched alkanes in silicalite-1: A temperature- programmed-equilibration study, Langmuir 15 (1999) 2534-2539.
[220] B. Millot, A. Méthivier, H. Jobic, H. Moueddeb, M. Bee, Diffusion of isobutane in ZSM-5 zeolite: A comparison of quasi- elastic neutron scattering and supported membrane results, J. Phys. Chem. B 103 (1999) 1096-1101.
[221] B. Millot, A. Méthivier, H. Jobic, H. Moueddeb, J.A. Dalmon, Permeation of linear and branched alkanes in ZSM-5 supported membranes, Microporous Mesoporous Mat. 38 (2000) 85-95.
[222] F. Salles, H. Jobic, T. Devic, P.L. Llewellyn, C. Serre, G. Férey, G. Maurin, Self and Transport Diffusivity of $CO_2$ in the Metal-Organic Framework MIL-47(V) Explored by Quasi-elastic Neutron Scattering Experiments and Molecular Dynamics Simulations, ACS Nano 4 (2010) 143-152.
[223] F. Salles, H. Jobic, A. Ghoufi, P.L. Llewellyn, C. Serre, S. Bourrelly, G. Férey, G. Maurin, Transport diffusivity of $CO_2$ in the highly flexible metal-organic framework MIL-53(Cr): A combination of quasi-elastic neutron scattering measurements and molecular dynamics simulations, Angew. Chem. Int. Ed. 48 (2009) 8335-8339.
[224] D. Tzoulaki, L. Heinke, H. Lim, J. Li, D. Olson, J. Caro, R. Krishna, C. Chmelik, J. Kärger, Assessing surface permeabilities from transient guest profiles in nanoporous host materials, Angew. Chem. Int. Ed. 48 (2009) 3525-3528.
[225] Q. Zhao, R.Q. Snurr, Self-Diffusion Studies of Binary Mixtures in NaX Zeolites Using Pulsed Field Gradient NMR and a Maxwell-Stefan Model, J. Phys. Chem. A 113 (2009) 3904-3910.
[226] H. Yucel, D.M. Ruthven, Diffusion of $CO_2$ in 4A and 5A zeolite crystals, J. Colloid Interface Sci. 74 (1980) 186-195.
[227] F. Hibbe, J.M. Van Baten, R. Krishna, C. Chmelik, J. Weitkamp, J. Kärger, In-Depth Study of Mass Transfer in Nanoporous Materials by Micro-Imaging, Chem. Ing. Tech. 83 (2011) 2211-2218.
[228] D.M. Ruthven, Principles of Adsorption and Adsorption Processes, John Wiley, New York, 1984.
[229] D.M. Ruthven, S. Farooq, K.S. Knaebel, Pressure swing adsorption, VCH Publishers, New York, 1994.

[230] R. Krishna, Diffusion of binary mixtures in microporous materials: Overshoot and roll-up phenomena, Int. Commun. Heat Mass Transf. 27 (2000) 893-902.
[231] R. Krishna, J.R. Long, Screening metal-organic frameworks by analysis of transient breakthrough of gas mixtures in a fixed bed adsorber, J. Phys. Chem. C 115 (2011) 12941-12950.
[232] Z.R. Herm, R. Krishna, J.R. Long, $CO_2/CH_4$, $CH_4/H_2$ and $CO_2/CH_4/H_2$ separations at high pressures using Mg2(dobdc), Microporous Mesoporous Mater. XXX (2011) XXX-XXX. (http://dx.doi.org/10.1016/j.micmat.2011.09.004)
[233] J.A. Mason, K. Sumida, Z.R. Herm, R. Krishna, J.R. Long, Evaluating Metal-Organic Frameworks for Post-Combustion Carbon Dioxide Capture via Temperature Swing Adsorption, Energy Environ. Sci. 3 (2011) 3030-3040.
[234] L.J.P. van den Broeke, R. Krishna, Experimental Verification of the Maxwell-Stefan Theory for Micropore Diffusion, Chem. Eng. Sci. 50 (1995) 2507-2522.
[235] R. Krishna, J.M. van Baten, A comparison of the $CO_2$ capture characteristics of zeolites and metal-organic frameworks, Sep. Purif. Technol. XX (2012) XXX-XXX. (http://dx.doi.org/10.1016/j.seppur.2011.11.031)
[236] G.R. Gavalas, Diffusion in Microporous Membranes: Measurements and Modeling, Ind. Eng. Chem. Res. 47 (2008) 5797-5811.
[237] R. Krishna, Diffusion of binary mixtures across zeolite membranes: Entropy effects on permeation selectivity, Int. Commun. Heat Mass Transf. 28 (2001) 337-346.
[238] R. Krishna, J.M. van Baten, In Silico Screening of Zeolite Membranes for $CO_2$ Capture, J. Membr. Sci. 360 (2010) 323-333.
[239] R. Krishna, J.M. van Baten, Maxwell-Stefan modeling of slowing-down effects in mixed gas permeation across porous membranes, J. Membr. Sci. 383 (2011) 289-300.
[240] R. Krishna, J.M. van Baten, A simplified procedure for estimation of mixture permeances from unary permeation data, J. Membr. Sci. 367 (2011) 204-210.
[241] S. Keskin, D.S. Sholl, Screening Metal-Organic Framework materials for membrane-based methane/carbon dioxide separations, J. Phys. Chem. C 111 (2007) 14055-14059.
[242] S. Keskin, D.S. Sholl, Efficient Methods for Screening of Metal Organic Framework Membranes for Gas Separations Using Atomically Detailed Models, Langmuir 25 (2009) 11786-11795.
[243] S. Keskin, D.S. Sholl, Assessment of a Metal−Organic Framework Membrane for Gas Separations Using Atomically Detailed Calculations: $CO_2$, $CH_4$, $N_2$, $H_2$ Mixtures in MOF-5, Ind. Eng. Chem. Res. 48 (2009) 914-922.
[244] S. Keskin, D.S. Sholl, Selecting metal organic frameworks as enabling materials in mixed matrix membranes for high efficiency natural gas purification, Energy & Environ. Sci. 3 (2010) 343-351.
[245] R. Krishna, S. Li, J.M. van Baten, J.L. Falconer, R.D. Noble, Investigation of slowing-down and speeding-up effects in binary mixture permeation across SAPO-34 and MFI membranes, Sep. Purif. Technol. 60 (2008) 230-236.
[246] R. Krishna, D. Paschek, Permeation of hexane isomers across ZSM-5 zeolite membranes, Ind. Eng. Chem. Res. 39 (2000) 2618-2622.
[247] R. Krishna, D. Paschek, Separation of hydrocarbon mixtures using zeolite membranes: a modelling approach combining molecular simulations with the Maxwell-Stefan theory, Sep. Purif. Technol. 21 (2000) 111-136.
[248] R. Krishna, R. Baur, Analytic solution of the Maxwell-Stefan equations for multicomponent permeation across a zeolite membrane, Chem. Eng. J. 97 (2004) 37-45.
[249] H. Bux, C. Chmelik, R. Krishna, J. Caro, Ethene/Ethane Separation by the MOF Membrane ZIF-8: Molecular Correlation of Permeation, Adsorption, Diffusion, J. Membr. Sci. 369 (2011) 284-289.

[250] H. Bux, C. Chmelik, J.M. Van Baten, R. Krishna, J. Caro, Novel MOF-Membrane for Molecular Sieving Predicted by IR-Diffusion Studies and Molecular Modeling, Adv. Mater. 22 (2010) 4741-4743.
[251] H. Bux, F. Liang, Y. Li, J. Cravillon, M. Wiebcke, J. Caro, Zeolitic Imidazolate Framework Membrane with Molecular Sieving Properties by Microwave-Assisted Solvothermal Synthesis, J. Am. Chem. Soc. 131 (2009) 16000-16001.
[252] J. Caro, M. Noack, Zeolite membranes - Recent developments and progress, Microporous Mesoporous Mat. 115 (2008) 215-233.
[253] J. Caro, M. Noack, P. Kolsch, R. Schafer, Zeolite membranes - state of their development and perspective, Microporous Mesoporous Mat. 38 (2000) 3-24.
[254] T.C. Bowen, J.C. Wyss, R.D. Noble, J.L. Falconer, Inhibition during multicomponent diffusion through ZSM-5 zeolite, Ind Eng Chem Res 43 (2004) 2598-2601.
[255] H.B. Chen, D.S. Sholl, Predictions of selectivity and flux for $CH_4/H_2$ separations using single walled carbon nanotubes as membranes, J. Membr. Sci. 269 (2006) 152-160.
[256] J. Coronas, J. Santamaria, Separations using zeolite membranes, Sep. Purif. Methods 28 (1999) 127-177.
[257] J. Coronas, J. Santamaria, State-of-the-art in zeolite membrane reactors, Top Catal 29 (2004) 29-44.
[258] H.H. Funke, A.M. Argo, C.D. Baertsch, J.L. Falconer, R.D. Noble, Separation of close-boiling hydrocarbons with silicalite zeolite membranes, J. Chem. Soc.-Faraday Trans. 92 (1996) 2499-2502.
[259] H.H. Funke, A.M. Argo, J.L. Falconer, R.D. Noble, Separations of cyclic, branched, and linear hydrocarbon mixtures through silicalite membranes, Ind. Eng. Chem. Res. 36 (1997) 137-143.
[260] H.H. Funke, K.R. Frender, K.M. Green, J.L. Wilwerding, B.A. Sweitzer, J.L. Falconer, R.D. Noble, Influence of adsorbed molecules on the permeation properties of silicalite membranes, J. Membr. Sci. 129 (1997) 77-82.
[261] H.H. Funke, M.G. Kovalchick, J.L. Falconer, R.D. Noble, Separation of hydrocarbon isomer vapors with silicalite zeolite membranes, Ind. Eng. Chem. Res. 35 (1996) 1575-1582.
[262] I.G. Giannakopoulos, V. Nikolakis, Separation of Propylene/Propane Mixtures Using Faujasite-Type Zeolite Membranes, Ind. Eng. Chem. Res. 44 (2005) 226-230.
[263] C.J. Gump, X. Lin, J.L. Falconer, R.D. Noble, Experimental configuration and adsorption effects on the permeation of $C_4$ isomers through ZSM-5 zeolite membranes, J. Membr. Sci. 173 (2000) 35-52.
[264] C.J. Gump, R.D. Noble, J.L. Falconer, Separation of hexane isomers through nonzeolite pores in ZSM-5 zeolite membranes, Ind. Eng. Chem. Res. 38 (1999) 2775-2781.
[265] C.J. Gump, V.A. Tuan, R.D. Noble, J.L. Falconer, Aromatic permeation through crystalline molecular sieve membranes, Ind. Eng. Chem. Res. 40 (2001) 565-577.
[266] F. Kapteijn, W.J.W. Bakker, J. Vandegraaf, G. Zheng, J. Poppe, J.A. Moulijn, Permeation and Separation Behavior of a Silicalite-1 Membrane, Catal. Today 25 (1995) 213-218.
[267] F. Kapteijn, W.J.W. Bakker, G.H. Zheng, J. Poppe, J.A. Moulijn, Permeation and Separation of Light-Hydrocarbons through a Silicalite-1 Membrane - Application of the Generalized Maxwell-Stefan Equations, Chem. Eng. J. Biochem. Eng. J. 57 (1995) 145-153.
[268] F. Kapteijn, J.M. van de Graaf, J.A. Moulijn, One-component permeation maximum: Diagnostic tool for silicalite-1 membranes? A.I.Ch.E.J. 46 (2000) 1096-1100.
[269] F. Kapteijn, W. Zhu, J.A. Moulijn, T.Q. Gardner, Zeolite membranes: modeling and application, in A. Cybulski and J.A. Moulijn (Ed.), Structured catalysts and reactors, Vol. pp. 700-746, CRC Taylor & Francis, Boca Raton, U.S.A., 2006.
[270] R. Krishna, J.M. van Baten, In silico screening of metal-organic frameworks in separation applications, Phys. Chem. Chem. Phys. 13 (2011) 10593-10616.
[271] S. Li, J.L. Falconer, R.D. Noble, R. Krishna, Interpreting unary, binary and ternary mixture permeation across a SAPO-34 membrane with loading-dependent Maxwell-Stefan diffusivities, J. Phys. Chem. C 111 (2007) 5075-5082.

[272] S. Li, J.L. Falconer, R.D. Noble, R. Krishna, Modeling permeation of $CO_2/CH_4$, $CO_2/N_2$, and $N_2/CH_4$ mixtures across SAPO-34 membrane with the Maxwell-Stefan equations, Ind. Eng. Chem. Res. 46 (2007) 3904-3911.
[273] M. Pera-Titus, C. Fité, V. Sebastián, E. Lorente, J. Llorens, F. Cunill, Modeling Pervaporation of Ethanol/Water Mixtures within 'Real' Zeolite NaA Membranes, Ind. Eng. Chem. Res. 47 (2008) 3213-3224.
[274] M. Pera-Titus, J. Llorens, J. Tejero, F. Cunill, Description of the pervaporation dehydration performance of A-type zeolite membranes: A modeling approach based on the Maxwell–Stefan theory, Catal. Today 118 (2006) 73-84.
[275] L. Sandström, E. Sjöberg, J. Hedlund, Very high flux MFI membrane for $CO_2$ separation, J. Membr. Sci. 380 (2011) 232-240.
[276] J.M. van de Graaf, F. Kapteijn, J.A. Moulijn, Modeling permeation of binary mixtures through zeolite membranes, A.I.Ch.E.J. 45 (1999) 497-511.
[277] J. van den Bergh, S. Ban, T.J.H. Vlugt, F. Kapteijn, Modeling the Loading Dependency of Diffusion in Zeolites: The Relevant Site Model, J. Phys. Chem. C 113 (2009) 17840–17850.
[278] J. van den Bergh, A. Tihaya, F. Kapteijn, High temperature permeation and separation characteristics of an all-silica DDR zeolite membrane, Microporous Mesoporous Mater. 132 (2010) 137-147.
[279] J. van den Bergh, W. Zhu, J. Gascon, J.A. Moulijn, F. Kapteijn, Separation and Permeation Characteristics of a DD3R Zeolite Membrane, J. Membr. Sci. 316 (2008) 35-45.
[280] J. van den Bergh, W. Zhu, J.C. Groen, F. Kapteijn, J.A. Moulijn, K. Yajima, K. Nakayama, T. Tomita, S. Yoshida, Natural Gas Purification with a DDR Zeolite Membrane; Permeation Modelling with Maxwell-Stefan Equations, Stud. Surf. Sci. Catal. 170 (2007) 1021-1027.
[281] L.J.P. van den Broeke, W.J.W. Bakker, F. Kapteijn, J.A. Moulijn, Binary permeation through a silicalite-1 membrane, A.I.Ch.E.J. 45 (1999) 976-985.
[282] W. Zhu, P. Hrabanek, L. Gora, F. Kapteijn, J.C. Jansen, J.A. Moulijn, Modelling of n-hexane and 3-methylpentane permeation through a silicalite-1 membrane, Stud. Surf. Sci. Catal. 154 (2004) 1934-1943.
[283] W. Zhu, P. Hrabanek, L. Gora, F. Kapteijn, J.A. Moulijn, Role of Adsorption in the Permeation of $CH_4$ and $CO_2$ through a Silicalite-1Membrane, Ind. Eng. Chem. Res. 45 (2006) 767-776.
[284] S. Khajavi, J.C. Jansen, F. Kapteijn, Application of hydroxy sodalite films as novel water selective membranes, J. Membr. Sci. 326 (2009) 153-160.
[285] R. Krishna, J.M. van Baten, Investigating the potential of MgMOF-74 membranes for $CO_2$ capture, J. Membr. Sci. 377 (2011) 249-260.
[286] Z.R. Herm, R. Krishna, J.R. Long, $CO_2/CH_4$, $CH_4/H_2$ and $CO_2/CH_4/H_2$ separations at high pressures using Mg2(dobdc), Microporous Mesoporous Mater. XXX (2012) XXX-XXX. (http://dx.doi.org/10.1016/j.micmat.2011.09.004)
[287] Z.R. Herm, J.A. Swisher, B. Smit, R. Krishna, J.R. Long, Metal-Organic Frameworks as Adsorbents for Hydrogen Purification and Pre-Combustion Carbon Dioxide Capture, J. Am. Chem. Soc. 133 (2011) 5664-5667.
[288] T.M. McDonald, D.M. D'Alessandro, R. Krishna, J.R. Long, Enhanced carbon dioxide capture upon incorporation of *N*,*N*′- dimethylethylenediamine in the metal-organic framework CuBTTri, Chem. Sci. 2 (2011) 2022-2028.
[289] C. Baerlocher, L.B. McCusker, Database of Zeolite Structures, International Zeolite Association, http://www.iza-structure.org/databases/, 10 January 2002.
[290] D. Dubbeldam, K.S. Walton, D.E. Ellis, R.Q. Snurr, Exceptional Negative Thermal Expansion in Isoreticular Metal–Organic Frameworks, Angew. Chem. Int. Ed. 46 (2007) 4496-4499.
[291] S.S.Y. Chui, S.M.F. Lo, J.P.H. Charmant, A.G. Orpen, I.D. Williams, A chemically functionalizable nanoporous material $[Cu_3(TMA)_2(H2O)_3]_n$, Science 283 (1999) 1148-1150.
[292] Q. Yang, C. Zhong, Electrostatic-Field-Induced Enhancement of Gas Mixture Separation in Metal-Organic Frameworks: A Computational Study, ChemPhysChem 7 (2006) 1417-1421.

[293] P.S. Bárcia, F. Zapata, J.A.C. Silva, A.E. Rodrigues, B. Chen, Kinetic Separation of Hexane Isomers by Fixed-Bed Adsorption with a Microporous Metal-Organic Framework, J. Phys. Chem. B 111 (2008) 6101-6103.
[294] J.Y. Lee, D.H. Olson, L. Pan, T.J. Emge, J. Li, Microporous Metal–Organic Frameworks with High Gas Sorption and Separation Capacity, Adv. Funct. Mater. 17 (2007) 1255-1262.
[295] L. Alaerts, C.E.A. Kirschhock, M. Maes, M. van der Veen, V. Finsy, A. Depla, J.A. Martens, G.V. Baron, P.A. Jacobs, J.F.M. Denayer, D. De Vos, Selective Adsorption and Separation of Xylene Isomers and Ethylbenzene with the Microporous Vanadium(IV) Terephthalate MIL-47, Angew. Chem. Int. Ed. 46 (2007) 4293-4297.
[296] V. Finsy, H. Verelst, L. Alaerts, D. De Vos, P.A. Jacobs, G.V. Baron, J.F.M. Denayer, Pore-Filling-Dependent Selectivity Effects in the Vapor-Phase Separation of Xylene Isomers on the Metal-Organic Framework MIL-47, J. Am. Chem. Soc. 130 (2008) 7110-7118.
[297] K. Barthelet, J. Marrot, D. Riou, G. Férey, A Breathing Hybrid Organic - Inorganic Solid with Very Large Pores and High Magnetic Characteristics, Angew. Chem. Int. Ed. 41 (2007) 281-284.
[298] D.S. Coombes, F. Corà, C. Mellot-Draznieks, R.G. Bell, Sorption-Induced Breathing in the Flexible Metal Organic Framework CrMIL-53: Force-Field Simulations and Electronic Structure Analysis, J. Phys. Chem. C 113 (2009) 544-552.
[299] R. Banerjee, A. Phan, B. Wang, C. Knobler, H. Furukawa, M. O'Keeffe, O.M. Yaghi, High-Throughput Synthesis of Zeolitic Imidazolate Frameworks and Application to $CO_2$ Capture, Science 319 (2008) 939-943.
[300] D. Britt, H. Furukawa, B. Wang, T.G. Glover, O.M. Yaghi, Highly efficient separation of carbon dioxide by a metal-organic framework replete with open metal sites, Proc. Natl. Acad. Sci. U.S.A. 106 (2009) 20637-20640.
[301] N.L. Rosi, J. Kim, M. Eddaoudi, B. Chen, M. O'Keeffe, O.M. Yaghi, Rod Packings and Metal-Organic Frameworks Constructed from Rod-Shaped Secondary Building Units, J. Am. Chem. Soc. 127 (2005) 1504-1518.
[302] P.D.C. Dietzel, B. Panella, M. Hirscher, R. Blom, H. Fjellvåg, Hydrogen adsorption in a nickel based coordination polymer with open metal sites in the cylindrical cavities of the desolvated framework, Chem. Commun. (2006) 959-961.
[303] P.D.C. Dietzel, V. Besikiotis, R. Blom, Application of metal–organic frameworks with coordinatively unsaturated metal sites in storage and separation of methane and carbon dioxide, J. Mater. Chem. 19 (2009) 7362-7370.
[304] S.R. Caskey, A.G. Wong-Foy, A.J. Matzger, Dramatic Tuning of Carbon Dioxide Uptake via Metal Substitution in a Coordination Polymer with Cylindrical Pores, J. Am. Chem. Soc. 130 (2008) 10870-10871.
[305] A.Ö. Yazaydın, R.Q. Snurr, T.H. Park, K. Koh, J. Liu, M.D. LeVan, A.I. Benin, P. Jakubczak, M. Lanuza, D.B. Galloway, J.J. Low, R.R. Willis, Screening of Metal-Organic Frameworks for Carbon Dioxide Capture from Flue Gas using a Combined Experimental and Modeling Approach, J. Am. Chem. Soc. 131 (2009) 18198-18199.
[306] E.D. Bloch, L. Murray, W.L. Queen, S. Chavan, S.N. Maximoff, J.P. Bigi, R. Krishna, V.K. Peterson, F. Grandjean, G.J. Long, B. Smit, S. Bordiga, C.M. Brown, J.R. Long, Selective Binding of $O_2$ over $N_2$ in a Redox-Active Metal-Organic Framework with Open Iron(II) Coordination Sites, J. Am. Chem. Soc. 133 (2011) 14814-14822.
[307] H.K. Chae, D.Y. Siberio-Pérez, J. Kim, Y.B. Go, M. Eddaoudi, A.J. Matzger, M. O'Keeffe, O.M. Yaghi, A route to high surface area, porosity and inclusion of large molecules in crystals, Nature 427 (2004) 523-527.
[308] H.J. Choi, M. Dincă, J.R. Long, Broadly Hysteretic $H_2$ Adsorption in the Microporous Metal-Organic Framework Co(1,4-benzenedipyrazolate), J. Am. Chem. Soc. 130 (2008) 7848-7850.
[309] F. Salles, G. Maurin, C. Serre, P.L. Llewellyn, C. Knöfel, H.J. Choi, Y. Filinchuk, L. Oliviero, A. Vimont, J.R. Long, G. Férey, Multistep $N_2$ Breathing in the Metal-Organic Framework Co(1,4-benzenedipyrazolate), J. Am. Chem. Soc. 132 (2010) 13782-13788.

[310] K. Sumida, M.R. Hill, S. Horike, A. Dailly, J.R. Long, Synthesis and Hydrogen Storage Properties of $Be_{12}(OH)_{12}$(1,3,5-benzenetribenzoate)$_4$, J. Am. Chem. Soc. 131 (2009) 15120-15121.

[311] A. Demessence, D.M. D'Alessandro, M.W. Foo, J.R. Long, Strong $CO_2$ Binding in a Water-Stable, Triazolate-Bridged Metal-Organic Framework Functionalized with Ethylenediamine, J. Am. Chem. Soc. 131 (2009) 8784-8786.

[312] M. Dogru, A. Sonnauer, A. Gavryushin, P. Knochel, T. Bein, A Covalent Organic Framework with 4 nm open pores, Chem. Commun. 47 (2011) 1707-1709.

[313] M.D. Foster, I. Rivin, M.M.J. Treacy, O.D. Friedrichs, A geometric solution to the largest-free-sphere problem in zeolite frameworks, Microporous Mesoporous Mater. 90 (2006) 32-38.

[314] T. Düren, F. Millange, G. Férey, K.S. Walton, R.Q. Snurr, Calculating Geometric Surface Areas as a Characterization Tool for Metal-Organic Frameworkss, J. Phys. Chem. C 111 (2007) 15350-15356.

[315] W. Smith, T.R. Forester, I.T. Todorov, The DL_POLY Molecular Simulation Package, Warrington, England, http://www.cse.clrc.ac.uk/msi/software/DL_POLY/index.shtml, March 2006.

[316] A. Corma, F. Rey, J. Rius, M.J. Sabater, S. Valencia, Supramolecular self-assembled molecules as organic directing agent for synthesis of zeolites, Nature 431 (2004) 287-290.

Table 1. Salient information on zeolite structures.

| **Zeolite** | **Channel or window size/ Å** |
|---|---|
| AFI | 12-ring 1D channels of 7.3 Å size |
| AFX | 490 $Å^3$ size cages connected to pockets of 98 $Å^3$ in size. Cages are separated by 3.4 Å × 3.9 Å size windows. |
| AWW | 1D connectivity. Cages separated by 8-ring windows of 3.9 Å size. There are 2 cages per unit cell. The volume of each cage is 221 $Å^3$. |
| BEA | Intersecting channels of two sizes: 12-ring of 7.1 Å - 7.3 Å and 10-ring of 5.6 – 5.6 Å |
| BOG | Intersecting channels: 12-ring 7.0 Å -7.0 Å and 10-ring of 5.5 Å - 5.8 Å |
| CHA | 316.4 $Å^3$ size cages separated by 3.77 Å × 4.23 Å size windows. |
| DDR | 277.8 $Å^3$ size cages separated by 3.65 Å × 4.37 Å size windows |
| ERI | 408.7 $Å^3$ size cages separated by 3.8 Å × 4.9 Å size windows |
| FAU | 785.7 $Å^3$ size cages separated by 7.4 Å size windows. The sodalite cages are blocked in simulations and are not accessible to guest molecules; these are excluded for pore volume determination. Cage size is calculated on the basis of the equivalent sphere volume. |
| FER | 10-ring 1D main channels of 4.2 Å -5.4 Å size, connected with 8-ring side pockets of 3.5 Å -4.8 Å size |
| GME | The main 12-ring channels are interconnected at right angles by a two-dimensional system of eight-ring channels, and thus form a three-dimensional channel system |

Table 2. Salient information on zeolite structures (continued)

| **Zeolite** | **Channel or window size/ Å** |
|---|---|
| ISV | Intersecting channels of two sizes: 12-ring of 6.1 Å -6.5 Å and 12-ring of 5.9 Å - 6.6 Å |
| ITQ-12 | 160 $Å^3$ sized cages separated by 3.71 Å × 4.17 Å sized windows. |
| ITQ-29 | 678 $Å^3$ sized cages separated by 4 Å × 4.22 Å sized windows. The sodalite cages are blocked in simulations and are not accessible to guest molecules. The structural information is from Corma [316]. |
| LTA-Si | 743.05 $Å^3$ size cages separated by 4.11 Å × 4.47 Å size windows. The sodalite cages are blocked in simulations and are not accessible to guest molecules. |
| LTL | 12-ring 1D channels of 7.1 Å size |
| MOR | 12-ring 1D main channels of 6.5 Å -7 Å size, connected with 8-ring side pockets of 2.6 Å -5.7 Å size |
| MFI | 10-ring intersecting channels of 5.1 Å – 5.5 Å and 5.3 Å – 5.6 Å size |
| MTW | 12-ring 1D channels of 5.6 Å -6 Å size |
| TON | 10-ring 1D channels of 4.6 Å -5.7 Å size |
| TSC | Two types of cages: LTA-type of 743.05 $Å^3$ and TSC-supercage of 2552.6 $Å^3$size. Two types of 8-ring windows: 4.02 Å × 4.17 Å and 3.1 Å × 5.41 Å. The sodalite cages are blocked in simulations and are not accessible to guest molecules; these are excluded for pore volume determination. |

Table 3. Unit cell dimensions, unit cell volumes, pore volumes of various all-silica zeolites. Also indicated are the framework density, $\rho$, (expressed as kg per $m^3$ framework), the factor to convert from molecules per unit cell to kmol/$m^3$ of accessible pore volume.

| Structure | *a* / Å | *b* / Å | *c* / Å | Unit cell volume/ $Å^3$ | Pore volume per unit cell/ $Å^3$ | Fractional pore volume | Pore volume/ $cm^3/g$ | Framework density/ $kg/m^3$ | Conversion factor |
|---|---|---|---|---|---|---|---|---|---|
| AFI | 23.77 | 13.73 | 8.48 | 2768.52 | 759.42 | 0.274 | 0.159 | 1729.88 | 2.1866 |
| AFX | 23.836 | 13.762 | 19.949 | 6543.89 | 2352.45 | 0.359 | 0.246 | 1463.71 | 0.7059 |
| AWW | 13.634 | 13.634 | 7.627 | 1417.75 | 441.31 | 0.311 | 0.184 | 1689.00 | 3.7628 |
| BEA | 12.66 | 12.66 | 26.41 | 4232.91 | 1728.05 | 0.408 | 0.271 | 1508.56 | 0.9609 |
| BOG | 20.24 | 23.80 | 12.80 | 6163.21 | 2305.42 | 0.374 | 0.241 | 1995.52 | 0.7203 |
| CHA | 15.08 | 23.91 | 13.80 | 4974.57 | 1898.40 | 0.382 | 0.264 | 1444.10 | 0.8747 |
| DDR | 24.01 | 13.86 | 40.89 | 13605.72 | 3333.53 | 0.245 | 0.139 | 1759.99 | 0.4981 |
| ERI | 22.95 | 13.25 | 14.81 | 4504.80 | 1635.01 | 0.363 | 0.228 | 1594.69 | 1.0156 |
| FAU | 24.28 | 24.28 | 24.28 | 14313.51 | 6285.60 | 0.439 | 0.328 | 1338.37 | 0.2642 |
| FER | 19.16 | 14.13 | 7.49 | 2026.65 | 573.24 | 0.283 | 0.160 | 1772.33 | 2.8968 |
| GME | 23.83 | 13.76 | 10.06 | 3298.48 | 1268.59 | 0.385 | 0.265 | 1451.94 | 1.3090 |

Table 4. Unit cell dimensions, unit cell volumes, pore volumes of various all-silica zeolites. Also indicated are the framework density, $\rho$, (expressed as kg per $m^3$ framework), the factor to convert from molecules per unit cell to kmol/$m^3$ of accessible pore volume.

| Structure | *a* / Å | *b* / Å | *c* / Å | Unit cell volume/ $Å^3$ | Pore volume per unit cell/ $Å^3$ | Fractional pore volume | Pore volume/ $cm^3/g$ | Framework density/ $kg/m^3$ | Conversion factor |
|---|---|---|---|---|---|---|---|---|---|
| ISV | 12.85 | 12.85 | 25.214 | 4165.34 | 1773.87 | 0.426 | 0.278 | 1533.03 | 0.9361 |
| ITQ-12 | 10.4364 | 15.0183 | 8.8553 | 1335.9 | 320 | 0.24 | 0.134 | 1442.03 | 5.18 |
| ITQ-29 | 11.87 | 11.87 | 11.87 | 1671.18 | 677.57 | 0.405 | 0.283 | 1442.03 | 2.4508 |
| LTA-Si | 24.61 | 24.61 | 24.61 | 14905.10 | 5944.38 | 0.399 | 0.310 | 1285.25 | 0.2794 |
| LTL | 31.98 | 18.47 | 7.48 | 4415.45 | 1221.27 | 0.277 | 0.170 | 1626.97 | 1.3597 |
| MFI | 20.02 | 19.90 | 13.38 | 5332.03 | 1584.94 | 0.297 | 0.165 | 1796.39 | 1.0477 |
| MOR | 18.09 | 20.52 | 7.52 | 2793.03 | 795.41 | 0.285 | 0.166 | 1714.69 | 2.0877 |
| MTW | 24.86 | 5.01 | 24.33 | 2887.49 | 620.55 | 0.215 | 0.111 | 1935.03 | 2.6759 |
| SOD-Si | 8.89 | 8.89 | 8.89 | 702.59 | 169.60 | 0.241 | 0.142 | 1704.10 | 9.7908 |
| TON | 13.86 | 17.42 | 5.04 | 1216.29 | 231.39 | 0.190 | 0.097 | 1968.76 | 7.1763 |
| TSC | 30.74 | 30.74 | 30.74 | 29053.36 | 13182.60 | 0.454 | 0.344 | 1318.73 | 0.1260 |

Table 5. Data on zeolite structures with cations (data on all-silica structures also included for comparison purposes). The number of atoms per unit cell of these structures are specified.

| **Zeolite** | **Si** | **Al** | **Si/Al** | **Na+** | **Ca++** |
|---|---|---|---|---|---|
| LTA-5A | 96 | 96 | 1 | 32 | 32 |
| LTA-4A | 96 | 96 | 1 | 96 | 0 |
| NaX | 106 | 86 | 1.23 | 86 | 0 |
| NaY | 144 | 48 | 3 | 48 | 0 |

Table 6. Unit cell dimensions, unit cell volumes, pore volumes of cation-exchanged zeolites. Also indicated are the framework density, $\rho$, (expressed as kg per $m^3$ of (framework +cations)), the factor to convert from molecules per unit cell to kmol/$m^3$ of accessible pore volume).

| Structure | *a* / Å | *b* / Å | *c* / Å | Unit cell volume/ $Å^3$ | Pore volume per unit cell/ $Å^3$ | Fractional pore volume | Pore volume/ $cm^3/g$ | Framework density/ $kg/m^3$ | Conversion factor |
|---|---|---|---|---|---|---|---|---|---|
| NaY (48 Na+) | 25.03 | 25.03 | 25.03 | 15677.56 | 6396.63 | 0.41 | 0.303 | 1333.2 | 0.2596 |
| NaY (54 Na+) | 25.03 | 25.03 | 25.03 | 15677.56 | 6396.63 | 0.41 | 0.303 | 1347.1 | 0.2596 |
| NaX | 25.03 | 25.03 | 25.03 | 15677.56 | 6248.00 | 0.40 | 0.280 | 1421.28 | 0.2658 |
| LTA-5A | 24.56 | 24.56 | 24.56 | 14805.39 | 5620.41 | 0.38 | 0.25 | 1508.38 | 0.2955 |
| LTA-4A | 24.56 | 24.56 | 24.56 | 14805.39 | 5552.02 | 0.38 | 0.25 | 1529.55 | 0.2991 |

Table 7. Salient structural information on MOFs and ZIFs.

| **MOF** | **Channel dimensions** |
|---|---|
| CuBTC | The CuBTC structure consists of two types of "cages" and two types of "windows" separating these cages. Large cages are inter-connected by 9 Å windows of square cross-section. The large cages are also connected to tetrahedral-shaped pockets of ca. 6 Å size through triangular-shaped windows of ca. 4.6 Å size |
| IRMOF-1 | Two alternating, inter-connected, cavities of 10.9 Å and 14.3 Å with window size of 8 Å. |
| MOF-177 | Tetrahedral $[Zn_4O]^{6+}$ units are linked by large, triangular tricarboxylate ligands. Six diamond-shaped channels (upper) with diameter of 10.8 Å surround a pore containing eclipsed $BTB^{3-}$ moieties. |
| MIL-47 | One-dimensional diamond-shaped channels with free internal diameter of ca 8.5 Å |
| MIL-53 (Cr)-lp | One-dimensional lozenge-shaped channels with free internal diameter of ca 8.5 Å |
| Zn(bdc)dabco | There exist two types of intersecting channels of about 7.5 Å × 7.5 Å along the *x*-axis and channels of 3.8 Å × 4.7 Å along *y* and *z* axes. |
| ZIF-8 | SOD topology consisting of cages separated by narrow windows of about 0.34 nm size. The volume of each cage is 1168 $Å^3$. |
| MgMOF-74 | One-dimensional hexagonal-shaped channels with free internal diameter of ca. 11 Å |
| ZnMOF-74 | One-dimensional hexagonal-shaped channels with free internal diameter of ca. 11 Å |
| NiMOF-74 | One-dimensional hexagonal-shaped channels with free internal diameter of ca. 11 Å |
| CoMOF-74 | One-dimensional hexagonal-shaped channels with free internal diameter of ca. 11 Å |

Table 8. Unit cell dimensions, unit cell volumes, pore volumes of various MOFs and ZIFs. Also indicated are the framework density, $\rho$, (expressed as kg per $m^3$ of framework), the factor to convert from molecules per unit cell to kmol/$m^3$ of accessible pore volume.

| Structure | *a* / Å | *b* / Å | *c* / Å | Unit cell volume/ $Å^3$ | Pore volume per unit cell/$Å^3$ | Fractional pore volume | Pore volume/ $cm^3/g$ | Framework density/ $kg/m^3$ | Conversion factor |
|---|---|---|---|---|---|---|---|---|---|
| CuBTC | 26.34 | 26.34 | 26.34 | 18280.82 | 13871.82 | 0.759 | 0.863 | 878.83 | 0.1218 |
| IRMOF1 | 25.83 | 25.83 | 25.83 | 17237.49 | 13996.27 | 0.812 | 1.369 | 593.21 | 0.1186 |
| MOF-177 | 37.072 | 37.072 | 30.033 | 35745.50 | 3001090 | 0.840 | 1.968 | 426.60 | 0.0553 |
| MIL-47 | 6.81 | 16.12 | 13.92 | 1527.32 | 929.34 | 0.608 | 0.606 | 1004.48 | 1.7868 |
| MIL-53 (Cr)-lp | 16.73 | 13.04 | 6.81 | 1486.14 | 801.60 | 0.539 | 0.518 | 1041.53 | 2.0716 |
| Zn(bdc)dabco | 10.93 | 10.93 | 9.61 | 1147.61 | 759.39 | 0.662 | 0.801 | 826.20 | 2.1867 |
| ZIF-8 | 16.99 | 16.99 | 16.99 | 4905.20 | 2336.97 | 0.476 | 0.515 | 924.25 | 0.711 |
| ZnMOF-74 | 25.93 | 25.93 | 6.84 | 3981.47 | 2867.85 | 0.709 | 0.582 | 1219.30 | 0.5881 |
| MgMOF-74 | 25.86 | 25.86 | 6.91 | 4005.02 | 2835.86 | 0.708 | 0.782 | 905.37 | 0.5856 |
| NiMOF-74 | 25.79 | 25.79 | 6.77 | 3898.34 | 2707.62 | 0.695 | 0.582 | 1193.81 | 0.6133 |
| CoMOF-74 | 25.89 | 25.89 | 6.80 | 3949.17 | 2793.08 | 0.707 | 0.599 | 1180.26 | 0.5945 |
| FeMOF-74 | 26.16 | 26.16 | 6.84 | 4055.94 | 2859.71 | 0.705 | 0.626 | 1126.43 | 0.5807 |
| Na-rhoZMOF | 31.06 | 31.06 | 31.062 | 29970.10 | 15165.37 | 0.506 | 0.427 | 1185.79 | 0.1095 |
| BeBTB | 24.3013 | 24.3013 | 54.57 | 32226.49 | 26013.82 | 0.807 | 1.908 | 423.09 | 0.0638 |
| Co(BDP) | 13.2529 | 13.253 | 13.995 | 2458.09 | 1643.88 | 0.669 | 0.927 | 721.55 | 1.0102 |
| CuBTT | 18.595 | 18.595 | 18.595 | 6429.67 | 3652.12 | 0.568 | 0.709 | 801.08 | 0.4547 |
| BTP-COF | 43.65 | 75.604 | 3.52 | 11616.40 | 8738.71 | 0.752 | 1.791 | 420.08 | 0.1900 |

Table 9. Molecular simulations of pore volumes and surface areas for the zeolites investigated.

| **Structure** | **Pore volume** / $cm^3$ $g^{-1}$ | **Surface area** / $m^2$ $g^{-1}$ | **Delaunay diameter**/ Å |
|---|---|---|---|
| MFI | 0.165 | 487.2 | 5.16 |
| ISV | 0.278 | 911.4 | 5.96 |
| BEA | 0.271 | 922.7 | 5.87 |
| BOG | 0.241 | 758.4 | 5.02 |
| GME | 0.265 | 717.6 | 7.09 |
| LTL | 0.170 | 520.6 | 7.26 |
| MOR | 0.166 | 416.7 | 7.47 |
| FER | 0.160 | 402.5 | 6.44 |
| FAU-Si | 0.328 | 1086 | 4.65 |
| ITQ-12 | 0134 | 230 | 4.88 |
| ITQ-29 | 0.283 | 773.3 | 5.69 |
| LTA-Si | 0.310 | 896 | 7.37 |
| TSC | 0.344 | 829 | |
| CHA | 0.264 | 757.5 | 3.98 |
| ERI | 0.228 | 635.3 | 4.10 |
| DDR | 0.139 | 350 | 4.02 |
| AFX | 0.246 | 674.5 | 3.77 |

Table 10. Molecular simulations of pore volumes and surface areas for the MOFs, ZIFs, and BTP-COF

| **Structure** | **Pore volume** / $cm^3$ $g^{-1}$ | **Surface area** / $m^2$ $g^{-1}$ | **Delaunay diameter**/ Å |
|---|---|---|---|
| IRMOF1 | 1.369 | 3522.2 | 7.38 |
| CuBTC | 0.848 | 2097.0 | 6.23 |
| MIL47 | 0.606 | 1472.8 | 8.03 |
| MIL53(Cr)-lp | 0.518 | 1280.5 | 7.40 |
| CoFA | 0.139 | | 3.41 |
| MnFA | 0.190 | | 3.66 |
| Zn(tbip) | 0.118 | | 3.96 |
| Zn(BDC)dabco | 0.801 | 2022.5 | 8.32 |
| Co(BDC)dabco | 0.796 | | 8.35 |
| PCN-19 | 0.432 | | 7.16 |
| ZIF-68 | 0.439 | 1066.0 | 7.52 |
| ZIF-7 | 0.223 | | 3.26 |
| ZIF-8 | 0.515 | 1164.7 | 3.26 |
| PCN-6prime | 3.228 | | 14.62 |
| MOF-177 | 1.968 | 4781.0 | 10.1 |
| ZnMOF-74 | 0.582 | 1176.0 | 9.49 |
| MgMOF-74 | 0.782 | 1640.0 | 10.66 |
| NiMOF-74 | 0.582 | 1239.0 | 9.80 |
| CoMOF-74 | 0.599 | 1274.0 | 9.52 |
| FeMOF-74 | 0.626 | 1277.3 | 11.1 |
| Co(BDP) | 0.927 | 2148.8 | 10 |
| BeBTB | 1.908 | 4706 | |
| CuBTT (blocked) | 0.709 | 1564.6 | 9.99 |
| BTP-COF | 1.791 | | 34.26 |

# All-silica Zeolites (in alphabetical order)

# AFI landscapes

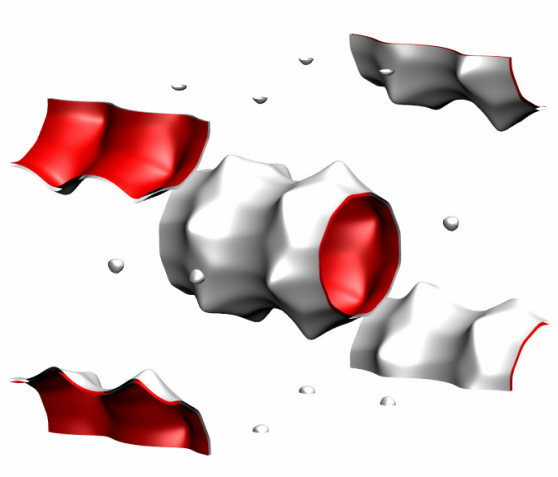

12-ring channel of AFI

Snapshots showing location of $CH_4$ and $CO_2$

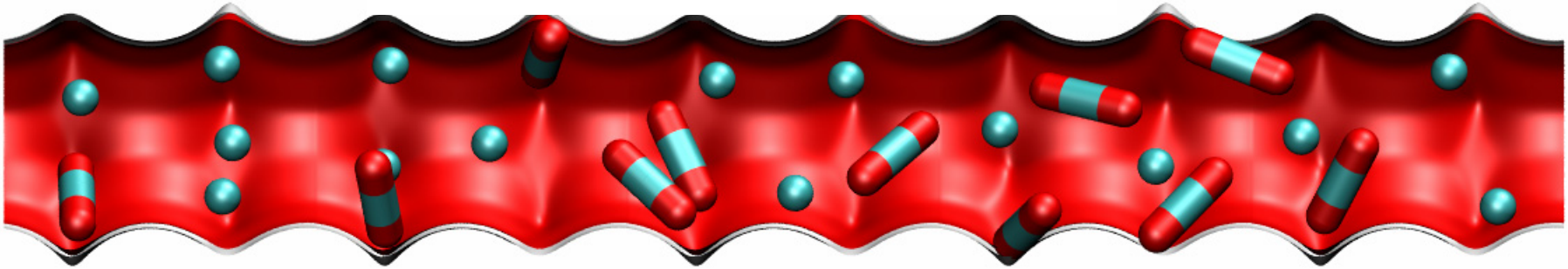

# AFI pore dimensions

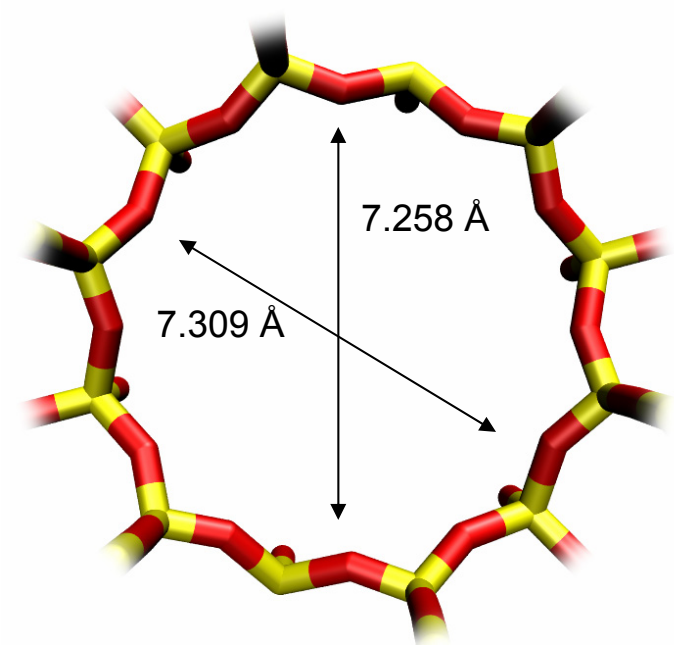


| | AFI |
|---|---|
| *a* /Å | 23.774 |
| *b* /Å | 13.726 |
| *c* /Å | 8.484 |
| Cell volume / Å$^3$ | 2768.515 |
| conversion factor for [molec/uc] to [mol per kg Framework] | 0.3467 |
| conversion factor for [molec/uc] to [kmol/m$^3$] | 2.1866 |
| $\rho$ [kg/m3] | 1729.876 |
| MW unit cell [g/mol(framework)] | 2884.07 |
| $\phi$, fractional pore volume | 0.274 |
| open space / Å$^3$/uc | 759.4 |
| Pore volume / cm$^3$/g | 0.159 |
| Surface area /m$^2$/g | 466.0 |
| DeLaunay diameter /Å | 7.26 |

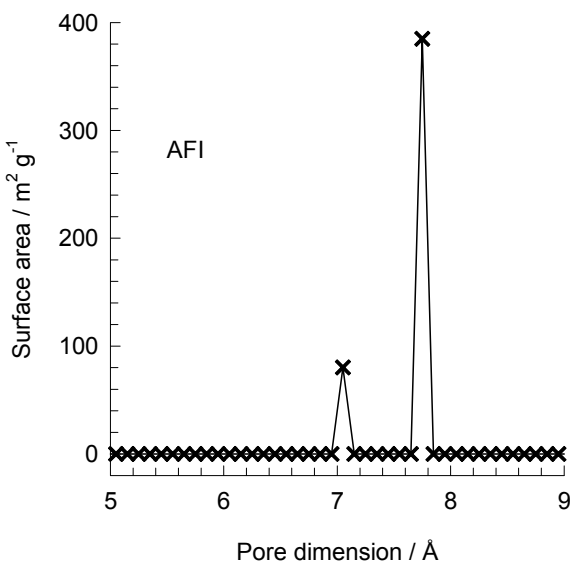


This plot of surface area versus pore dimension is determined using a combination of the DeLaunay triangulation method for pore dimension determination, and the procedure of Düren for determination of the surface area. The computational details will be described in detail in a forthcoming publication.

# AFX pore landscape

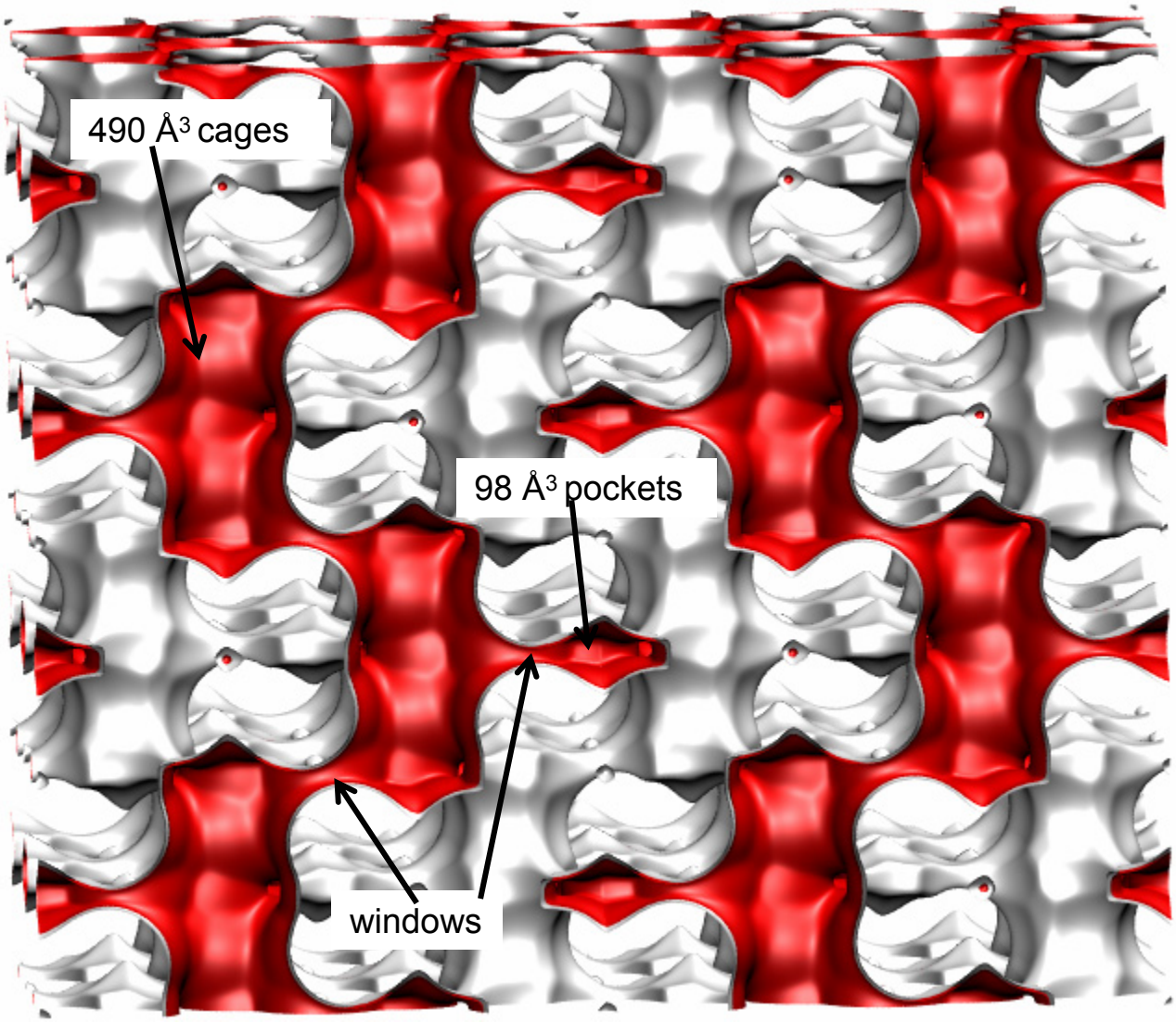

# AFX window sizes and pore dimensions

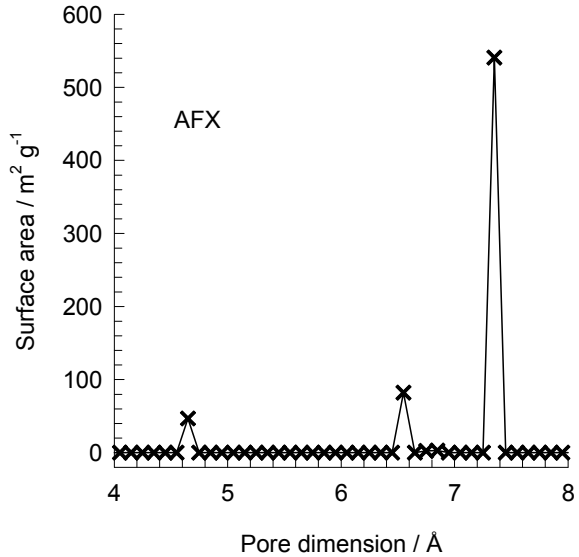


| | AFX |
|---|---|
| *a* /Å | 23.836 |
| *b* /Å | 13.762 |
| *c* /Å | 19.949 |
| Cell volume / Å$^3$ | 6543.891 |
| conversion factor for [molec/uc] to [mol per kg Framework] | 0.1734 |
| conversion factor for [molec/uc] to [kmol/m$^3$] | 0.7059 |
| $\rho$ [kg/m3] | 1463.713 |
| MW unit cell [g/mol(framework)] | 5768.141 |
| $\phi$, fractional pore volume | 0.359 |
| open space / Å$^3$/uc | 2352.5 |
| Pore volume / cm$^3$/g | 0.246 |
| Surface area /m$^2$/g | 674.0 |
| DeLaunay diameter /Å | 3.44 |

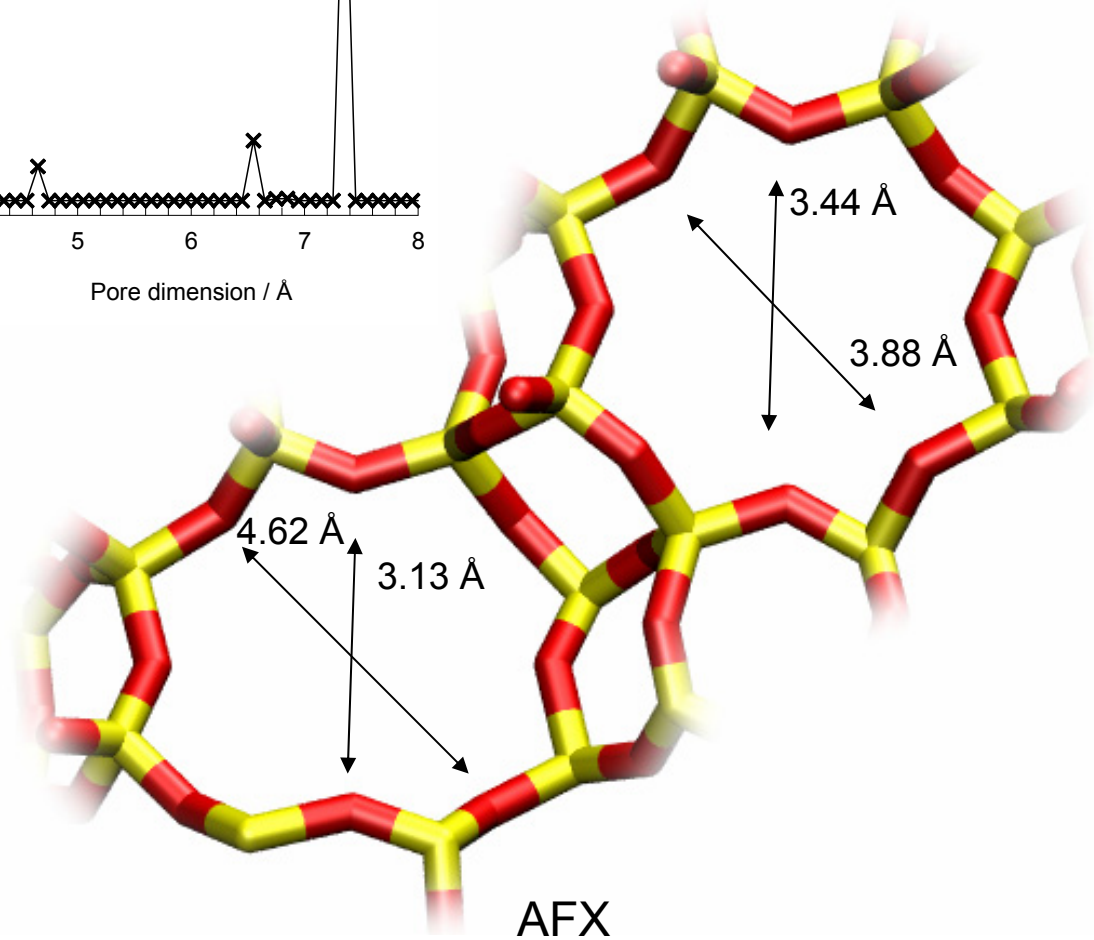


The window dimension calculated using the van der Waals diameter of framework atoms = 2.7 Å are indicated above by the arrows.

# AWW landscapes

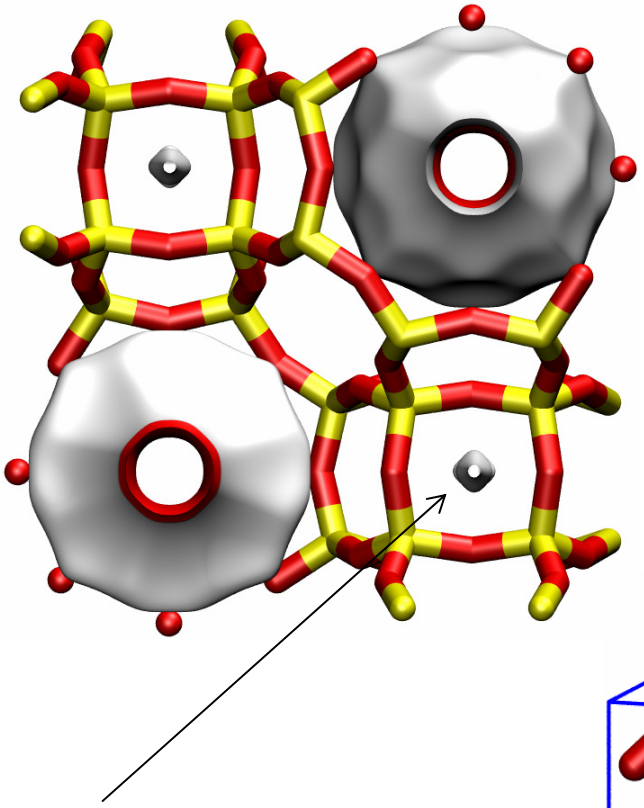

These inaccessible pockets are blocked in the simulations

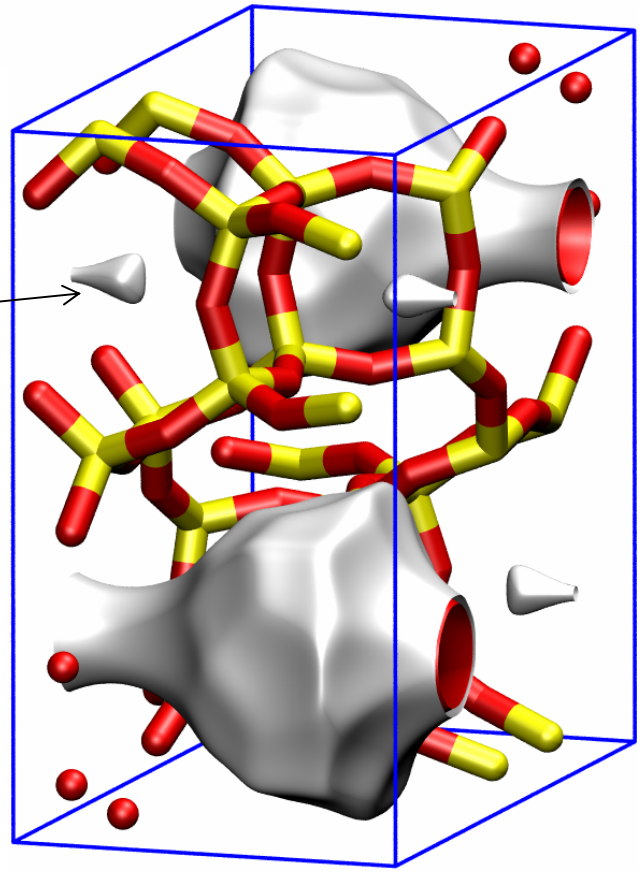

# AWW pore dimensions

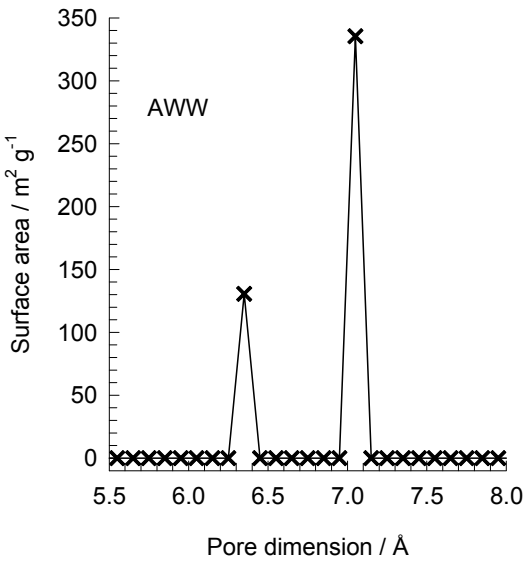


This plot of surface area versus pore dimension is determined using a combination of the DeLaunay triangulation method for pore dimension determination, and the procedure of Düren for determination of the surface area. The computational details will be described in detail in a forthcoming publication.

| | AWW |
|---|---|
| *a* /Å | 13.634 |
| *b* /Å | 13.634 |
| *c* /Å | 7.627 |
| Cell volume / Å$^3$ | 1417.752 |
| conversion factor for [molec/uc] to [mol per kg Framework] | 0.6935 |
| conversion factor for [molec/uc] to [kmol/m$^3$] | 3.7628 |
| $\rho$ [kg/m3] | 1689.007 |
| MW unit cell [g/mol (framework)] | 1442.035 |
| $\phi$, fractional pore volume | 0.311 |
| open space / Å$^3$/uc | 441.3 |
| Pore volume / cm$^3$/g | 0.184 |
| Surface area /m$^2$/g | 468.2 |
| DeLaunay diameter /Å | 4.11 |

# AWW snapshots

Mixture of $CH_4$ and $CO_2$

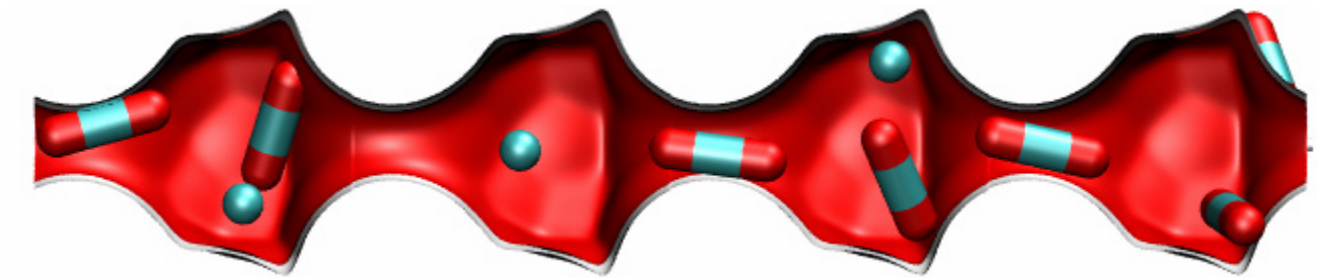

Mixture of $N_2$ and $CO_2$

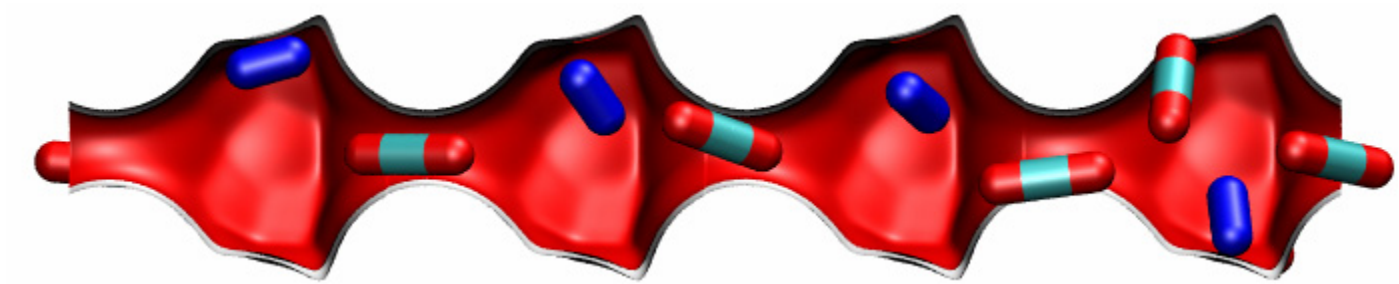

Mixture of $H_2$ and $CO_2$

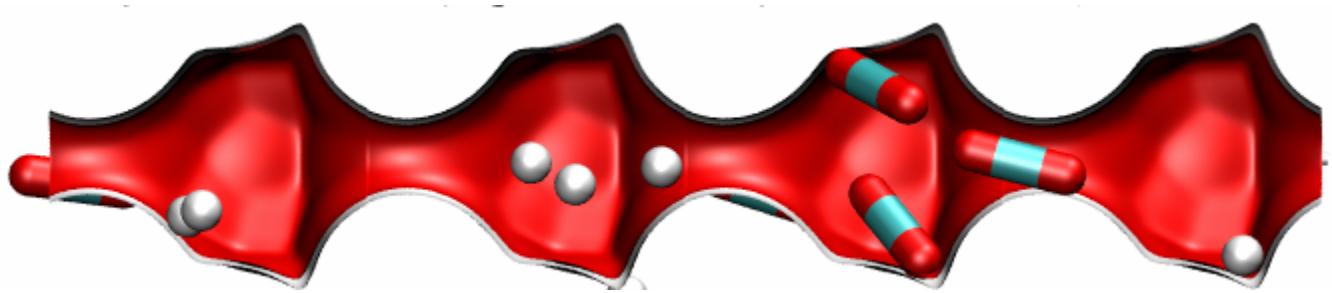

# BEA pore landscape

| | BEA |
|---|---|
| *a* /Å | 12.661 |
| *b* /Å | 12.661 |
| *c* /Å | 26.406 |
| Cell volume / Å$^3$ | 4232.906 |
| conversion factor for [molec/uc] to [mol per kg Framework] | 0.2600 |
| conversion factor for [molec/uc] to [kmol/m$^3$] | 0.9609 |
| $\rho$ [kg/m3] | 1508.558 |
| MW unit cell [g/mol(framework)] | 3845.427 |
| $\phi$, fractional pore volume | 0.408 |
| open space / Å$^3$/uc | 1728.1 |
| Pore volume / cm$^3$/g | 0.271 |
| Surface area /m$^2$/g | 923.0 |
| DeLaunay diameter /Å | 5.87 |

# BEA pore dimensions

This plot of surface area versus pore dimension is determined using a combination of the DeLaunay triangulation method for pore dimension determination, and the procedure of Düren for determination of the surface area. The computational details will be described in detail in a forthcoming publication.

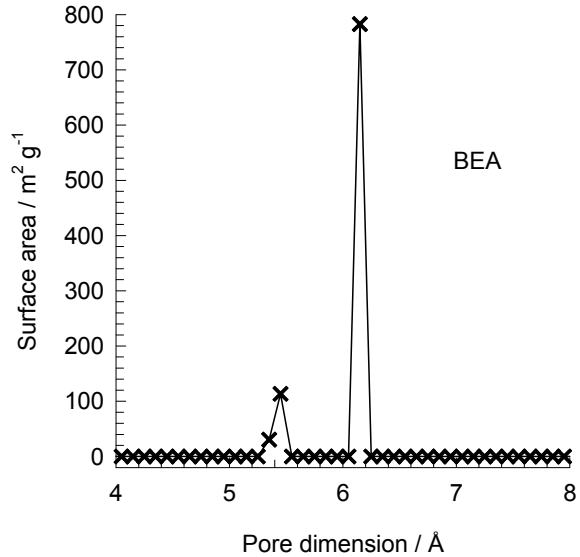


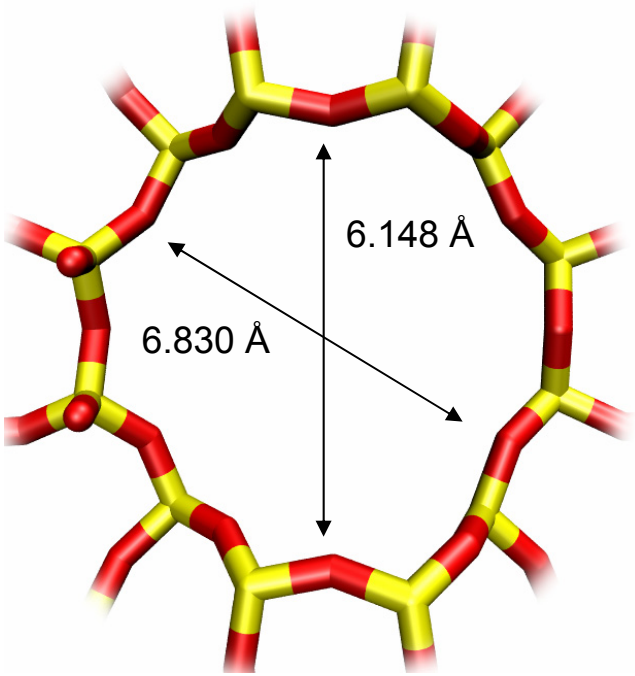


BEA [1 0 0]

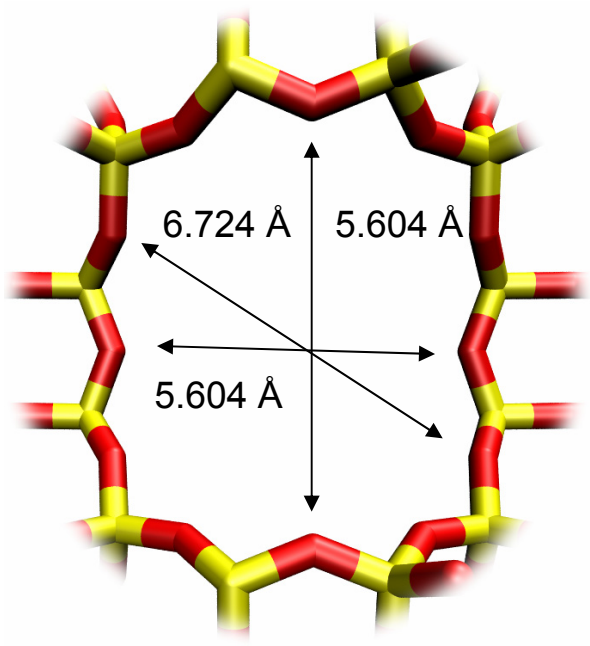


BEA [0 0 1]

# BOG pore landscape

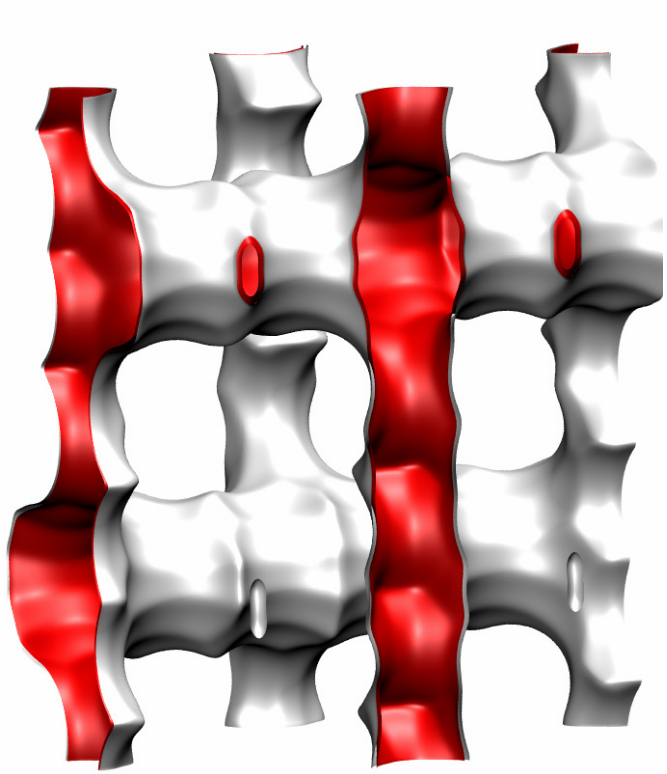

| | BOG |
|---|---|
| *a* /Å | 20.236 |
| *b* /Å | 23.798 |
| *c* /Å | 12.798 |
| Cell volume / Å$^3$ | 6163.214 |
| conversion factor for [molec/uc] to [mol per kg Framework] | 0.1734 |
| conversion factor for [molec/uc] to [kmol/m$^3$] | 0.7203 |
| $\rho$ [kg/m3] | 1995.523 |
| MW unit cell [g/mol(framework)] | 5768.141 |
| $\phi$, fractional pore volume | 0.374 |
| open space / Å$^3$/uc | 2305.4 |
| Pore volume / cm$^3$/g | 0.241 |
| Surface area /m$^2$/g | 758.0 |
| DeLaunay diameter /Å | 5.02 |

# BOG pore dimensions

This plot of surface area versus pore dimension is determined using a combination of the DeLaunay triangulation method for pore dimension determination, and the procedure of Düren for determination of the surface area. The computational details will be described in detail in a forthcoming publication.

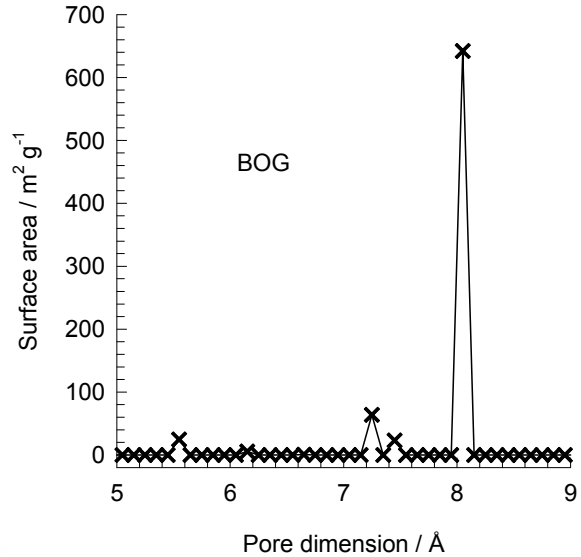


BOG has an intersecting channel system:
12-ring channels intersecting with 10-ring channels

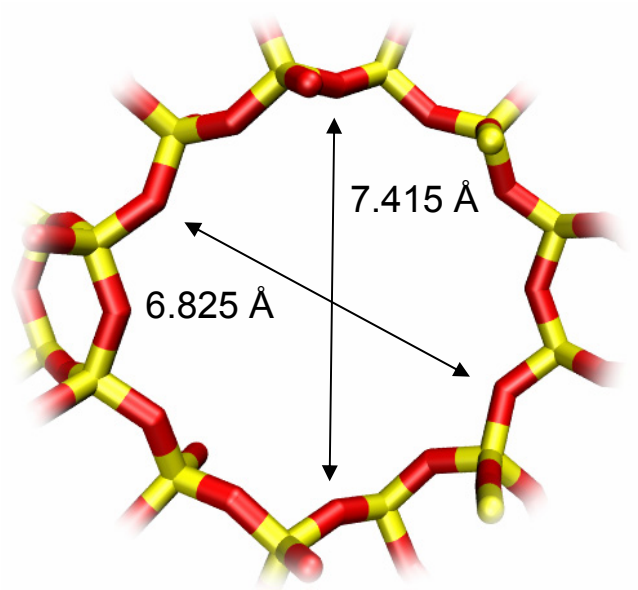


BOG [1 0 0]

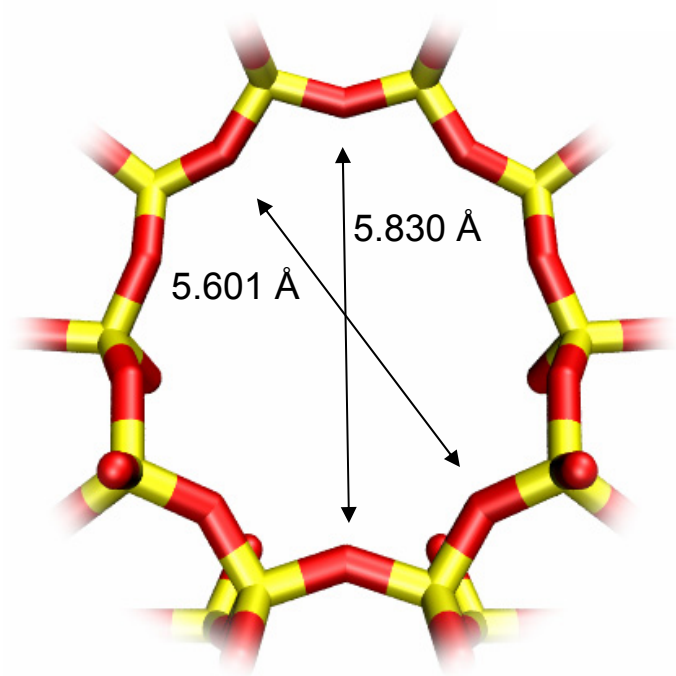


BOG [0 1 0]

# CHA landscape

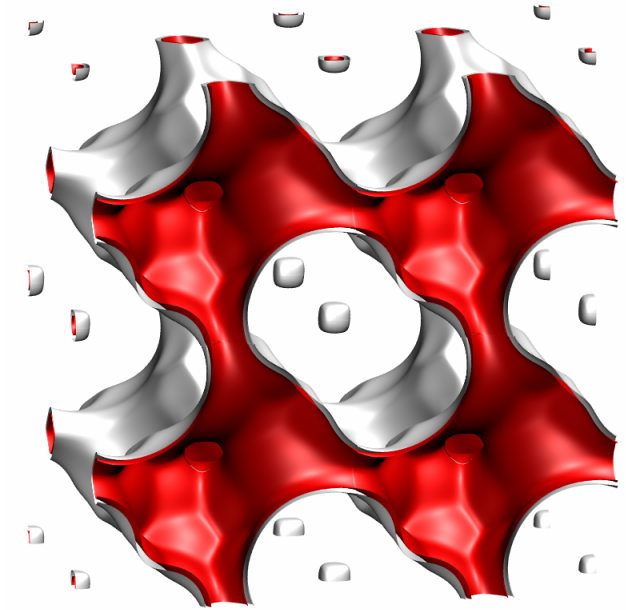

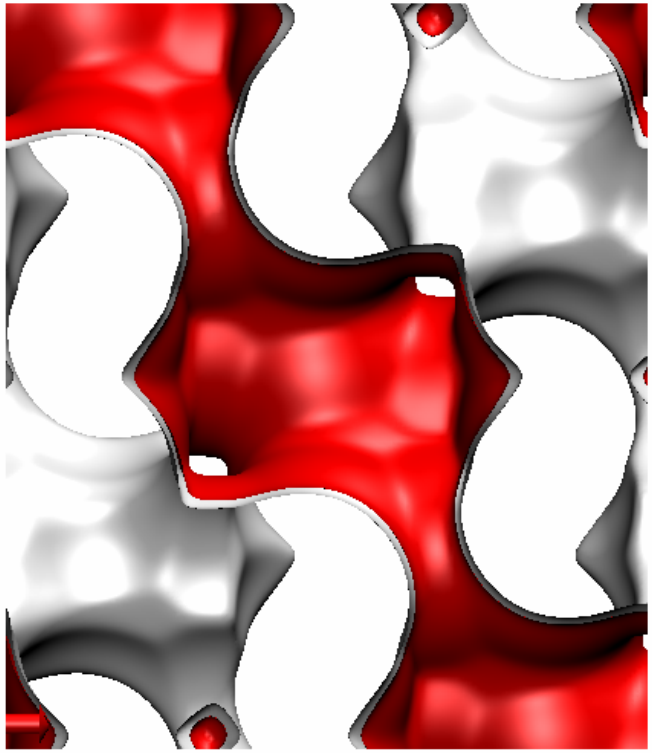

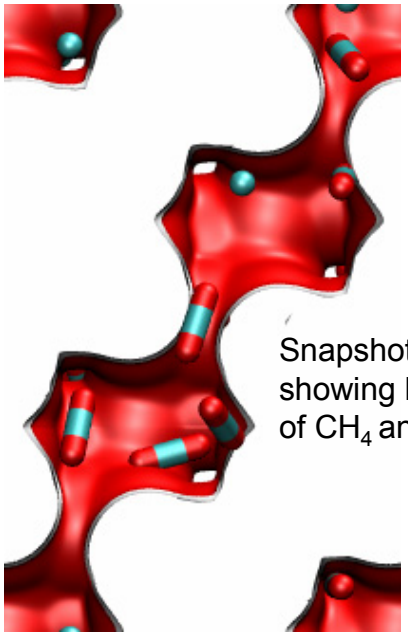

Snapshots showing location of $CH_4$ and $CO_2$

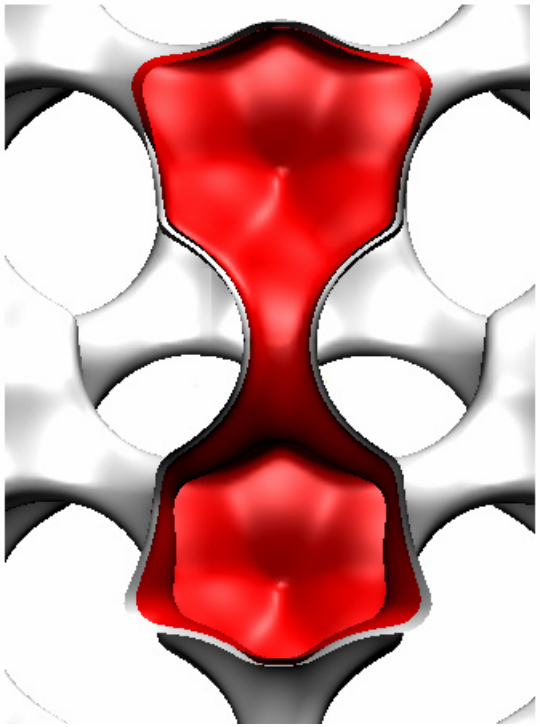

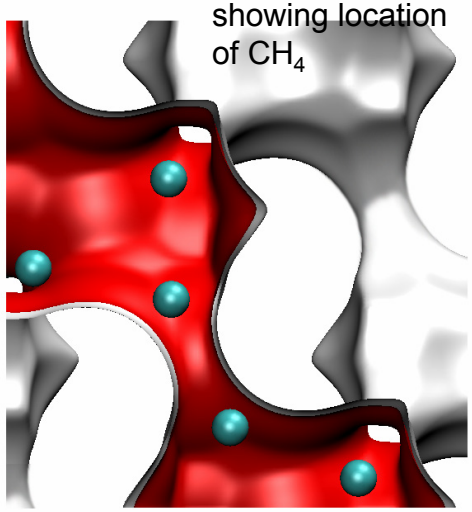

Snapshots showing location of $CH_4$

# CHA window and pore dimensions

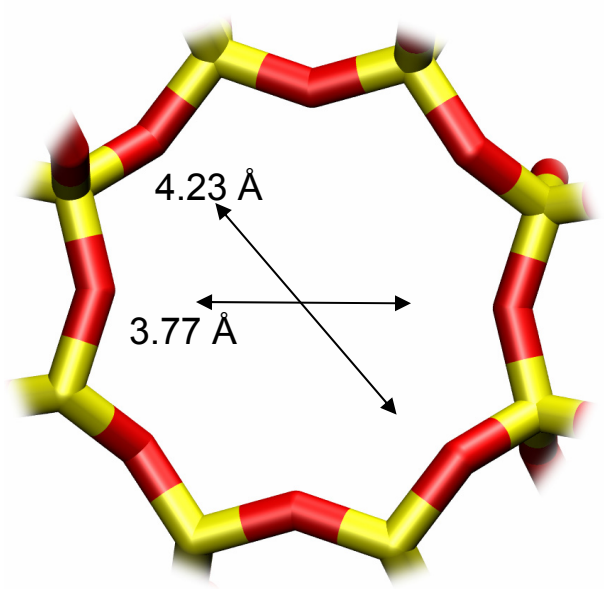


CHA

The window dimensions calculated using the van der Waals diameter of framework atoms = 2.7 Å are indicated above by the arrows.

This plot of surface area versus pore dimension is determined using a combination of the DeLaunay triangulation method for pore dimension determination, and the procedure of Düren for determination of the surface area. The computational details will be described in detail in a forthcoming publication.

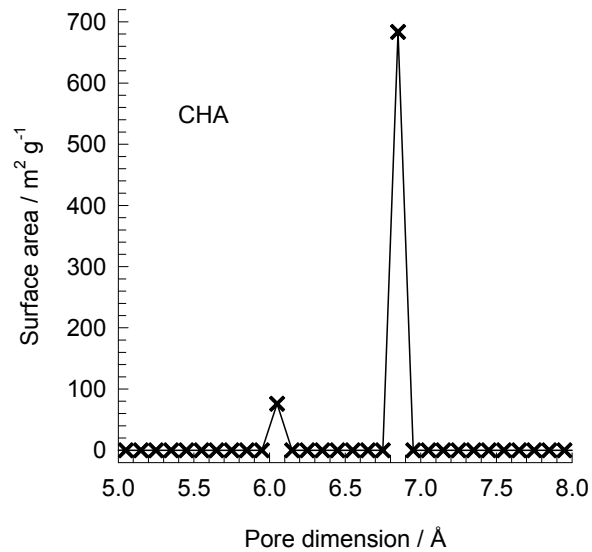


| | CHA |
|---|---|
| *a* /Å | 15.075 |
| *b* /Å | 23.907 |
| *c* /Å | 13.803 |
| Cell volume / Å$^3$ | 4974.574 |
| conversion factor for [molec/uc] to [mol per kg Framework] | 0.2312 |
| conversion factor for [molec/uc] to [kmol/m$^3$] | 0.8747 |
| $\rho$ [kg/m3] | 1444.1 |
| MW unit cell [g/mol(framework)] | 4326.106 |
| $\phi$, fractional pore volume | 0.382 |
| open space / Å$^3$/uc | 1898.4 |
| Pore volume / cm$^3$/g | 0.264 |
| Surface area /m$^2$/g | 758.0 |
| DeLaunay diameter /Å | 3.77 |

# DDR landscape

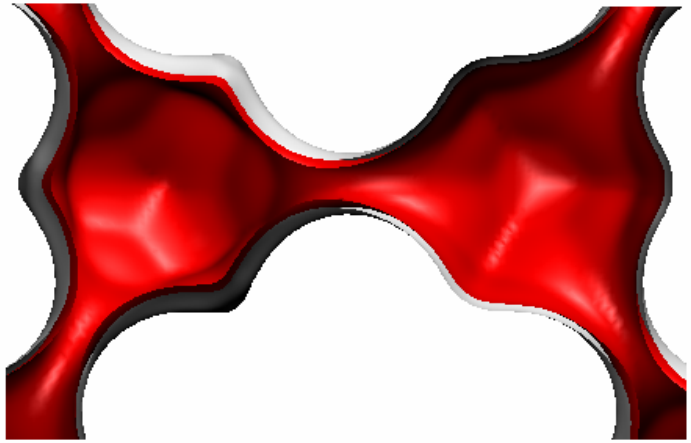

Snapshots showing location of $CH_4$ and $CO_2$

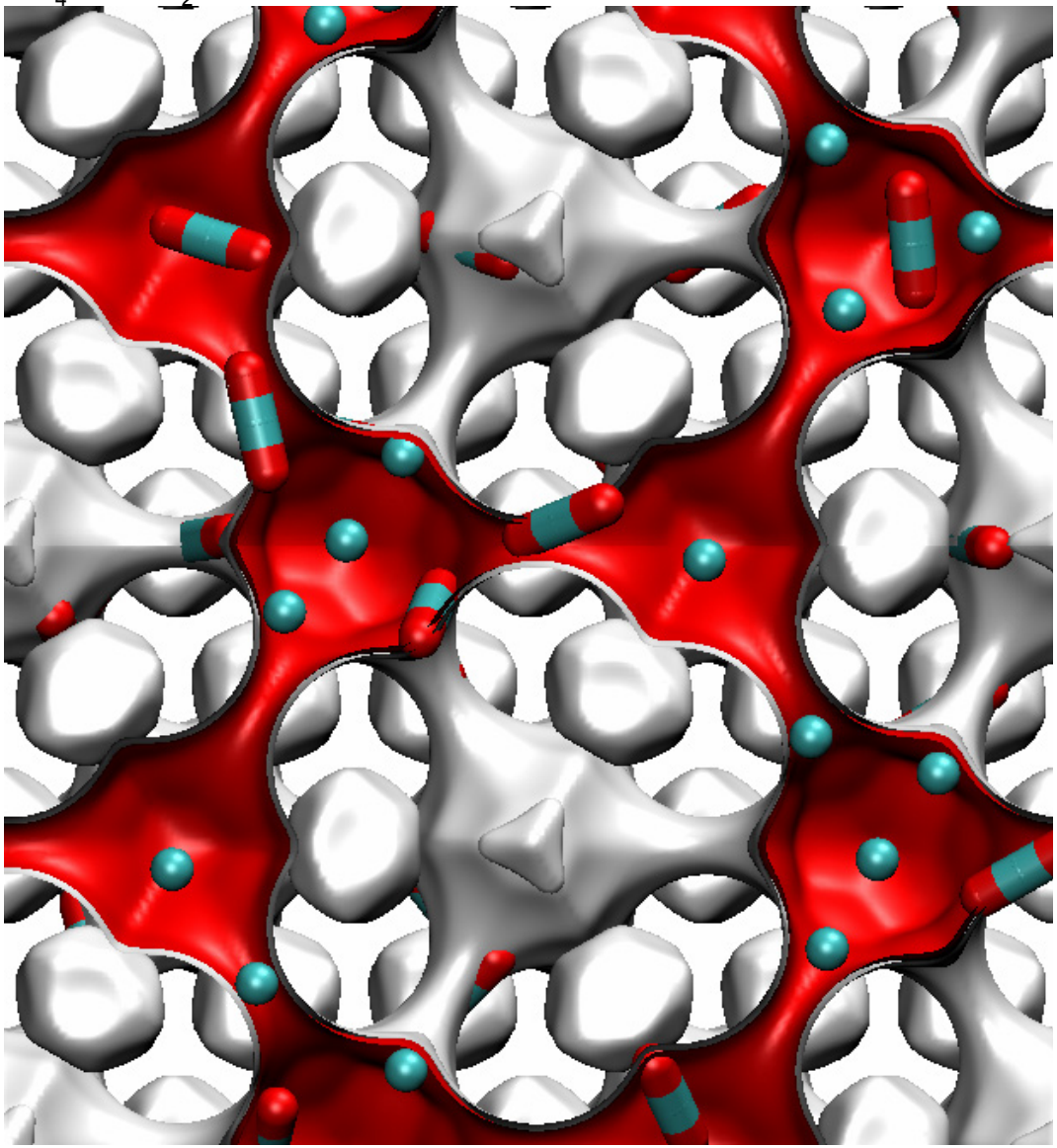

# DDR window and pore dimensions

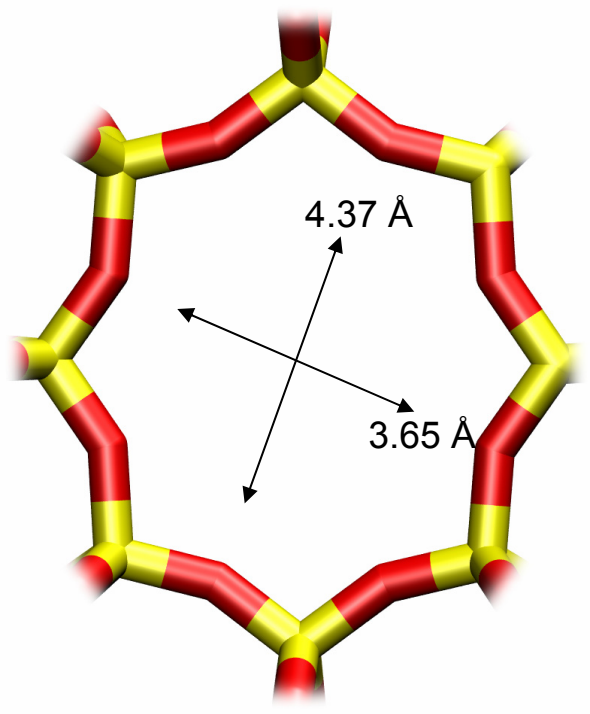


DDR

The window dimensions calculated using the van der Waals diameter of framework atoms = 2.7 Å are indicated above by the arrows.

This plot of surface area versus pore dimension is determined using a combination of the DeLaunay triangulation method for pore dimension determination, and the procedure of Düren for determination of the surface area. The computational details will be described in detail in a forthcoming publication.

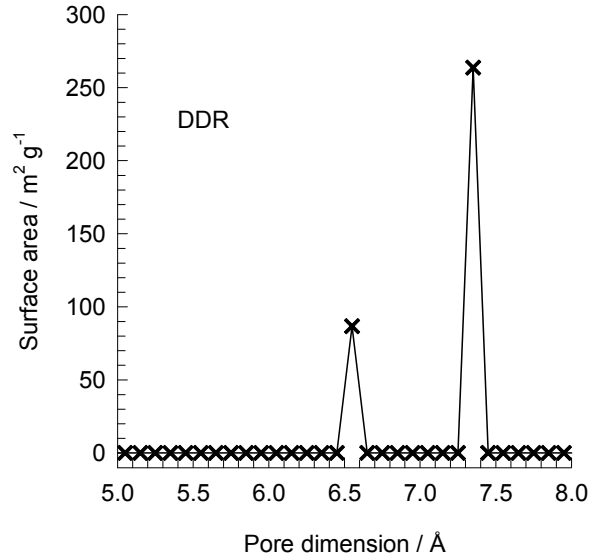


| | DDR |
|---|---|
| *a* /Å | 24.006 |
| *b* /Å | 13.86 |
| *c* /Å | 40.892 |
| Cell volume / Å$^3$ | 13605.72 |
| conversion factor for [molec/uc] to [mol per kg Framework] | 0.0693 |
| conversion factor for [molec/uc] to [kmol/m$^3$] | 0.4981 |
| $\rho$ [kg/m3] | 1759.991 |
| MW unit cell [g/mol(framework)] | 14420.35 |
| $\phi$, fractional pore volume | 0.245 |
| open space / Å$^3$/uc | 3333.5 |
| Pore volume / cm$^3$/g | 0.139 |
| Surface area /m$^2$/g | 350.0 |
| DeLaunay diameter /Å | 3.65 |

# ERI pore landscape

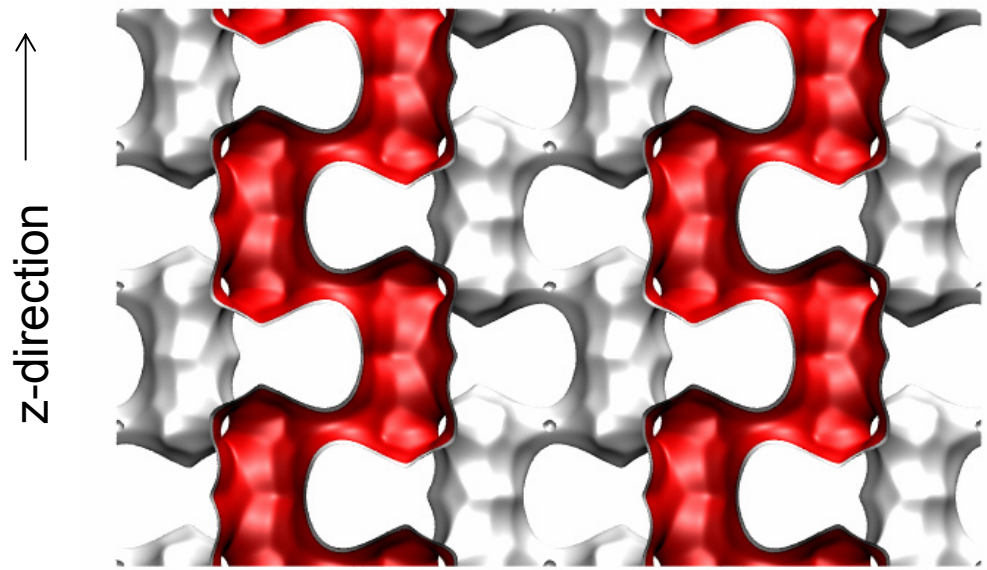


x-y projection

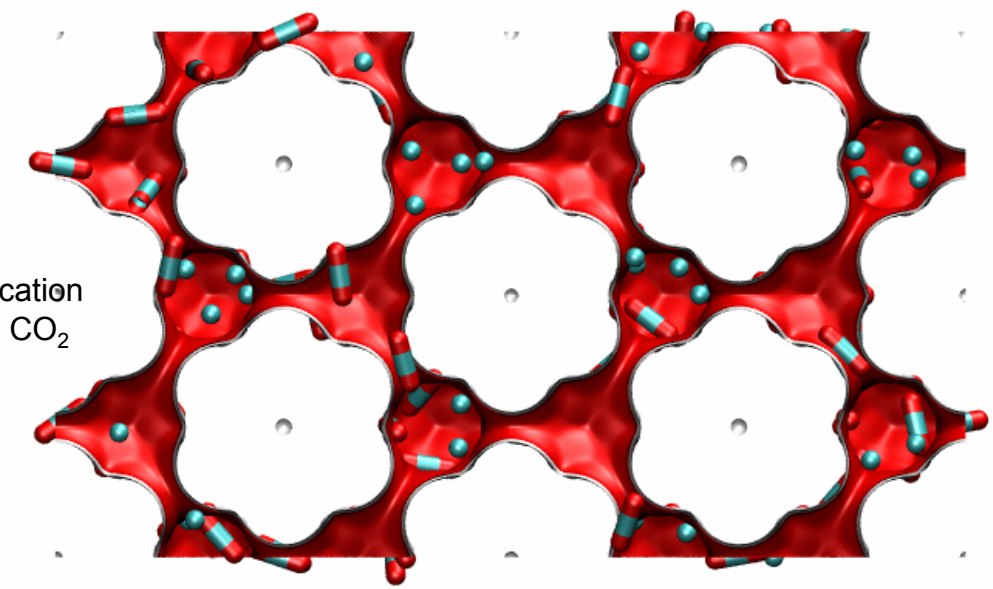

Snapshots showing location of $CH_4$ and $CO_2$

# ERI window and pore dimensions

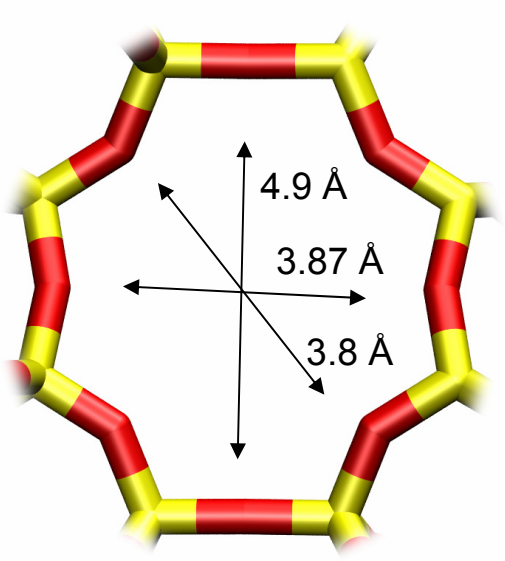


ERI

The window dimensions calculated using the van der Waals diameter of framework atoms = 2.7 Å are indicated above by the arrows.

This plot of surface area versus pore dimension is determined using a combination of the DeLaunay triangulation method for pore dimension determination, and the procedure of Düren for determination of the surface area. The computational details will be described in detail in a forthcoming publication.

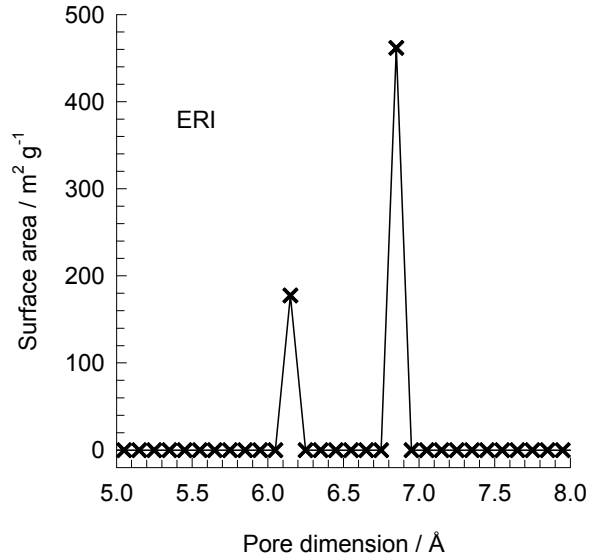


| | ERI |
|---|---|
| *a* /Å | 22.953 |
| *b* /Å | 13.252 |
| *c* /Å | 14.81 |
| Cell volume / Å$^3$ | 4504.804 |
| conversion factor for [molec/uc] to [mol per kg Framework] | 0.2312 |
| conversion factor for [molec/uc] to [kmol/m$^3$] | 1.0156 |
| $\rho$ [kg/m3] | 1594.693 |
| MW unit cell [g/mol(framework)] | 4326.106 |
| $\phi$, fractional pore volume | 0.363 |
| open space / Å$^3$/uc | 1635.0 |
| Pore volume / cm$^3$/g | 0.228 |
| Surface area /m$^2$/g | 635.0 |
| DeLaunay diameter /Å | 3.81 |

# FAU-Si pore landscape

12-ring
window of FAU

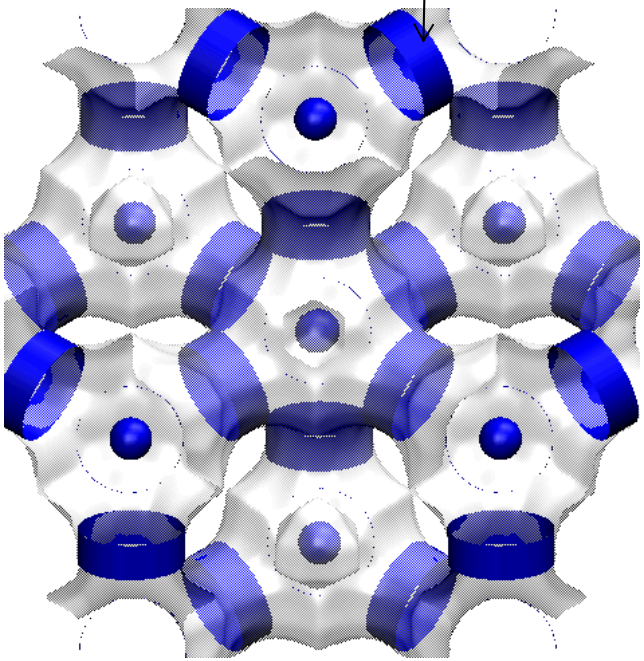

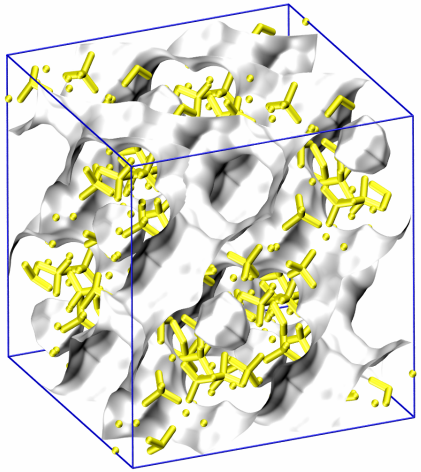

The volume of one FAU cage is 786 Å$^3$, larger in size than that of LTA (743 Å$^3$) and DDR (278 Å$^3$).

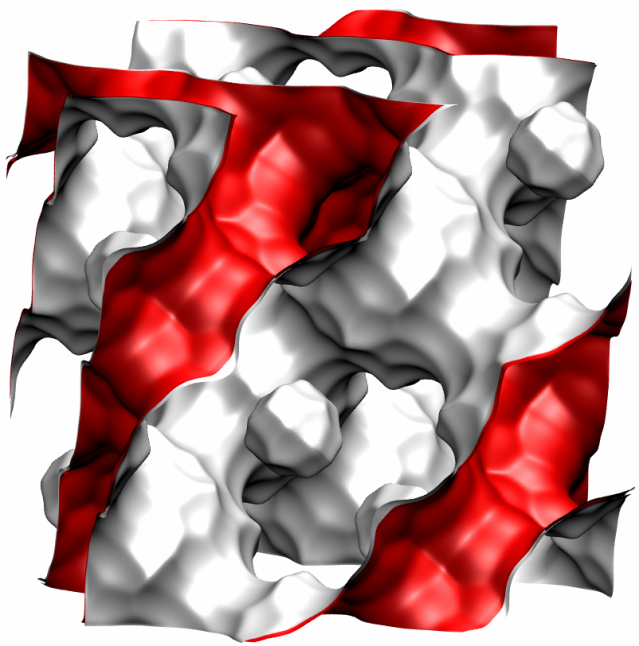

# FAU-Si window and pore dimensions

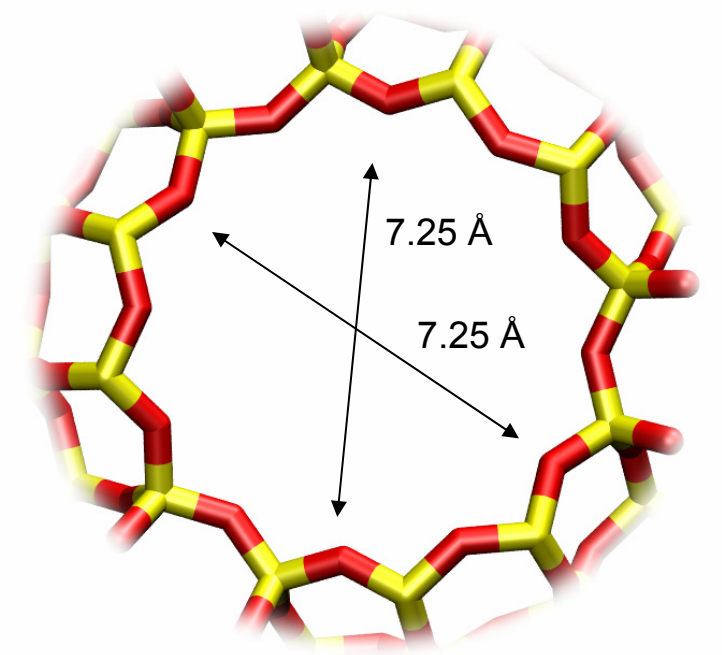


This plot of surface area versus pore dimension is determined using a combination of the DeLaunay triangulation method for pore dimension determination, and the procedure of Düren for determination of the surface area. The computational details will be described in detail in a forthcoming publication.

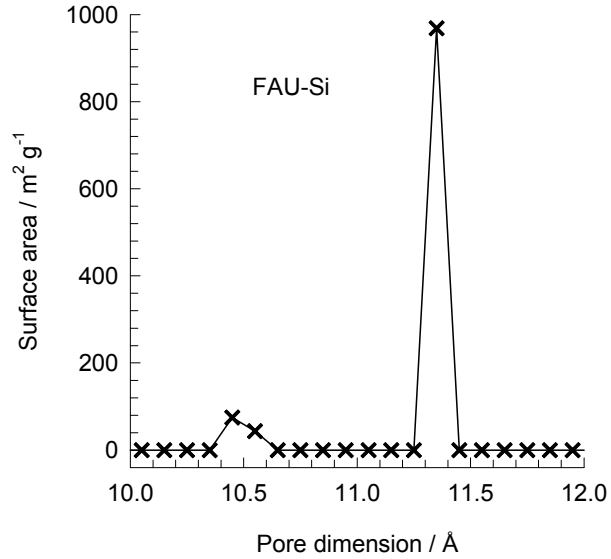


| | FAU-Si |
|---|---|
| *a* /Å | 24.28 |
| *b* /Å | 24.28 |
| *c* /Å | 24.28 |
| Cell volume / Å$^3$ | 14313.51 |
| conversion factor for [molec/uc] to [mol per kg Framework] | 0.0867 |
| conversion factor for [molec/uc] to [kmol/m$^3$] | 0.2642 |
| $\rho$ [kg/m3] | 1338.369 |
| MW unit cell [g/mol (framework)] | 11536.28 |
| $\phi$, fractional pore volume | 0.439 |
| open space / Å$^3$/uc | 6285.6 |
| Pore volume / cm$^3$/g | 0.328 |
| Surface area /m$^2$/g | 1086.0 |
| DeLaunay diameter /Å | 7.37 |

# FER pore landscape

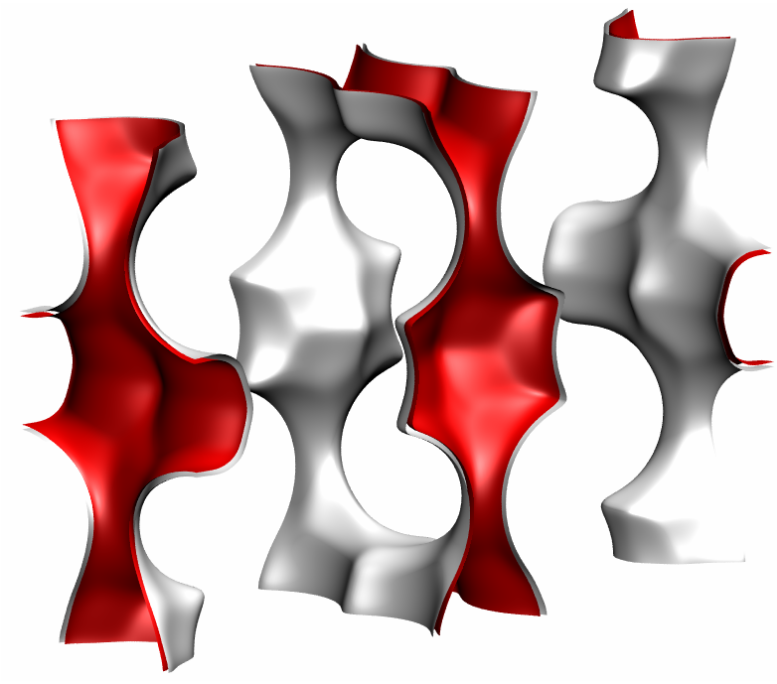

| | FER |
|---|---|
| *a* /Å | 19.156 |
| *b* /Å | 14.127 |
| *c* /Å | 7.489 |
| Cell volume / Å$^3$ | 2026.649 |
| conversion factor for [molec/uc] to [mol per kg Framework] | 0.4623 |
| conversion factor for [molec/uc] to [kmol/m$^3$] | 2.8968 |
| $\rho$ [kg/m3] | 1772.33 |
| MW unit cell [g/mol (framework)] | 2163.053 |
| $\phi$, fractional pore volume | 0.283 |
| open space / Å$^3$/uc | 573.2 |
| Pore volume / cm$^3$/g | 0.160 |
| Surface area /m$^2$/g | 403.0 |
| DeLaunay diameter /Å | 4.65 |

# FER pore dimensions

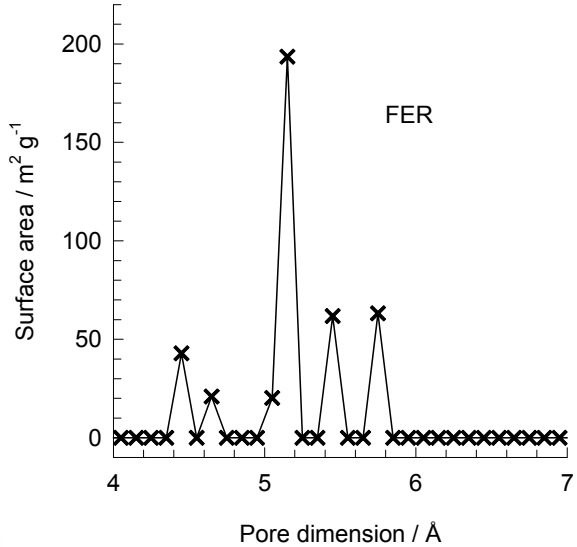


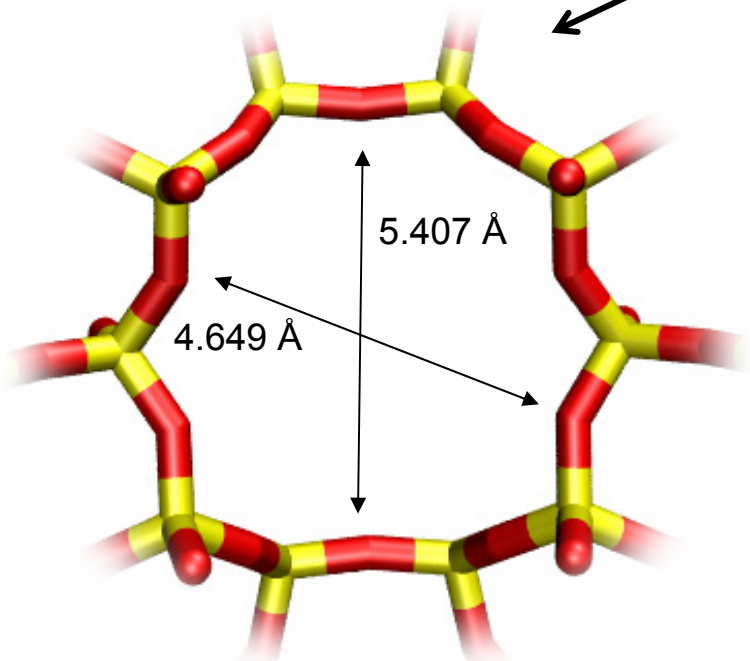


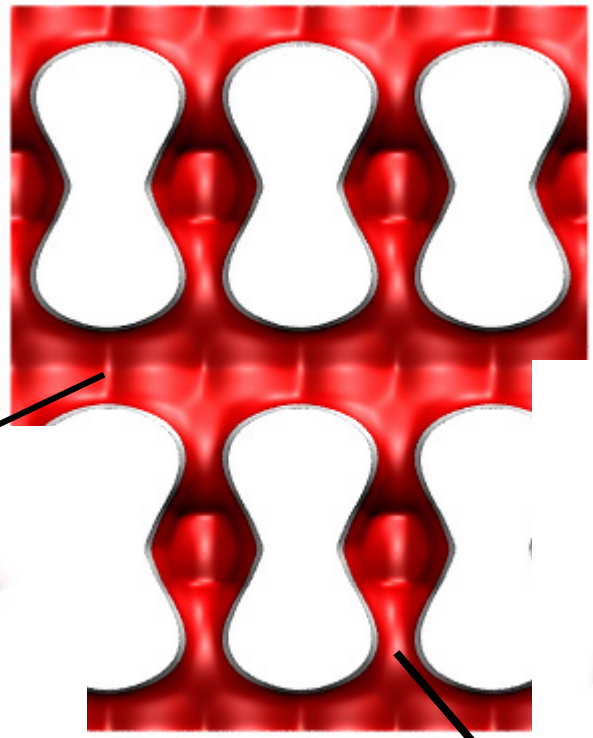

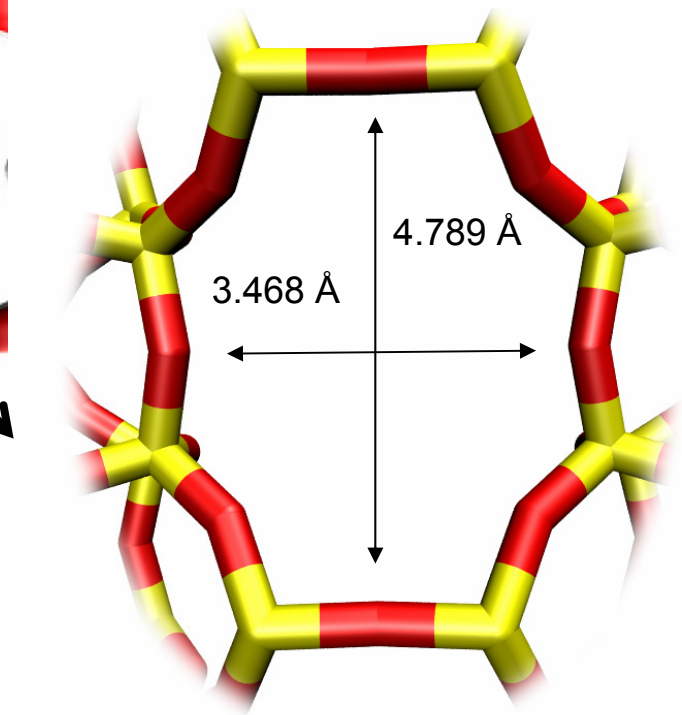


FER channel [0 0 1]

FER [0 1 0]

# GME landscapes

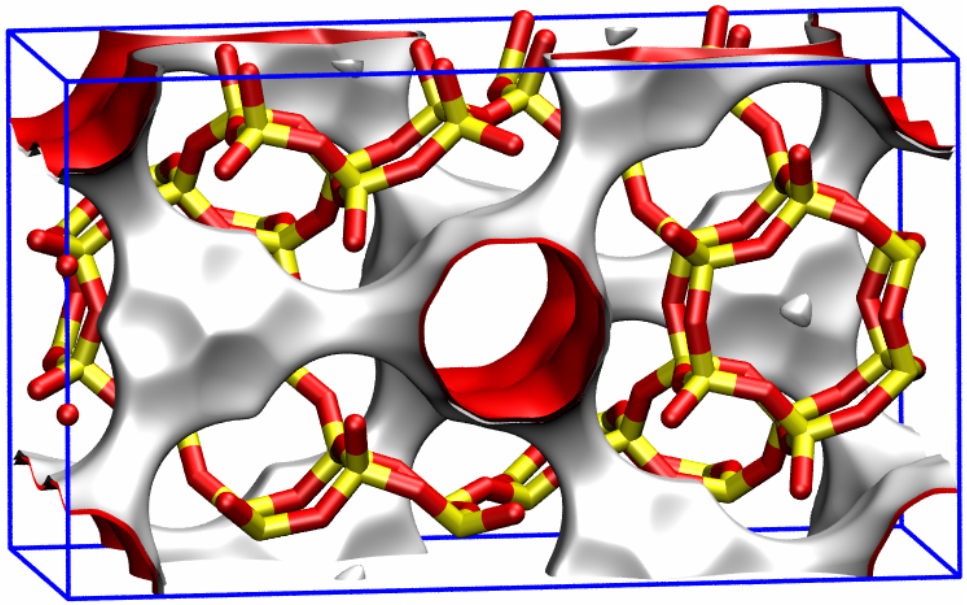

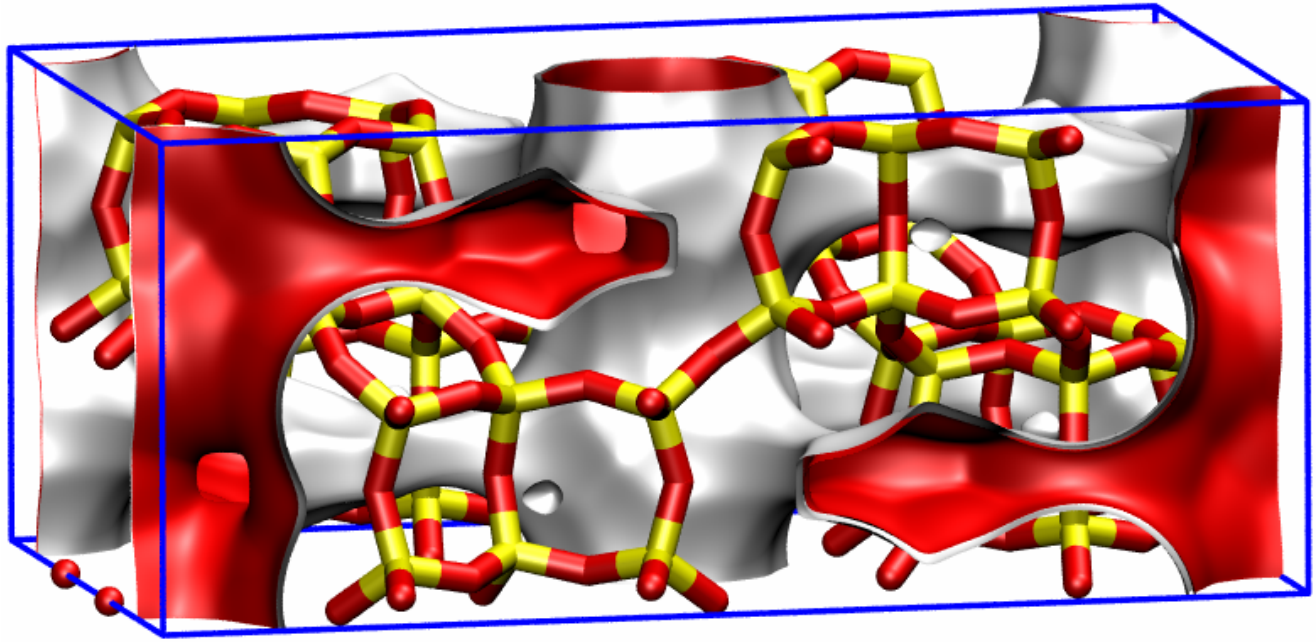

# GME pore dimensions

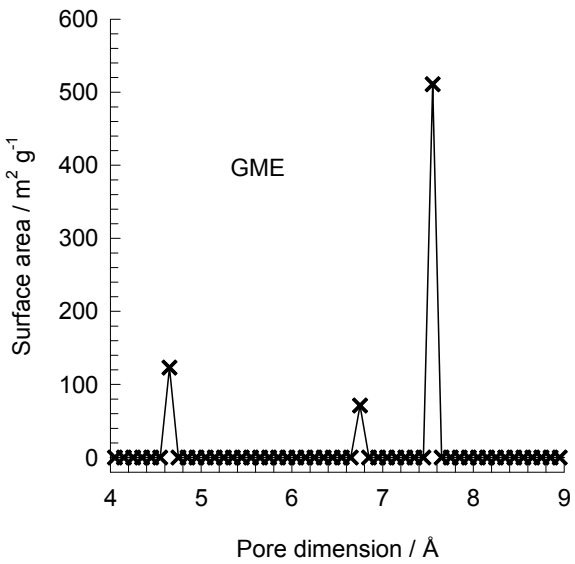


This plot of surface area versus pore dimension is determined using a combination of the DeLaunay triangulation method for pore dimension determination, and the procedure of Düren for determination of the surface area. The computational details will be described in detail in a forthcoming publication.

| | GME |
|---|---|
| *a* /Å | 23.826 |
| *b* /Å | 13.756 |
| *c* /Å | 10.064 |
| Cell volume / $Å^3$ | 3298.481 |
| conversion factor for [molec/uc] to [mol per kg Framework] | 0.3467 |
| conversion factor for [molec/uc] to [kmol/$m^3$] | 1.3090 |
| $\rho$ [kg/m3] | 1451.938 |
| MW unit cell [g/mol(framework)] | 2884.07 |
| $\phi$, fractional pore volume | 0.385 |
| open space / $Å^3$/uc | 1268.6 |
| Pore volume / $cm^3$/g | 0.265 |
| Surface area /$m^2$/g | 717.0 |
| DeLaunay diameter /Å | 7.09 |

# ISV pore landscape

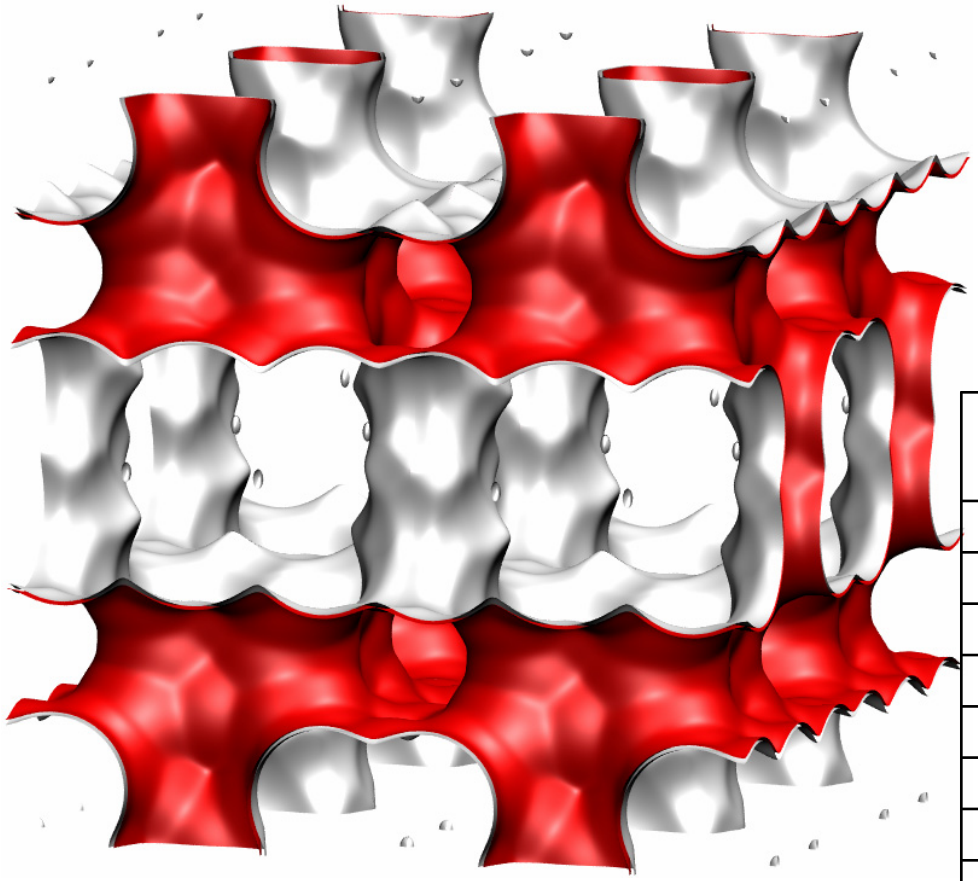

| | ISV |
|---|---|
| *a* /Å | 12.853 |
| *b* /Å | 12.853 |
| *c* /Å | 25.214 |
| Cell volume / Å$^3$ | 4165.343 |
| conversion factor for [molec/uc] to [mol per kg Framework] | 0.2600 |
| conversion factor for [molec/uc] to [kmol/m$^3$] | 0.9361 |
| $\rho$ [kg/m3] | 1533.027 |
| MW unit cell [g/mol(framework)] | 3845.427 |
| $\phi$, fractional pore volume | 0.426 |
| open space / Å$^3$/uc | 1773.9 |
| Pore volume / cm$^3$/g | 0.278 |
| Surface area /m$^2$/g | 911.0 |
| DeLaunay diameter /Å | 5.96 |

# ISV pore dimensions

This plot of surface area versus pore dimension is determined using a combination of the DeLaunay triangulation method for pore dimension determination, and the procedure of Düren for determination of the surface area. The computational details will be described in detail in a forthcoming publication.

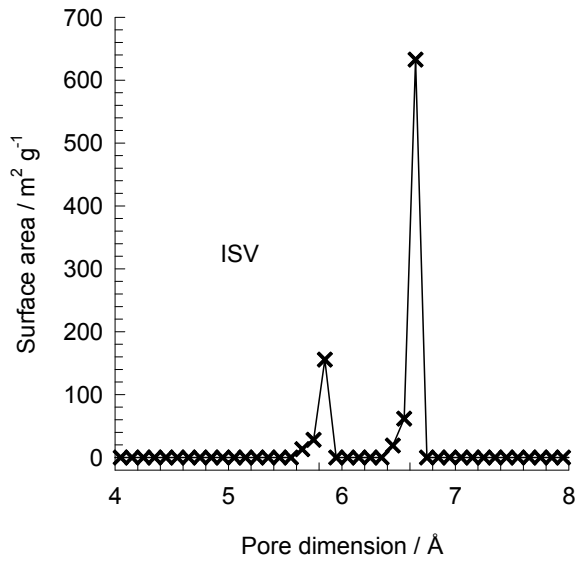


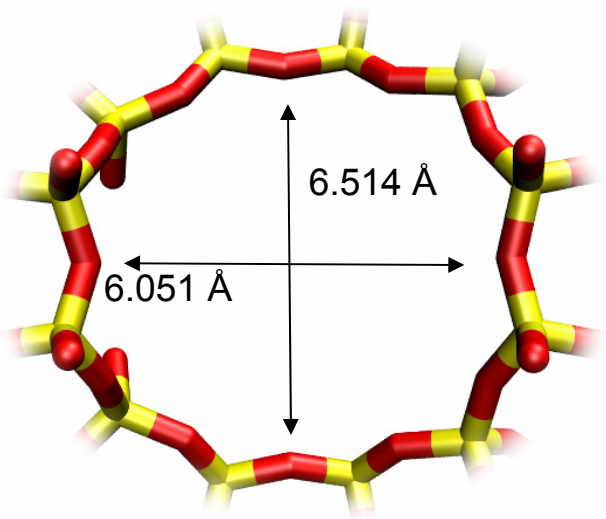


ISV [1 0 0]

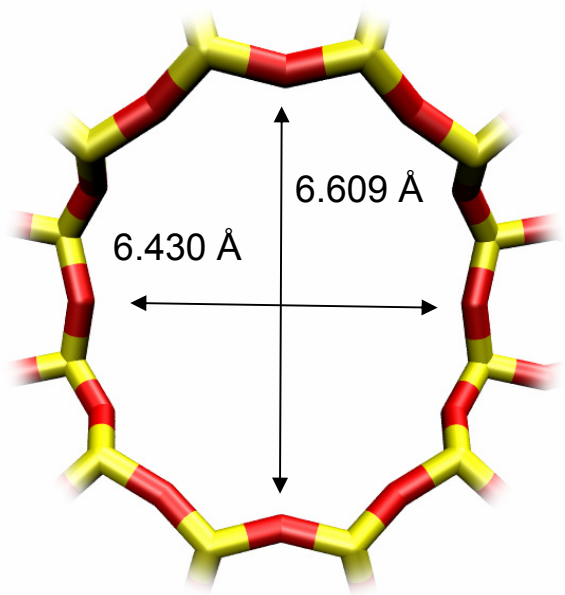


ISV [0 0 1]

# ITQ-12 pore landscape

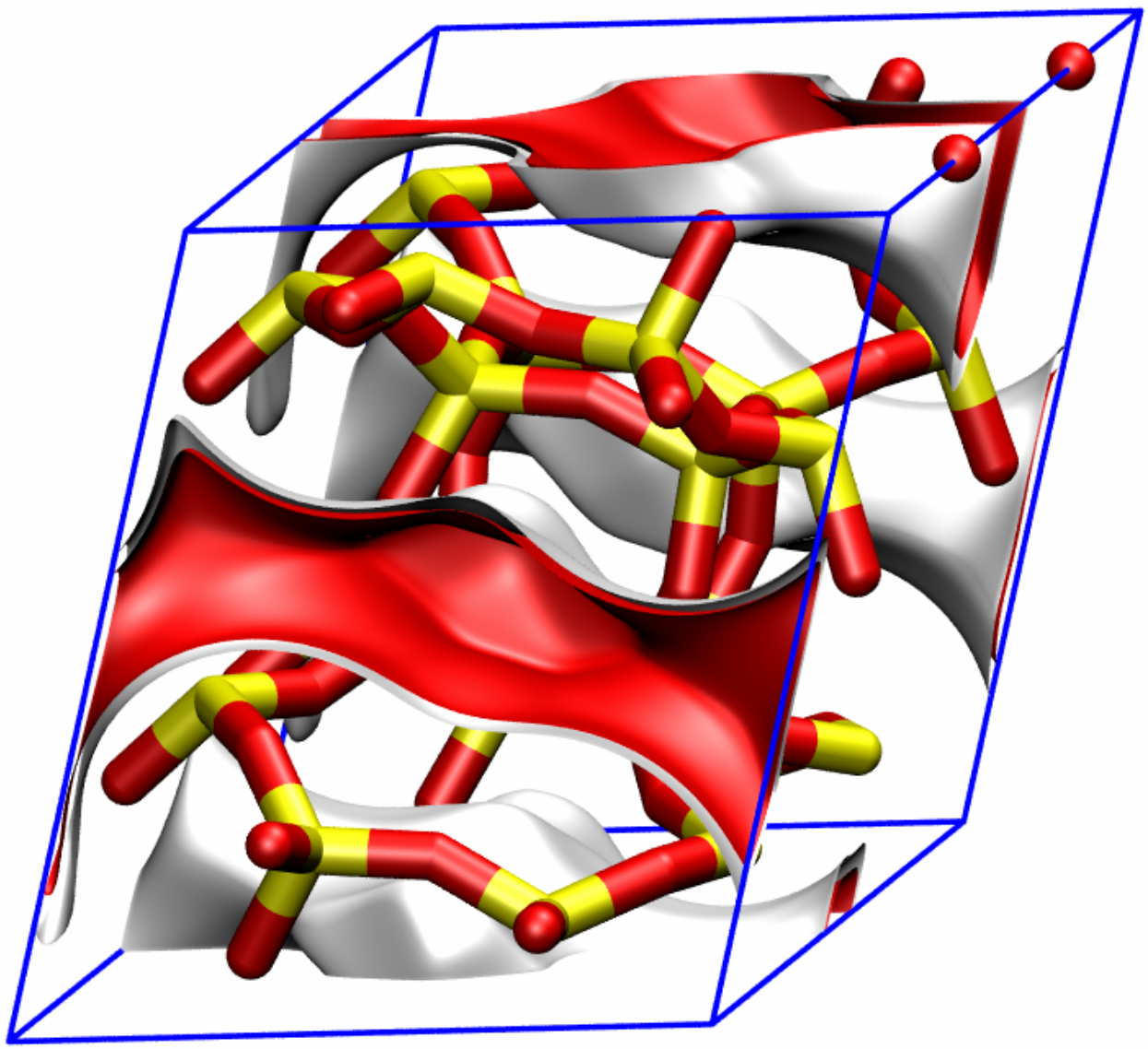

# ITQ-12 pore landscape

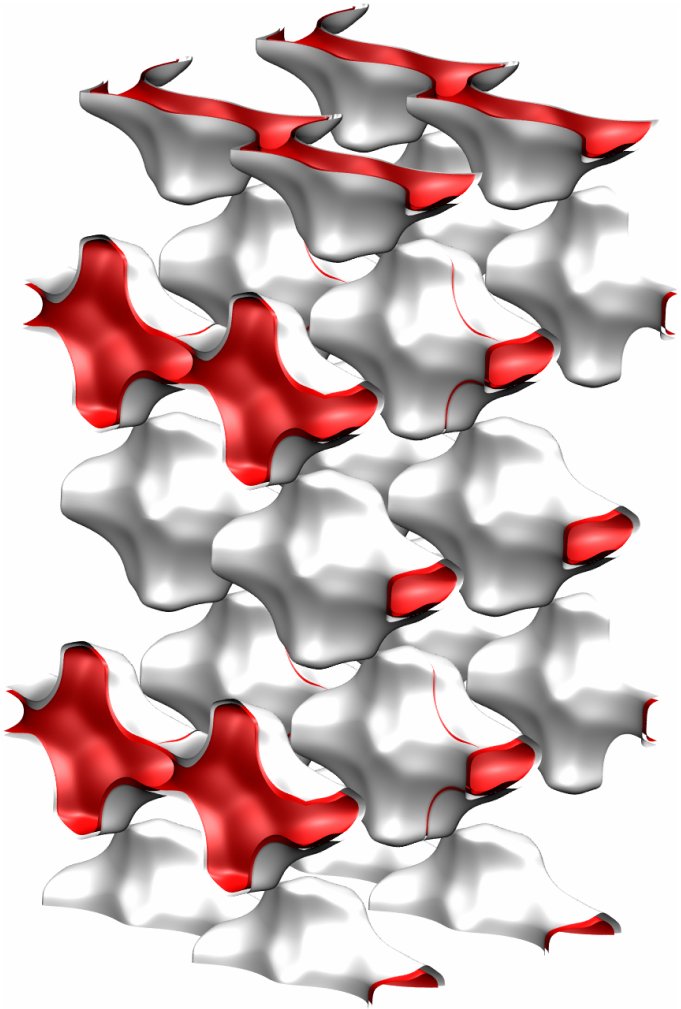

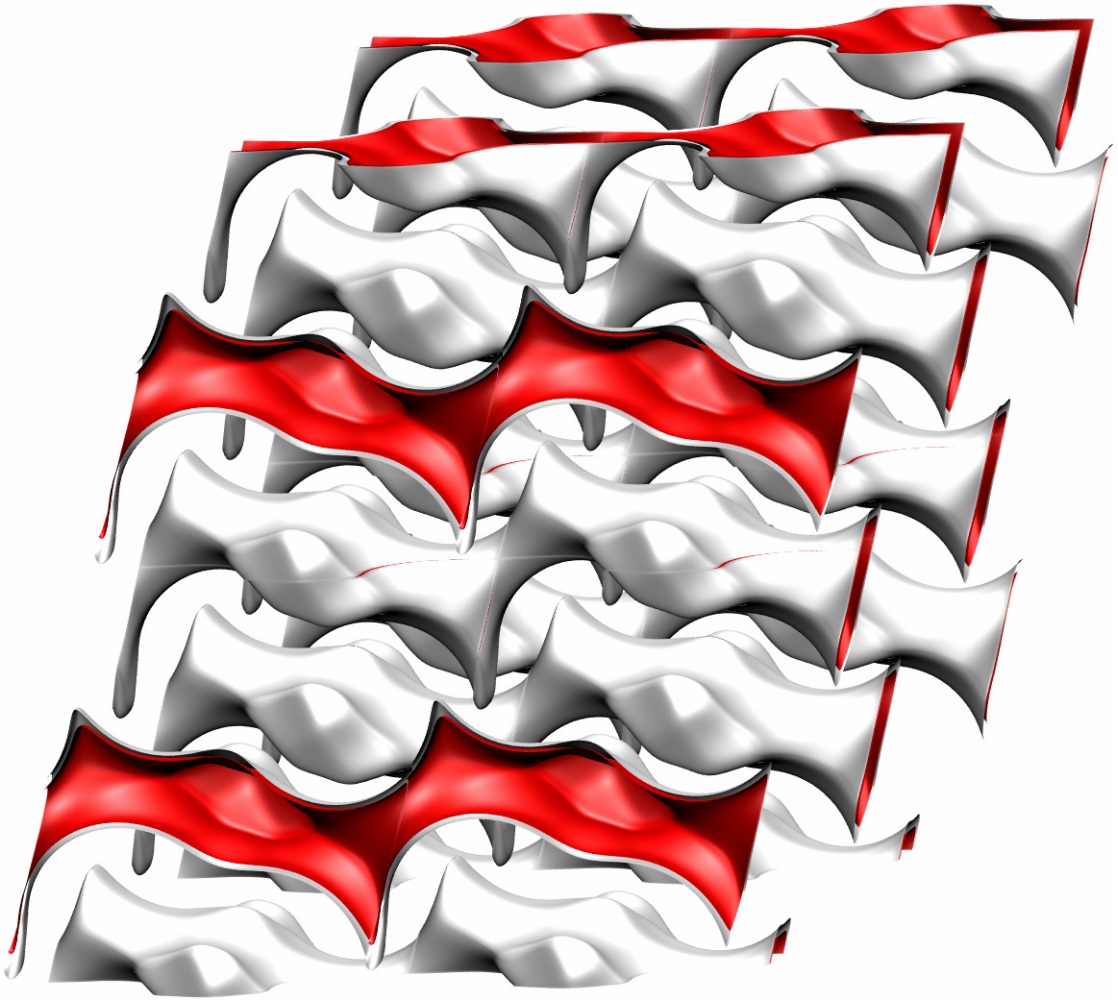

# ITQ-12 window and pore dimensions

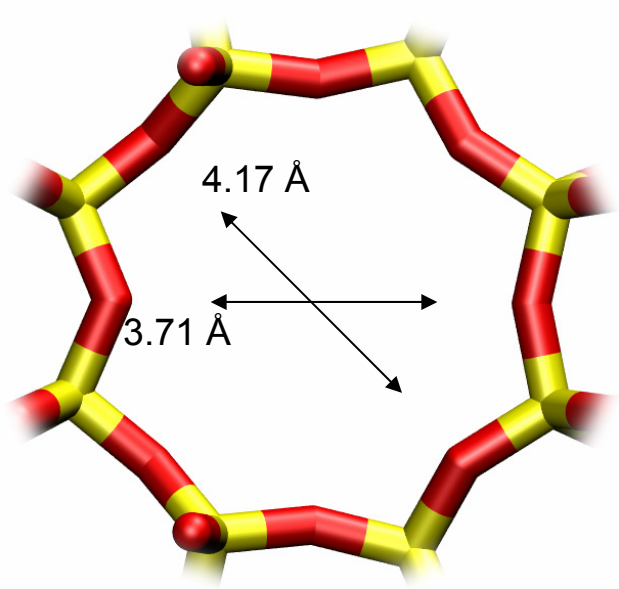


ITQ-12

The window dimensions calculated using the van der Waals diameter of framework atoms = 2.7 Å are indicated above by the arrows.

This plot of surface area versus pore dimension is determined using a combination of the DeLaunay triangulation method for pore dimension determination, and the procedure of Düren for determination of the surface area. The computational details will be described in detail in a forthcoming publication.

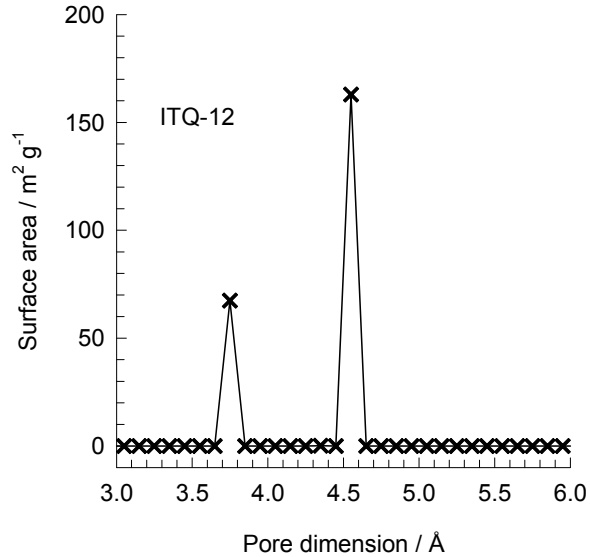


| | ITQ-12 |
|---|---|
| *a* /Å | 10.4364 |
| *b* /Å | 15.0183 |
| *c* /Å | 8.8553 |
| Cell volume / Å$^3$ | 1335.915 |
| conversion factor for [molec/uc] to [mol per kg Framework] | 0.6935 |
| conversion factor for [molec/uc] to [kmol/m$^3$] | 5.1856 |
| $\rho$ [kg/m3] | 1792.475 |
| MW unit cell [g/mol (framework)] | 1442.035 |
| $\phi$, fractional pore volume | 0.240 |
| open space / Å$^3$/uc | 320.2 |
| Pore volume / cm$^3$/g | 0.134 |
| Surface area /m$^2$/g | 230.0 |
| DeLaunay diameter /Å | |

# ITQ-29 pore landscape

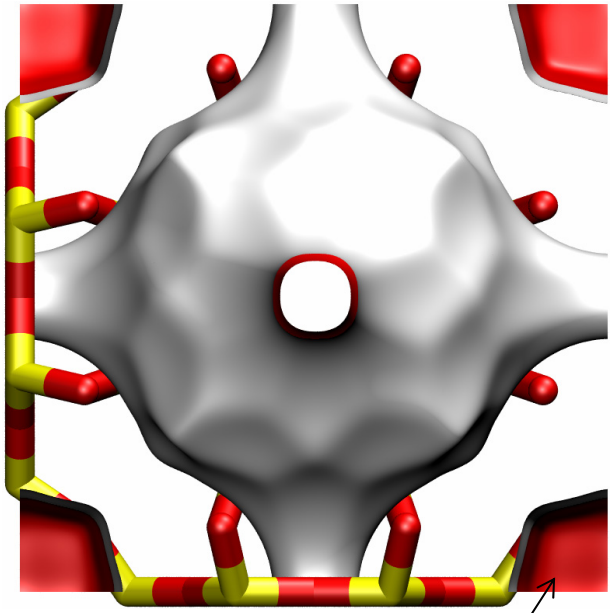

The structural information for ITQ-29 is not available in the IZA atlas and is taken from Corma, Nature, 437 (2004) 287. The window size is slightly smaller than that of LTA Si.

Inaccessible sodalite cages have been blocked in these simulations

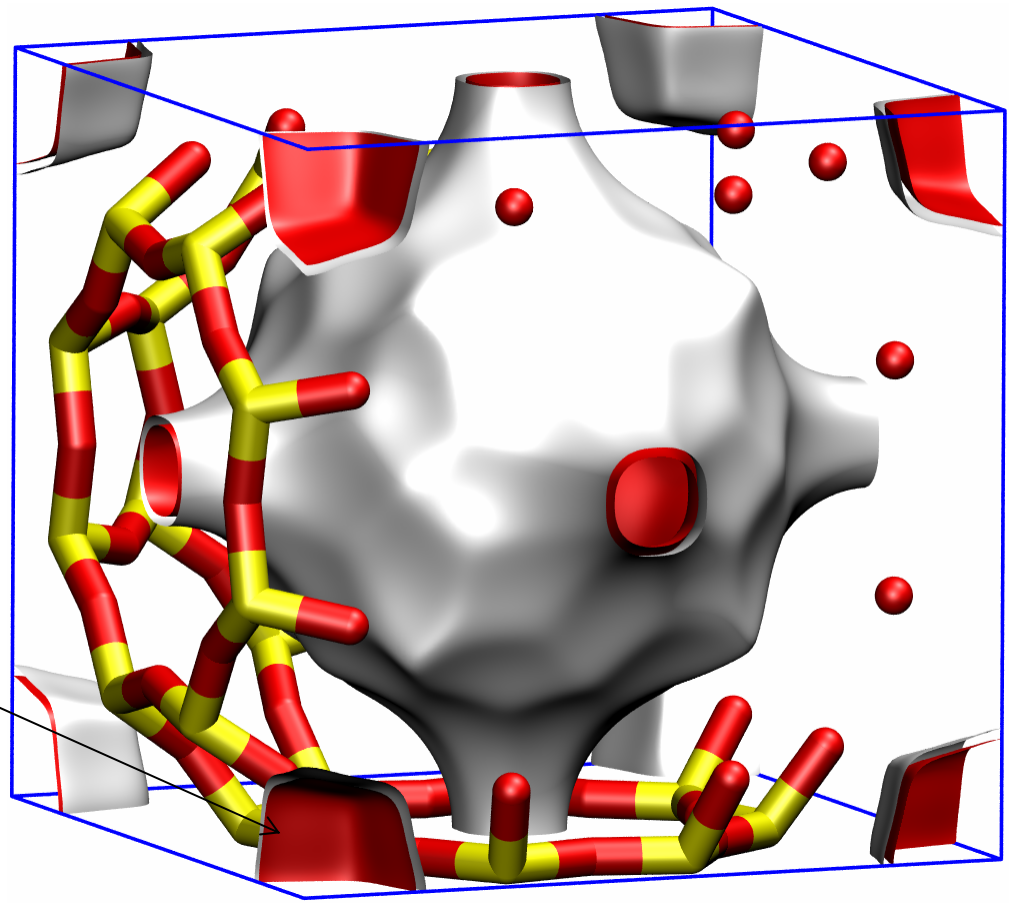

# ITQ-29 window and pore dimensions

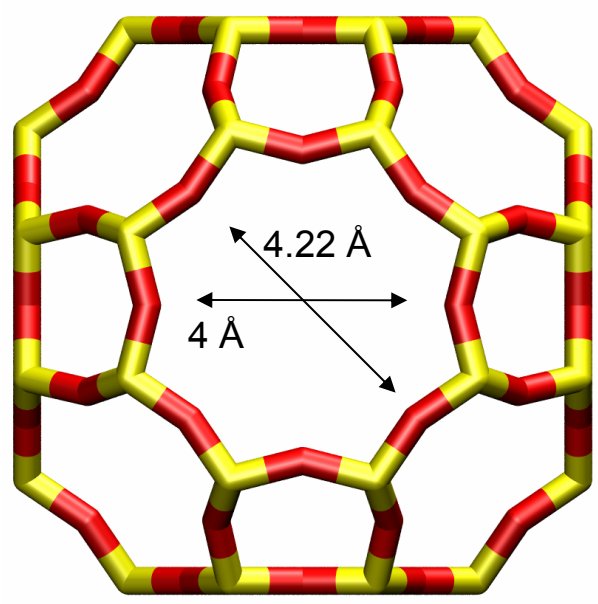


The window dimension calculated using the van der Waals diameter of framework atoms = 2.7 Å is indicated above by the arrows.

This plot of surface area versus pore dimension is determined using a combination of the DeLaunay triangulation method for pore dimension determination, and the procedure of Düren for determination of the surface area. The computational details will be described in detail in a forthcoming publication.

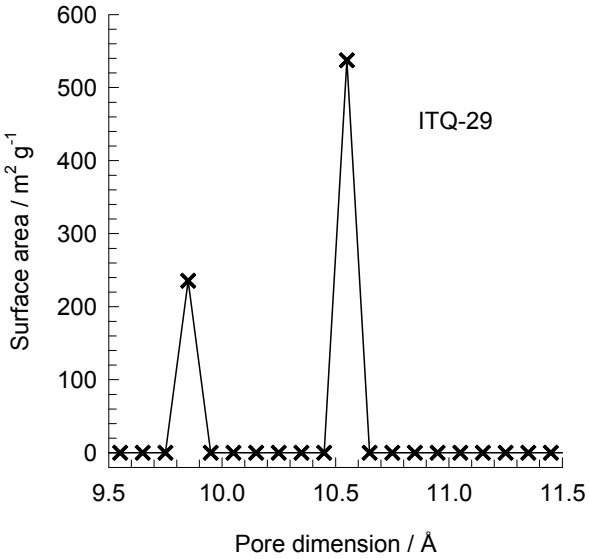


| | ITQ-29 |
|---|---|
| *a* /Å | 11.867 |
| *b* /Å | 11.867 |
| *c* /Å | 11.867 |
| Cell volume / Å$^3$ | 1671.178 |
| conversion factor for [molec/uc] to [mol per kg Framework] | 0.6935 |
| conversion factor for [molec/uc] to [kmol/m$^3$] | 2.4508 |
| $\rho$ [kg/m3] | 1432.877 |
| MW unit cell [g/mol(framework)] | 1442.035 |
| $\phi$, fractional pore volume | 0.405 |
| open space / Å$^3$/uc | 677.6 |
| Pore volume / cm$^3$/g | 0.283 |
| Surface area /m$^2$/g | 773.0 |
| DeLaunay diameter /Å | 3.98 |

# LTA-Si landscapes

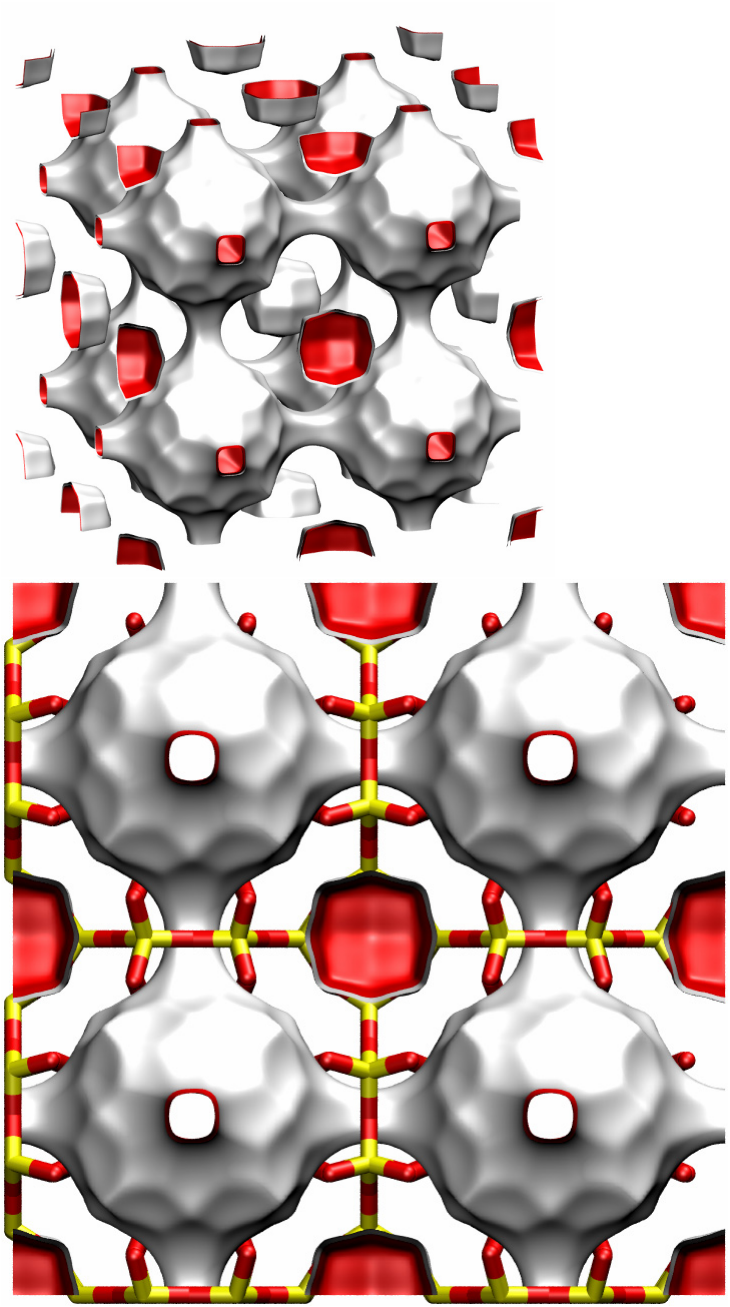

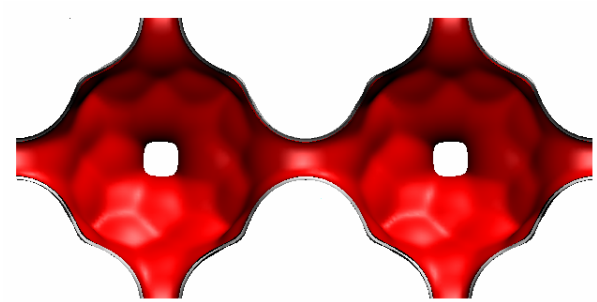

Snapshots showing location of $CH_4$ and $CO_2$

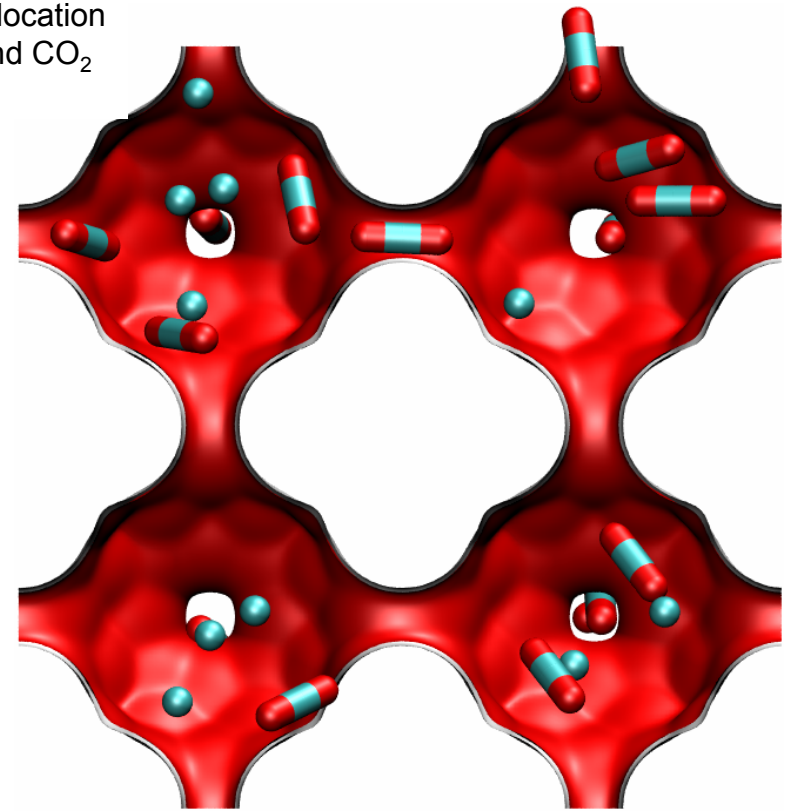

# LTA-Si window and pore dimensions

8-ring window of LTA

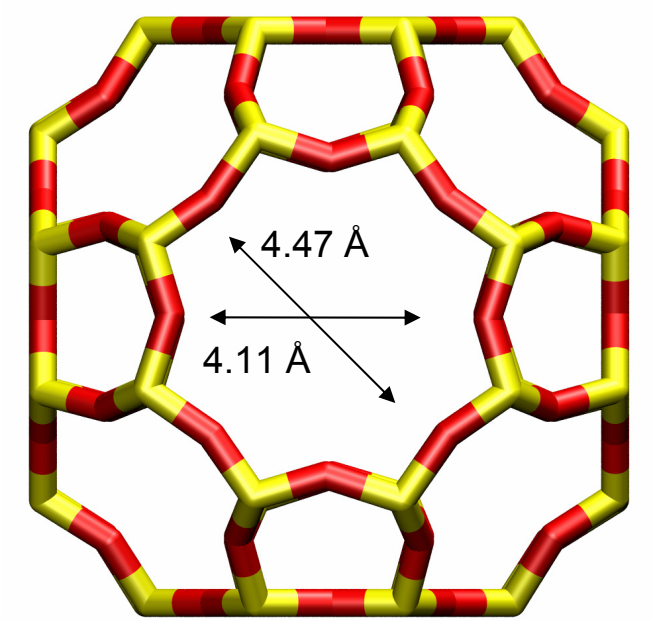


The window dimension calculated using the van der Waals diameter of framework atoms = 2.7 Å is indicated above by the arrows.

This plot of surface area versus pore dimension is determined using a combination of the DeLaunay triangulation method for pore dimension determination, and the procedure of Düren for determination of the surface area. The computational details will be described in detail in a forthcoming publication.

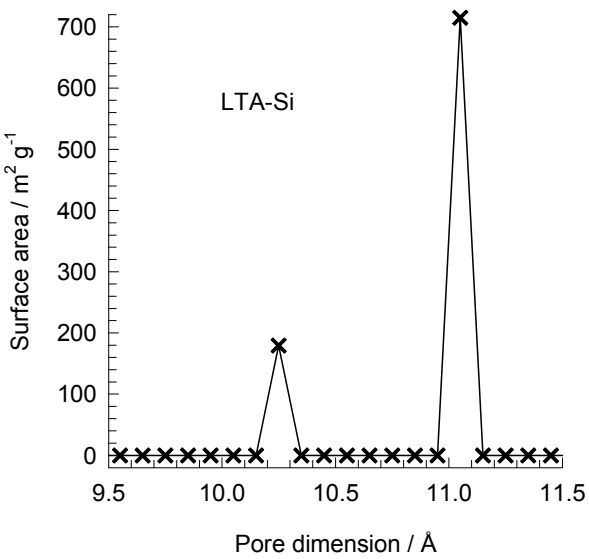


| | LTA-Si |
|---|---|
| *a* /Å | 24.61 |
| *b* /Å | 24.61 |
| *c* /Å | 24.61 |
| Cell volume / Å$^3$ | 14905.1 |
| conversion factor for [molec/uc] to [mol per kg Framework] | 0.0867 |
| conversion factor for [molec/uc] to [kmol/m$^3$] | 0.2794 |
| $\rho$ [kg/m3] | 1285.248 |
| MW unit cell [g/mol(framework)] | 11536.28 |
| $\phi$, fractional pore volume | 0.399 |
| open space / Å$^3$/uc | 5944.4 |
| Pore volume / cm$^3$/g | 0.310 |
| Surface area /m$^2$/g | 896.0 |
| DeLaunay diameter /Å | 4.10 |

# LTL pore landscapes

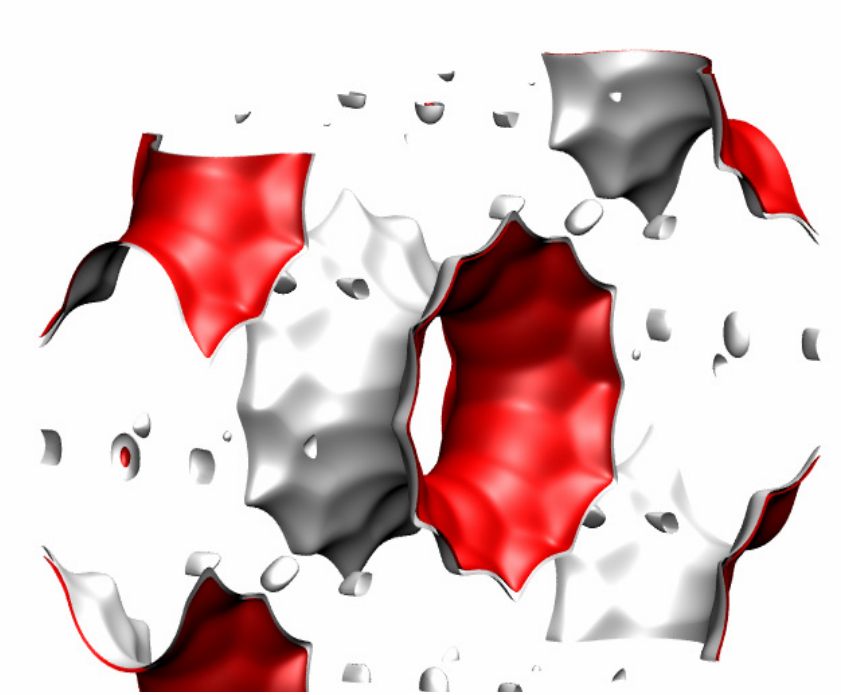

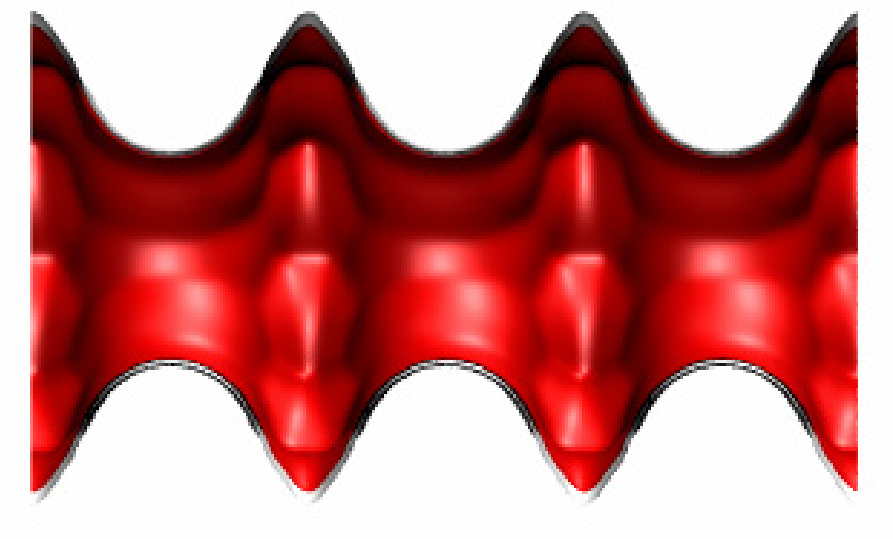

# LTL pore dimensions

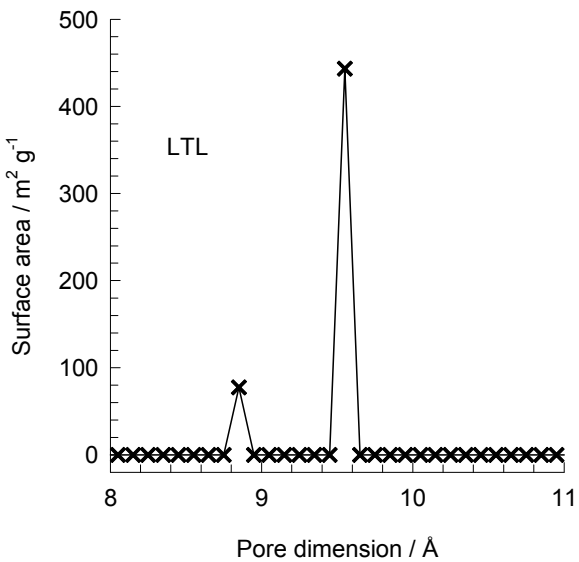


This plot of surface area versus pore dimension is determined using a combination of the DeLaunay triangulation method for pore dimension determination, and the procedure of Düren for determination of the surface area. The computational details will be described in detail in a forthcoming publication.

| | LTL |
|---|---|
| *a* /Å | 31.984 |
| *b* /Å | 18.466 |
| *c* /Å | 7.476 |
| Cell volume / $Å^3$ | 4415.449 |
| conversion factor for [molec/uc] to [mol per kg Framework] | 0.2312 |
| conversion factor for [molec/uc] to [kmol/$m^3$] | 1.3597 |
| $\rho$ [kg/m3] | 1626.965 |
| MW unit cell [g/mol(framework)] | 4326.106 |
| $\phi$, fractional pore volume | 0.277 |
| open space / $Å^3$/uc | 1221.3 |
| Pore volume / $cm^3$/g | 0.170 |
| Surface area /$m^2$/g | 521.0 |
| DeLaunay diameter /Å | 7.47 |

# MFI pore landscape

| | MFI |
|---|---|
| *a* /Å | 20.022 |
| *b* /Å | 19.899 |
| *c* /Å | 13.383 |
| Cell volume / Å$^3$ | 5332.025 |
| conversion factor for [molec/uc] to [mol per kg Framework] | 0.1734 |
| conversion factor for [molec/uc] to [kmol/m$^3$] | 1.0477 |
| $\rho$ [kg/m3] | 1796.386 |
| MW unit cell [g/mol(framework)] | 5768.141 |
| $\phi$, fractional pore volume | 0.297 |
| open space / Å$^3$/uc | 1584.9 |
| Pore volume / cm$^3$/g | 0.165 |
| Surface area /m$^2$/g | 487.0 |
| DeLaunay diameter /Å | 5.16 |

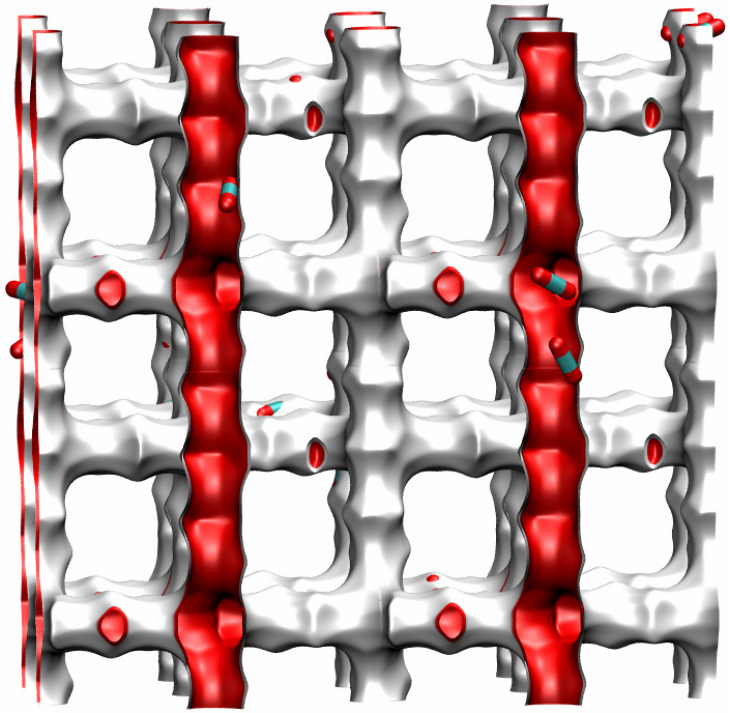

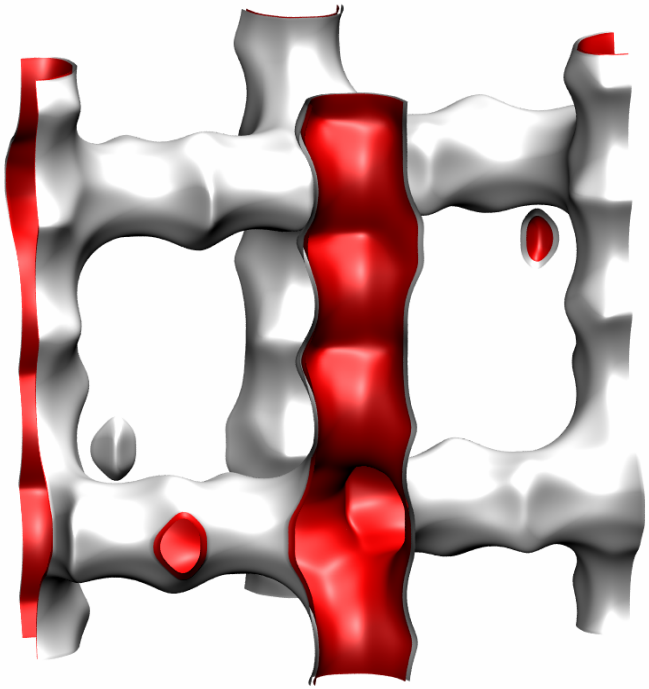

# MFI pore dimensions

10 ring channel of MFI viewed along [100]

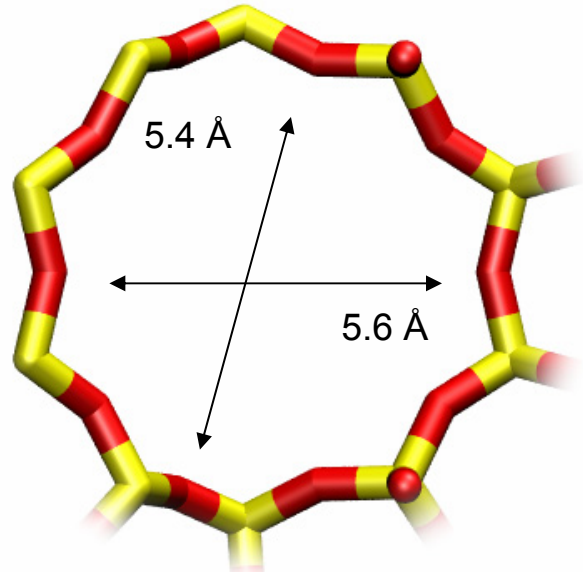


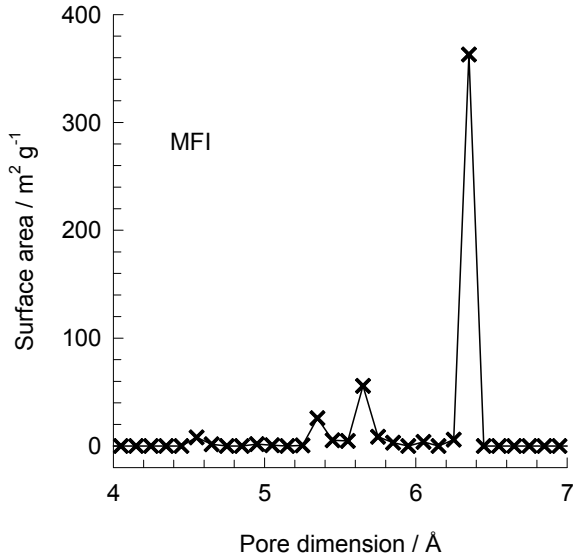


10 ring channel of MFI viewed along [010]

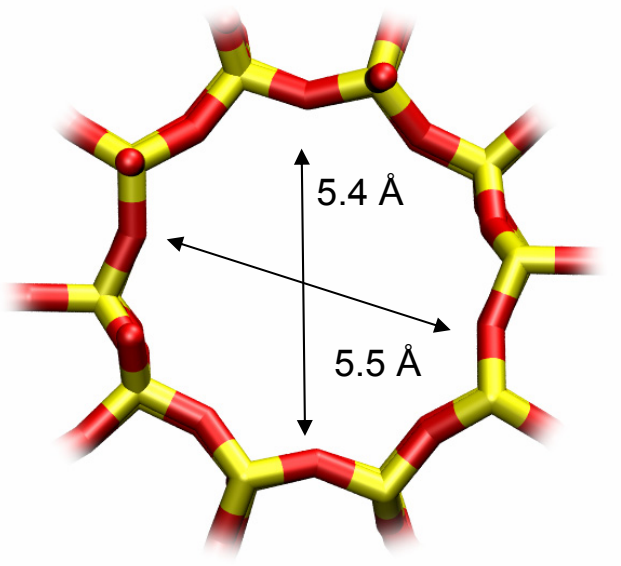


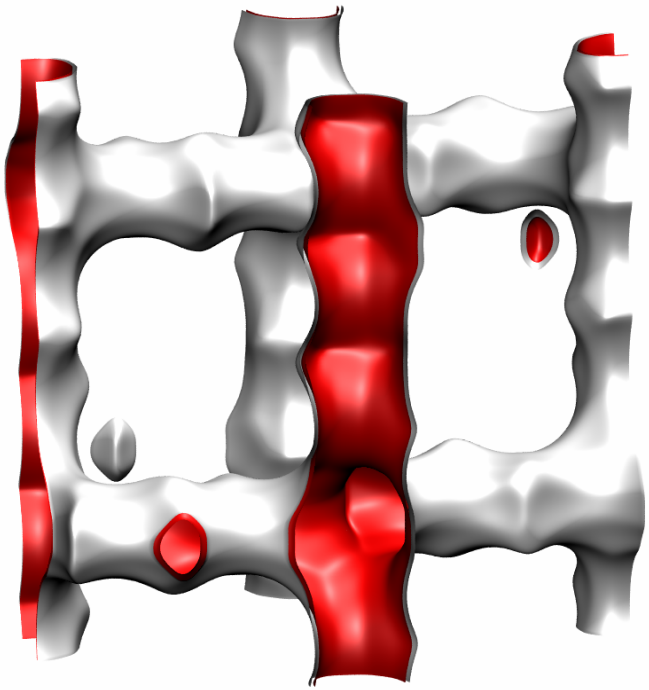

# MOR pore landscape

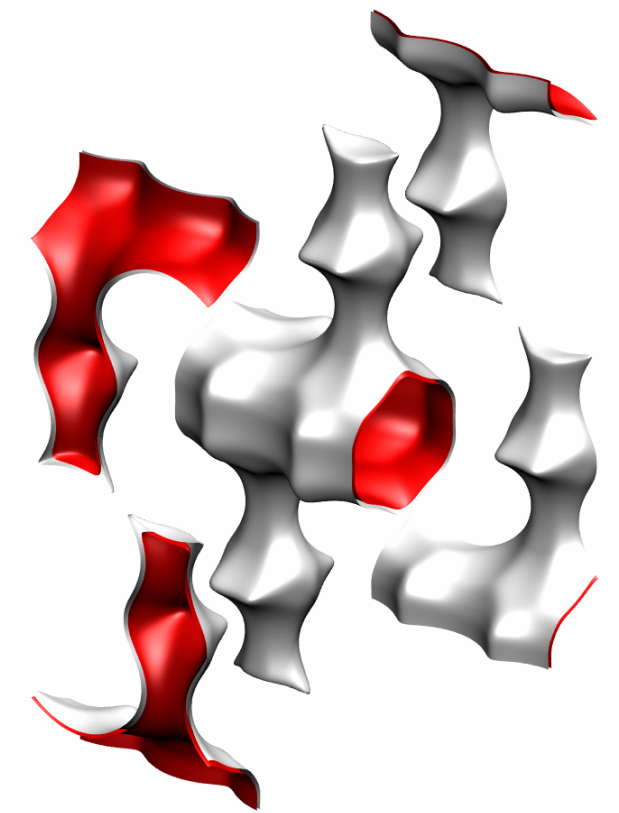

| | MOR |
|---|---|
| *a* /Å | 18.094 |
| *b* /Å | 20.516 |
| *c* /Å | 7.524 |
| Cell volume / Å$^3$ | 2793.033 |
| conversion factor for [molec/uc] to [mol per kg Framework] | 0.3467 |
| conversion factor for [molec/uc] to [kmol/m$^3$] | 2.0877 |
| $\rho$ [kg/m3] | 1714.691 |
| MW unit cell [g/mol(framework)] | 2884.07 |
| $\phi$, fractional pore volume | 0.285 |
| open space / Å$^3$/uc | 795.4 |
| Pore volume / cm$^3$/g | 0.166 |
| Surface area /m$^2$/g | 417.0 |
| DeLaunay diameter /Å | 6.44 |

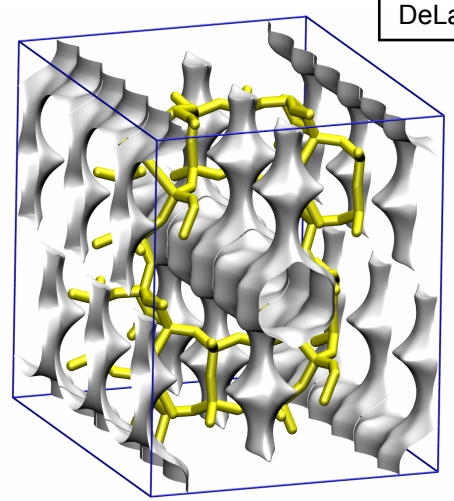

# MOR pore dimensions

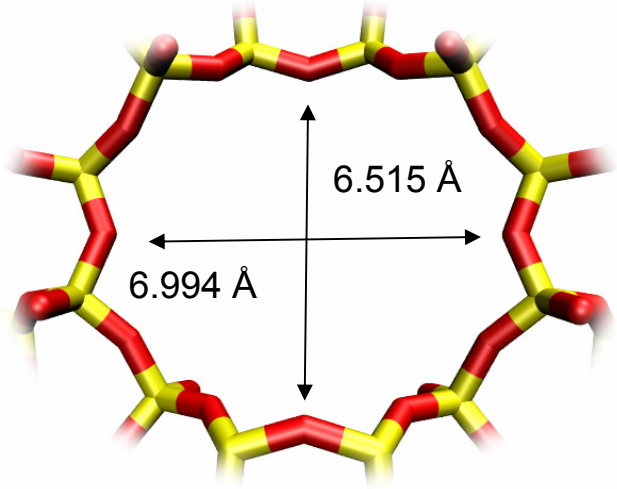


MOR Channel [1 0 0]

12-ring
main channels

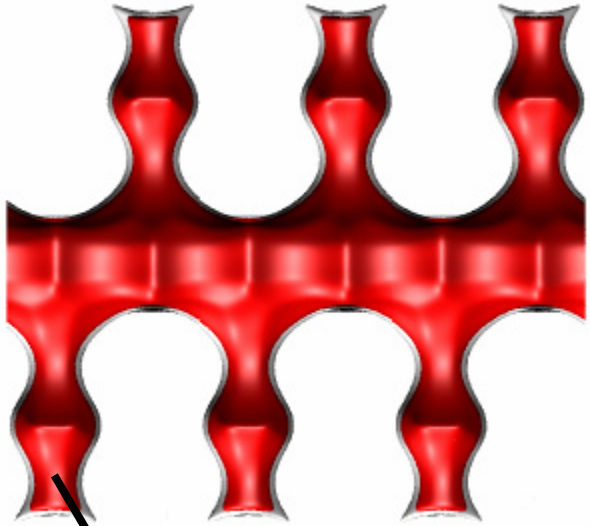

8-ring

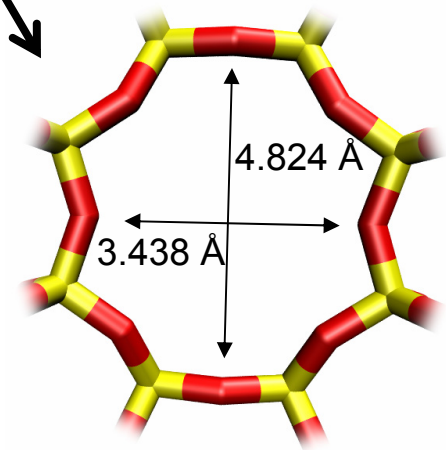


MOR [0 1 0]

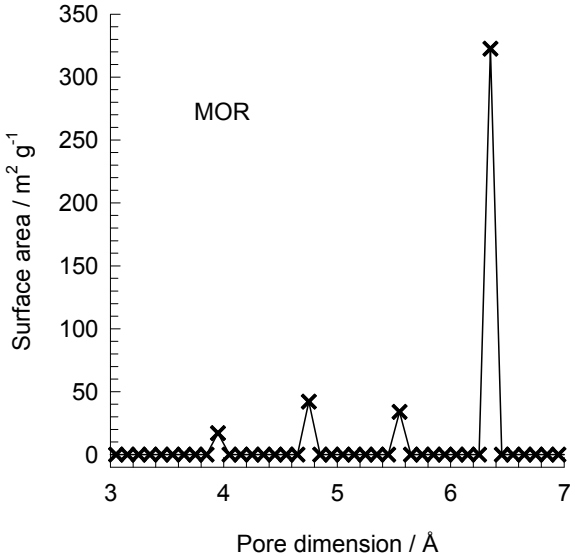


This plot of surface area versus pore dimension is determined using a combination of the DeLaunay triangulation method for pore dimension determination, and the procedure of Düren for determination of the surface area. The computational details will be described in detail in a forthcoming publication.

# MTW pore landscape

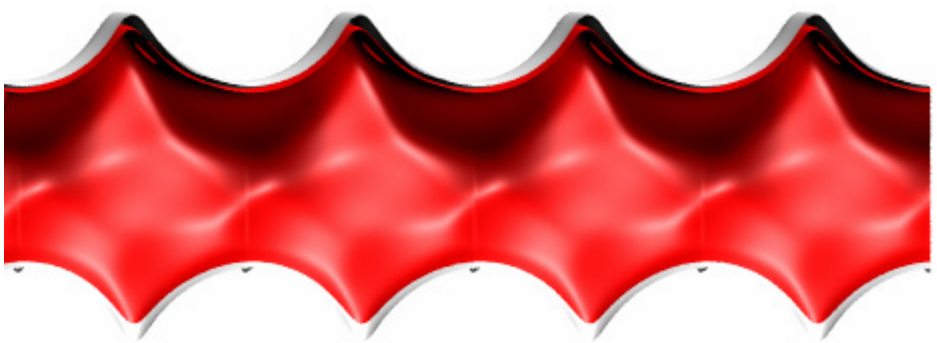

MTW has 1D, 12-ring channels

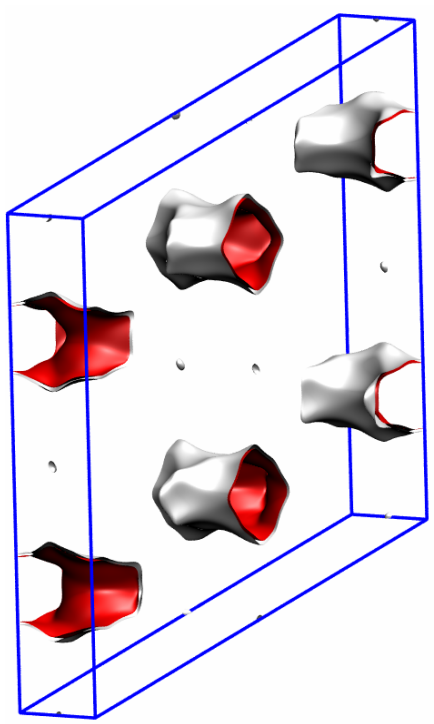

# MTW pore dimensions

This plot of surface area versus pore dimension is determined using a combination of the DeLaunay triangulation method for pore dimension determination, and the procedure of Düren for determination of the surface area. The computational details will be described in detail in a forthcoming publication.

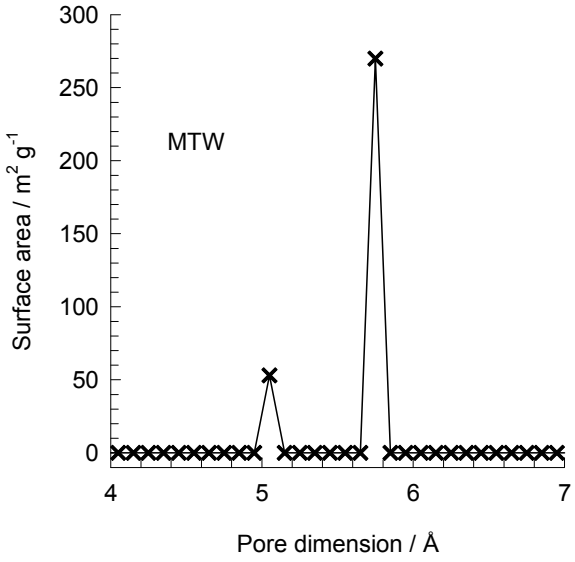


MTW has 1D, 12-ring channels

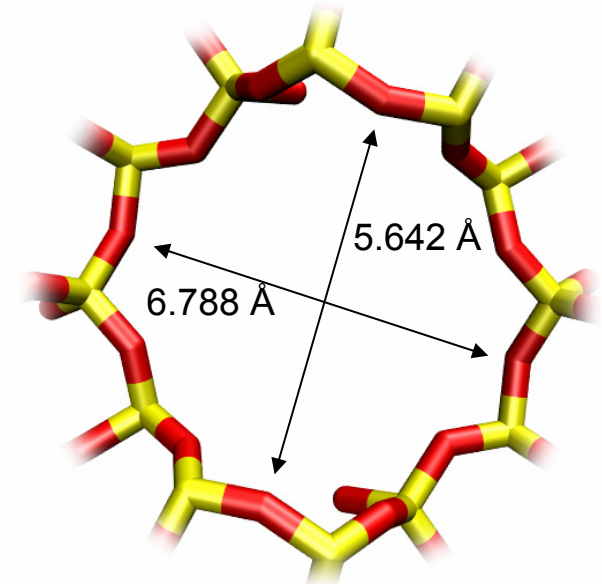


| | MTW |
|---|---|
| *a* /Å | 24.863 |
| *b* /Å | 5.012 |
| *c* /Å | 24.326 |
| Cell volume / Å$^3$ | 2887.491 |
| conversion factor for [molec/uc] to [mol per kg Framework] | 0.2972 |
| conversion factor for [molec/uc] to [kmol/m$^3$] | 2.6759 |
| $\rho$ [kg/m3] | 1935.031 |
| MW unit cell [g/mol(framework)] | 3364.749 |
| $\phi$, fractional pore volume | 0.215 |
| open space / Å$^3$/uc | 620.6 |
| Pore volume / cm$^3$/g | 0.111 |
| Surface area /m$^2$/g | 323.0 |
| DeLaunay diameter /Å | 5.69 |

# SOD-Si pore landscape

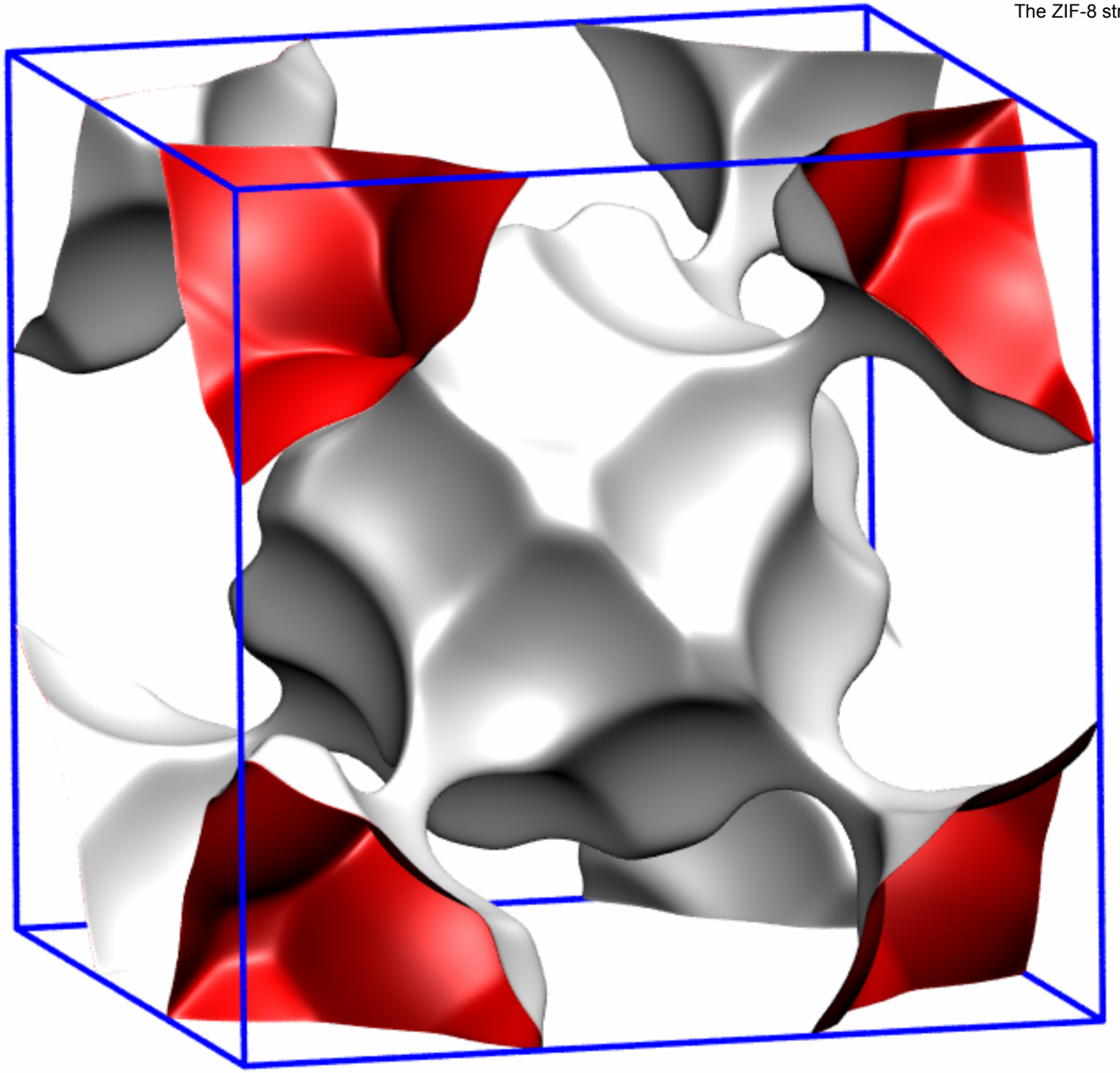

The ZIF-8 structure is analogous to that of SOD.

# SOD-Si dimensions

| | SOD-Si |
|---|---|
| *a* /Å | 8.89 |
| *b* /Å | 8.89 |
| *c* /Å | 8.89 |
| Cell volume / $Å^3$ | 702.5954 |
| conversion factor for [molec/uc] to [mol per kg Framework] | 1.3869 |
| conversion factor for [molec/uc] to [kmol/$m^3$] | 9.7908 |
| $\rho$ [kg/m3] | 1704.106 |
| MW unit cell [g/mol(framework)] | 721.0176 |
| $\phi$, fractional pore volume | 0.241 |
| open space / $Å^3$/uc | 169.6 |
| Pore volume / $cm^3$/g | 0.142 |
| Surface area /$m^2$/g | |
| DeLaunay diameter /Å | 2.47 |

# TON pore landscape

10-ring channel of TON

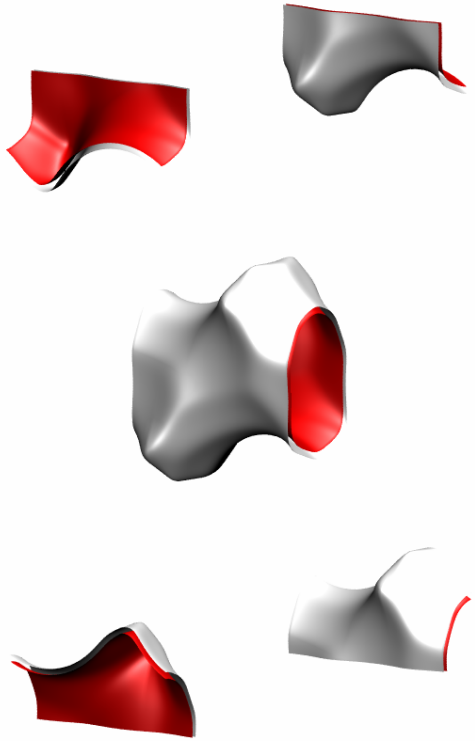

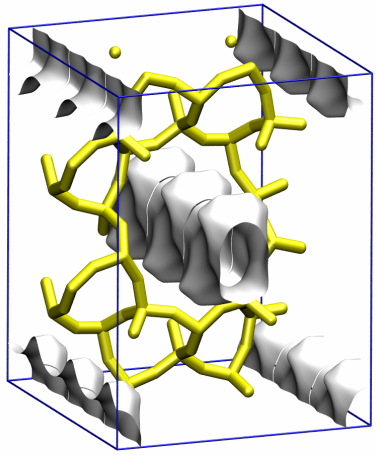

# TON pore dimensions

This plot of surface area versus pore dimension is determined using a combination of the DeLaunay triangulation method for pore dimension determination, and the procedure of Düren for determination of the surface area. The computational details will be described in detail in a forthcoming publication.

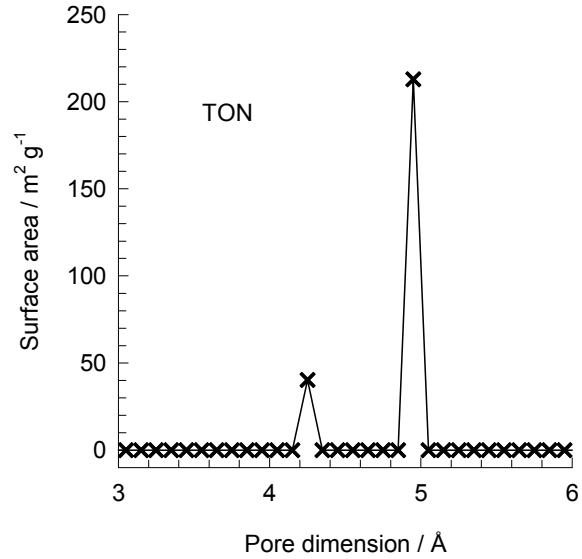


## 10-ring channel of TON

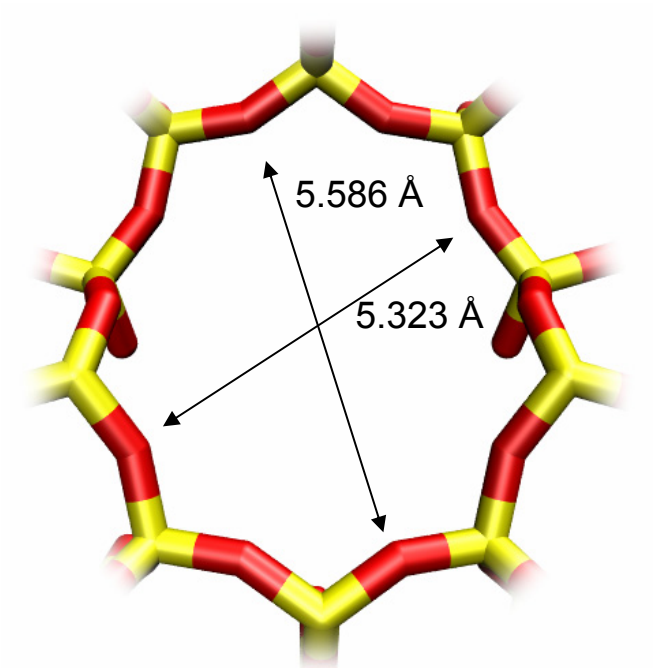


| | TON |
|---|---|
| *a* /Å | 13.859 |
| *b* /Å | 17.42 |
| *c* /Å | 5.038 |
| Cell volume / Å$^3$ | 1216.293 |
| conversion factor for [molec/uc] to [mol per kg Framework] | 0.6935 |
| conversion factor for [molec/uc] to [kmol/m$^3$] | 7.1763 |
| $\rho$ [kg/m3] | 1968.764 |
| MW unit cell [g/mol(framework)] | 1442.035 |
| $\phi$, fractional pore volume | 0.190 |
| open space / Å$^3$/uc | 231.4 |
| Pore volume / cm$^3$/g | 0.097 |
| Surface area /m$^2$/g | 253.0 |
| DeLaunay diameter /Å | 4.88 |

# TSC landscape

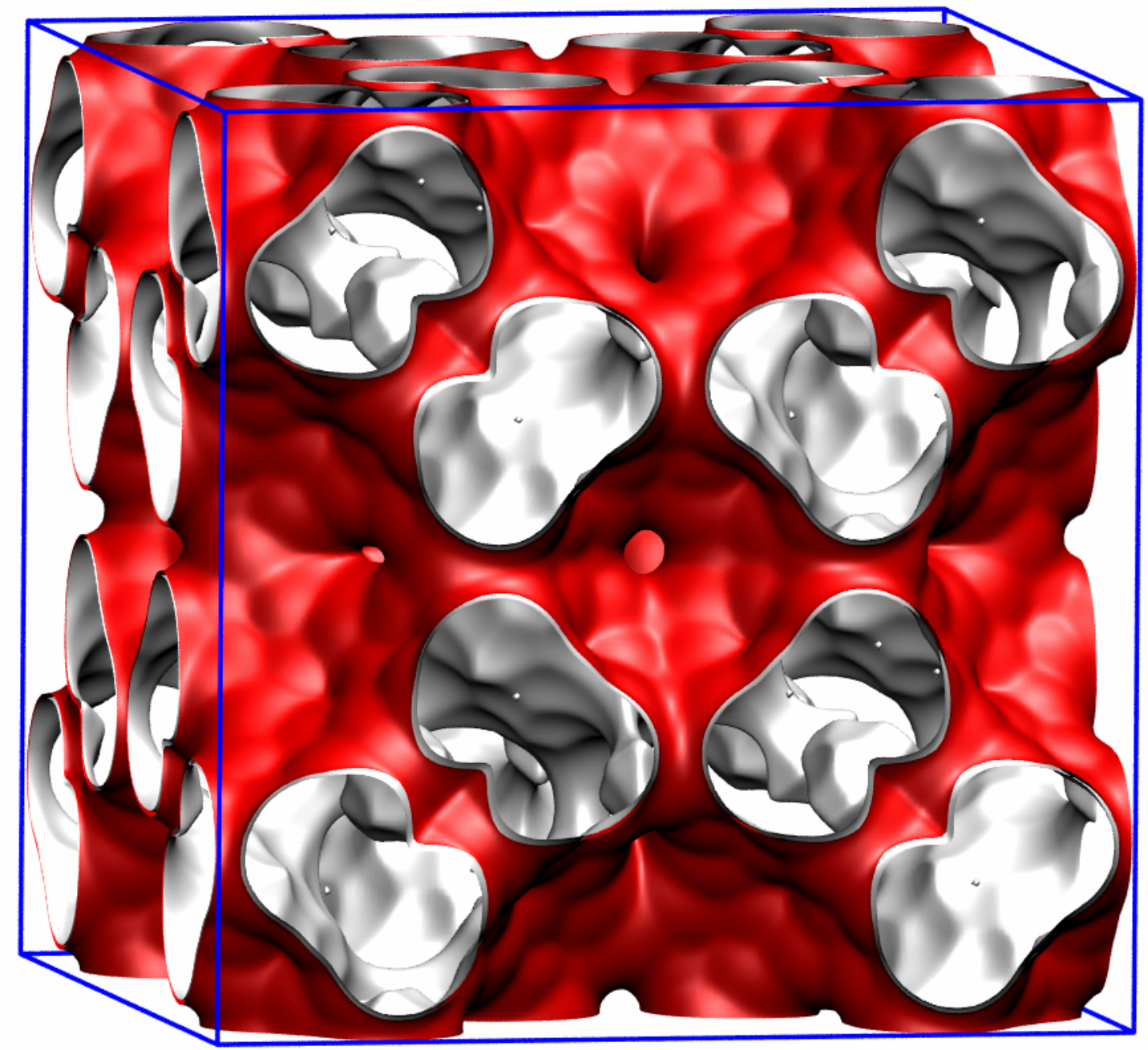

Unit cell of TSC

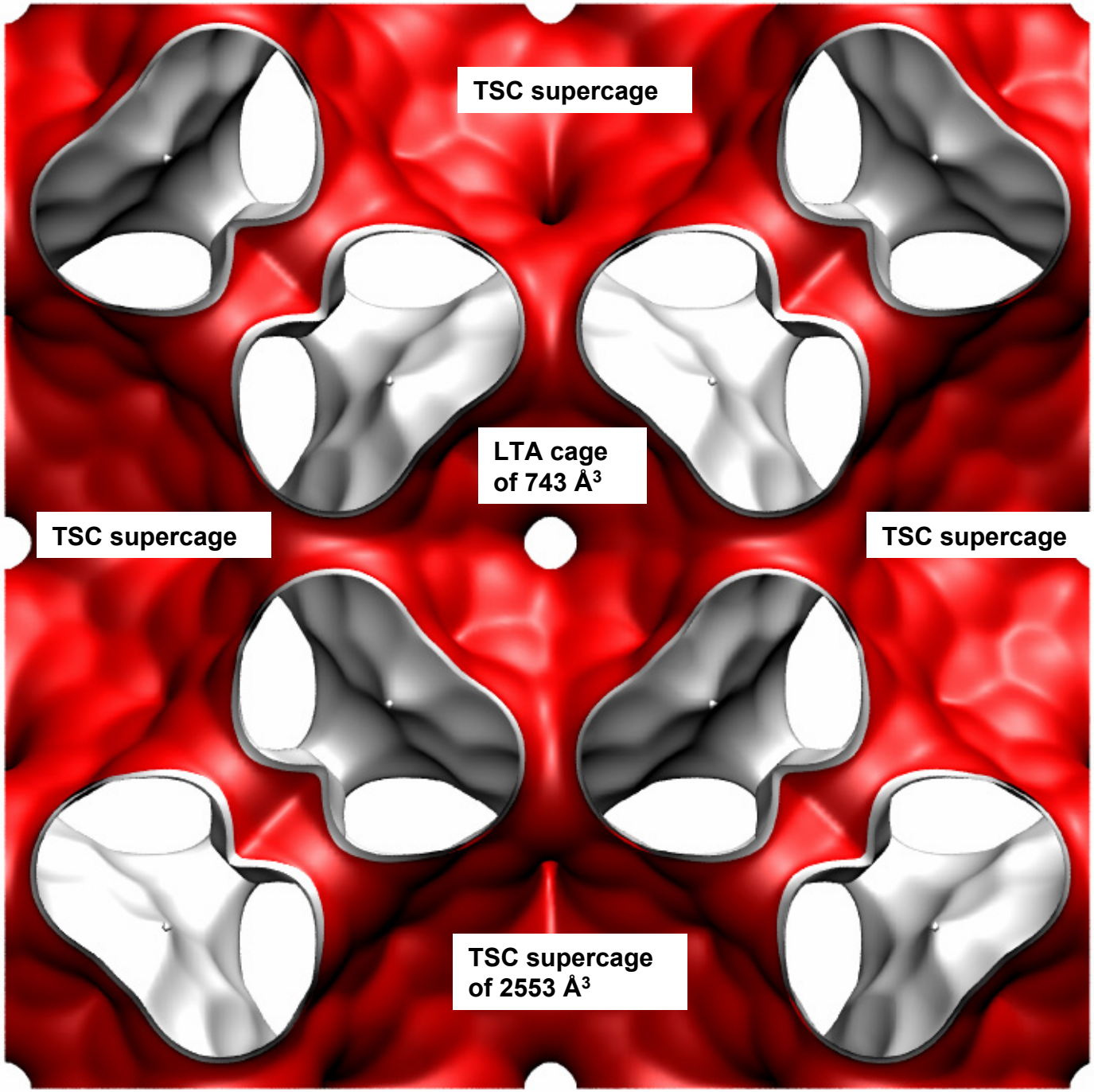


**8-ring windows of two sizes:**
**4.2x4.2 Å along [100]**
**3.1x5.6 Å along [110]**

# Front plane of unit cell of TSC

# TSC window and pore dimensions

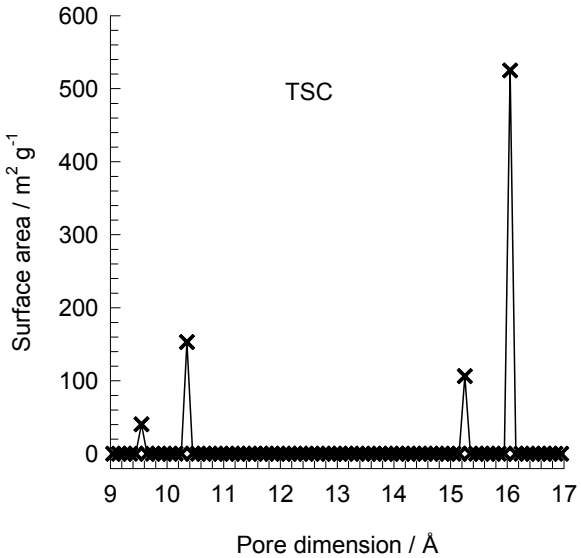


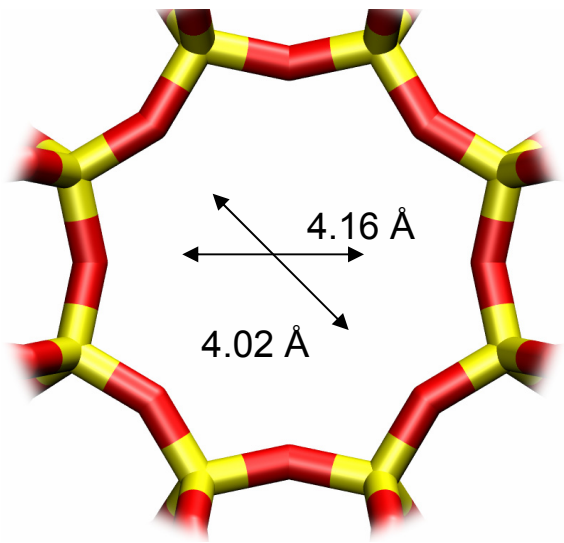


TSC
(supercage - cage)

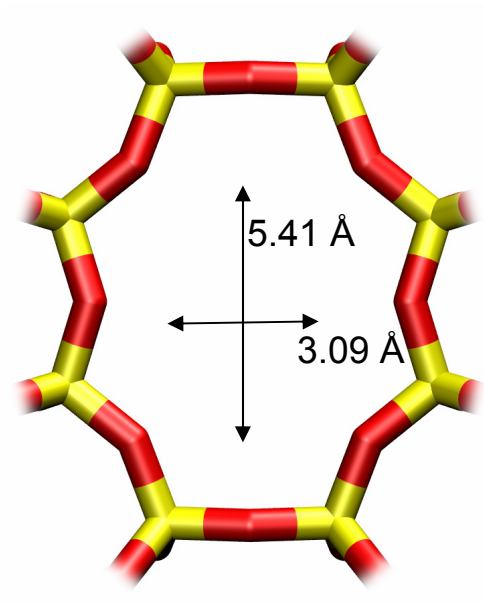


TSC
(supercage - pocket)

| | TSC |
|---|---|
| *a* /Å | 30.742 |
| *b* /Å | 30.742 |
| *c* /Å | 30.742 |
| Cell volume / Å$^3$ | 29053.36 |
| conversion factor for [molec/uc] to [mol per kg Framework] | 0.0433 |
| conversion factor for [molec/uc] to [kmol/m$^3$] | 0.1260 |
| $\rho$ [kg/m3] | 1318.729 |
| MW unit cell [g/mol(framework)] | 23072.56 |
| $\phi$, fractional pore volume | 0.454 |
| open space / Å$^3$/uc | 13182.6 |
| Pore volume / cm$^3$/g | 0.344 |
| Surface area /m$^2$/g | 829.0 |
| DeLaunay diameter /Å | 4.02 |

The window dimension calculated using the van der Waals diameter of framework atoms = 2.7 Å are indicated above by the arrows. It is likely that the pockets are inaccessible due to the narrow constriction of 3.092 Å. Another point to note is that the dimensions provided in the IZA website do not appear to be correct for the window on the left.

# Zeolites with cations

# NaY (144 Si, 48 Al, 48 Na+, Si/Al=3)

Blue spheres are cations

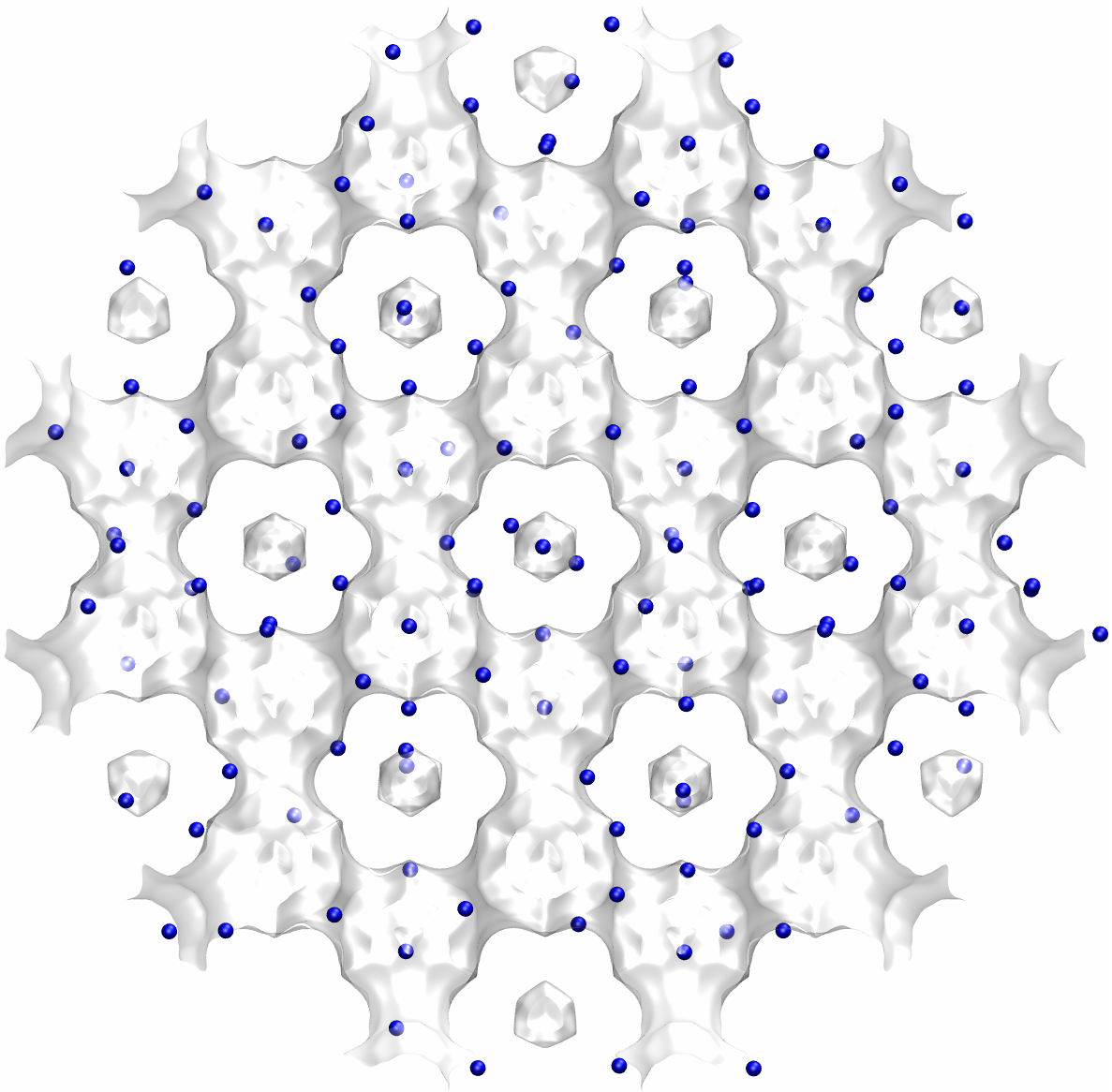

| | FAU-48Al |
|---|---|
| *a* /Å | 25.028 |
| *b* /Å | 25.028 |
| *c* /Å | 25.028 |
| Cell volume / Å$^3$ | 15677.56 |
| conversion factor for [molec/uc] to [mol per kg Framework] | 0.0794 |
| conversion factor for [molec/uc] to [kmol/m$^3$] | 0.2596 |
| $\rho$ [kg/m3] (with cations) | 1333.19 |
| MW unit cell [g/mol(framework+cations)] | 12586.78 |
| $\phi$, fractional pore volume | 0.408 |
| open space / Å$^3$/uc | 6396.6 |
| Pore volume / cm$^3$/g | 0.306 |
| Surface area /m$^2$/g | |
| DeLaunay diameter /Å | 7.37 |

# NaY (138 Si, 54 Al, 54 Na+, Si/Al=2.55)

Blue spheres are cations

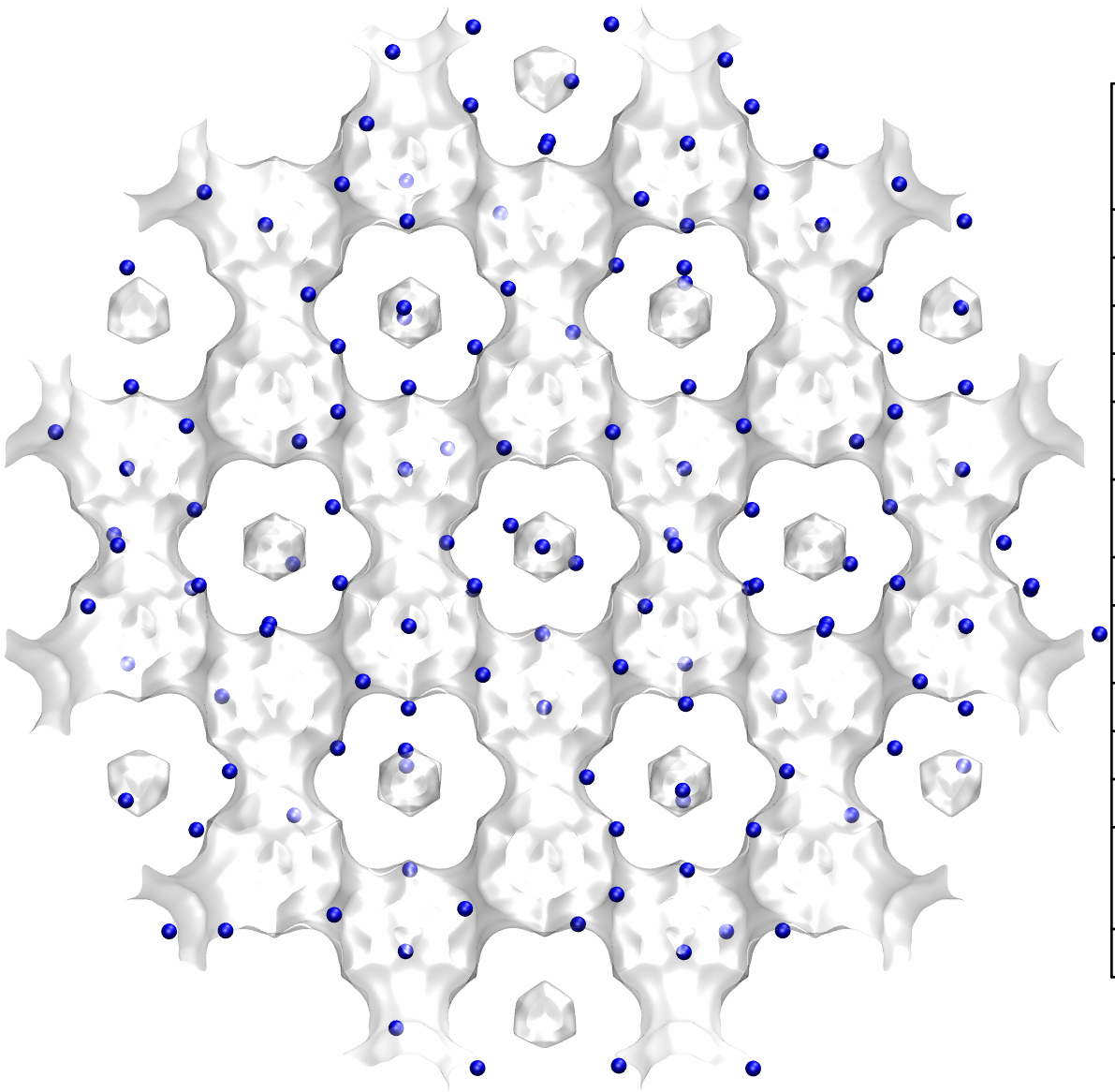

| | FAU-54Al |
|---|---|
| *a* /Å | 25.028 |
| *b* /Å | 25.028 |
| *c* /Å | 25.028 |
| Cell volume / Å$^3$ | 15677.56 |
| conversion factor for [molec/uc] to [mol per kg Framework] | 0.0786 |
| conversion factor for [molec/uc] to [kmol/m$^3$] | 0.2596 |
| $\rho$ [kg/m3] (with cations) | 1347.1 |
| MW unit cell [g/mol(framework+cations)] | 12718.08 |
| $\phi$, fractional pore volume | 0.408 |
| open space / Å$^3$/uc | 6396.6 |
| Pore volume / cm$^3$/g | 0.303 |
| Surface area /m$^2$/g | |
| DeLaunay diameter /Å | 7.37 |

# NaX (106 Si, 86 Al, 86 Na+, Si/Al=1.23)

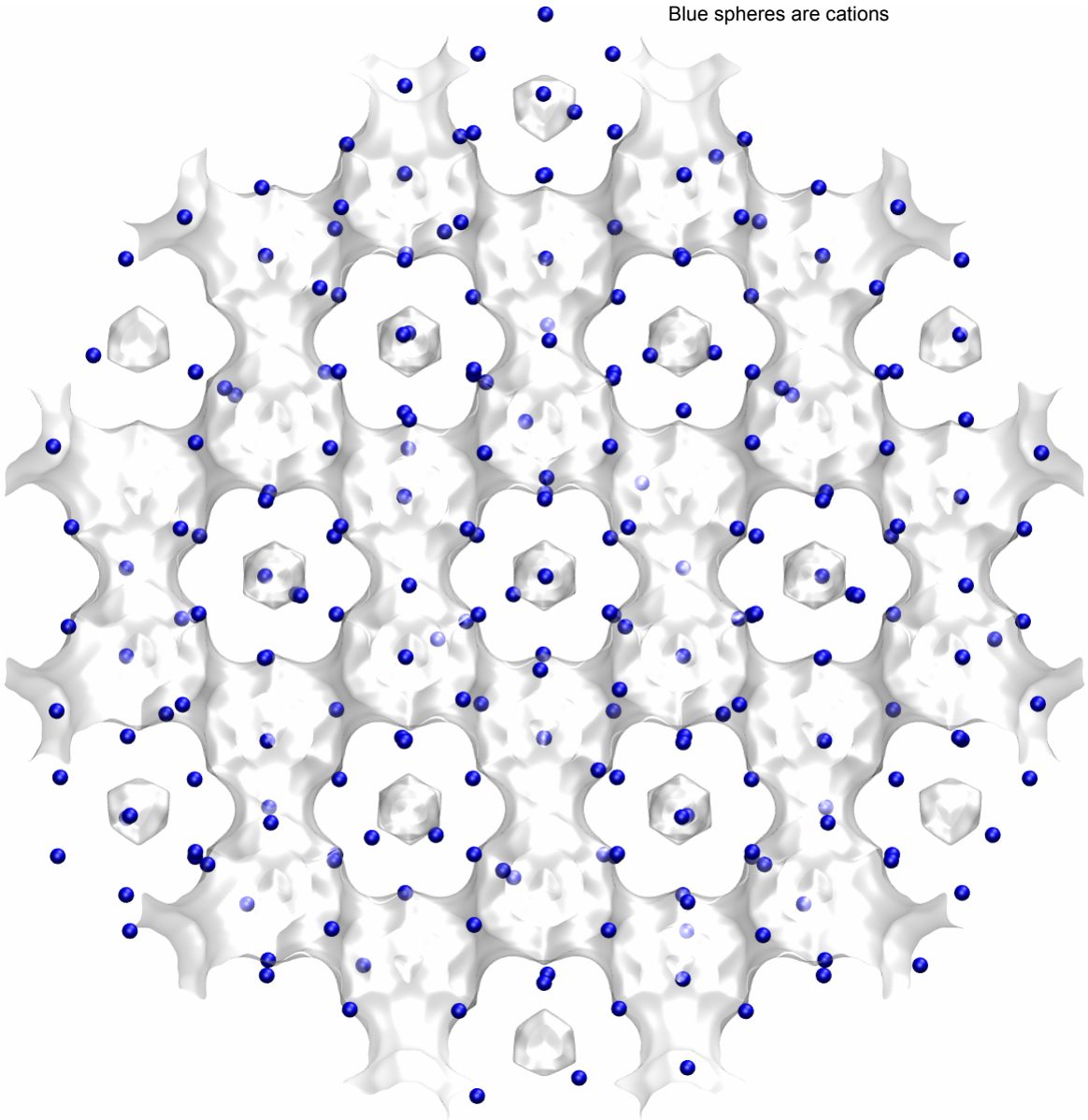


| | FAU-86Al |
|---|---|
| *a* /Å | 25.028 |
| *b* /Å | 25.028 |
| *c* /Å | 25.028 |
| Cell volume / Å$^3$ | 15677.56 |
| conversion factor for [molec/uc] to [mol per kg Framework] | 0.0745 |
| conversion factor for [molec/uc] to [kmol/m$^3$] | 0.2658 |
| $\rho$ [kg/m3] (with cations) | 1421.277 |
| MW unit cell [g/mol(framework+cations)] | 13418.42 |
| $\phi$, fractional pore volume | 0.399 |
| open space / Å$^3$/uc | 6248.0 |
| Pore volume / cm$^3$/g | 0.280 |
| Surface area /m$^2$/g | |
| DeLaunay diameter /Å | 7.37 |

# LTA-5A

## LTA-5A (32 Na+, 32 Ca++)

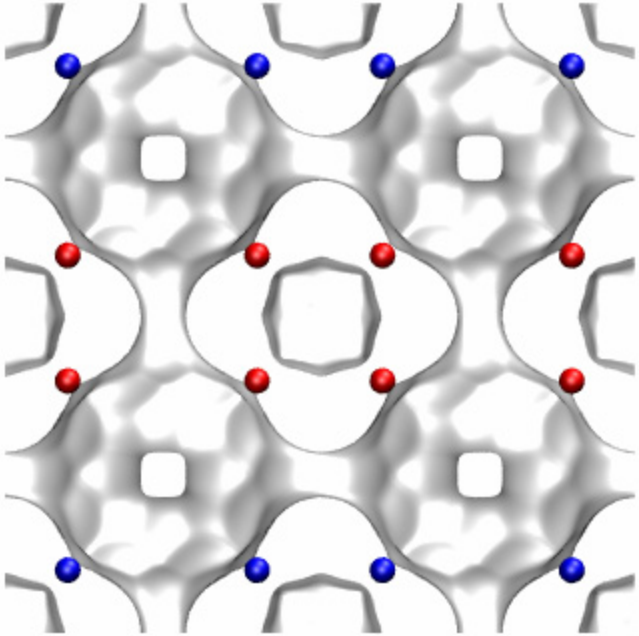

# LTA-5A

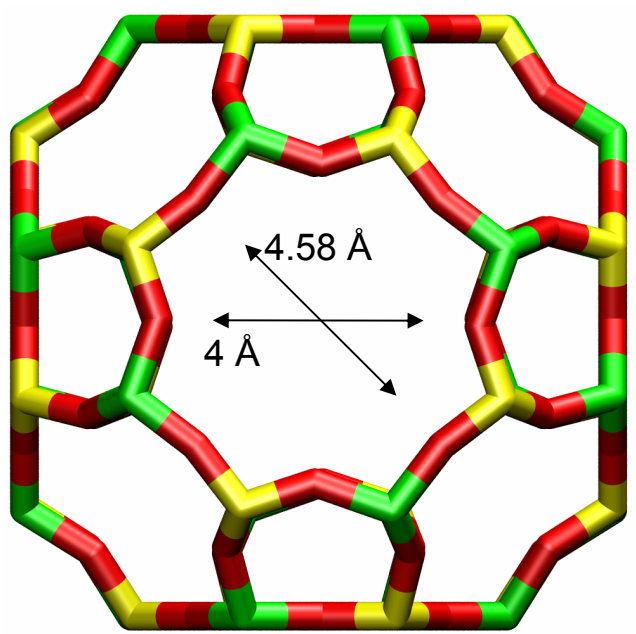


LTA-5A

The window dimension calculated using the van der Waals diameter of framework atoms = 2.7 Å is indicated above by the arrow.

| | LTA-5A |
|---|---|
| *a* /Å | 24.555 |
| *b* /Å | 24.555 |
| *c* /Å | 24.555 |
| Cell volume / Å$^3$ | 14805.39 |
| conversion factor for [molec/uc] to [mol per kg Framework] | 0.0744 |
| conversion factor for [molec/uc] to [kmol/m$^3$] | 0.2955 |
| $\rho$ [kg/m3] (with cations) | 1508.376 |
| MW unit cell [g/mol(framework+cations)] | 13448.48 |
| $\phi$, fractional pore volume | 0.380 |
| open space / Å$^3$/uc | 5620.4 |
| Pore volume / cm$^3$/g | 0.252 |
| Surface area /m$^2$/g | |
| DeLaunay diameter /Å | 4.00 |

# LTA-4A

## LTA-4A (96 Na+)

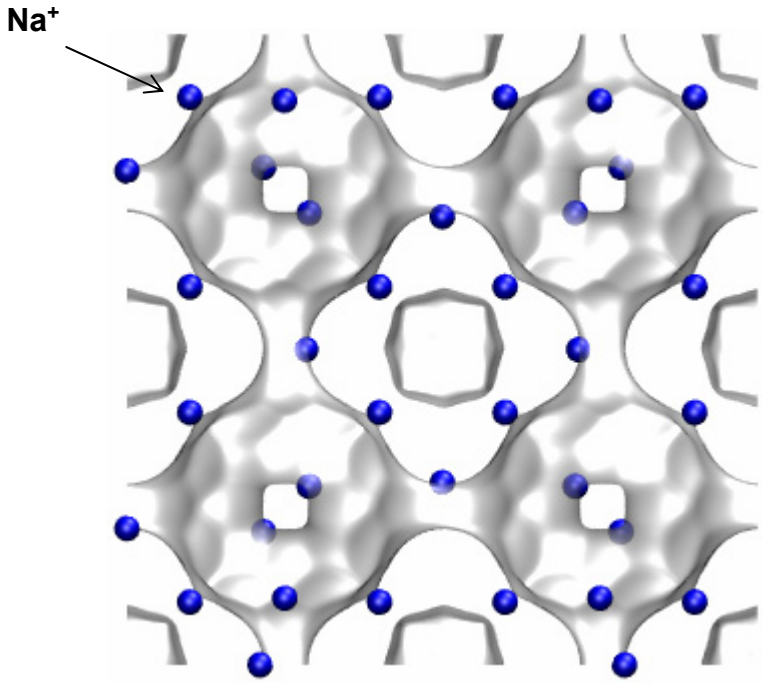

# LTA-4A

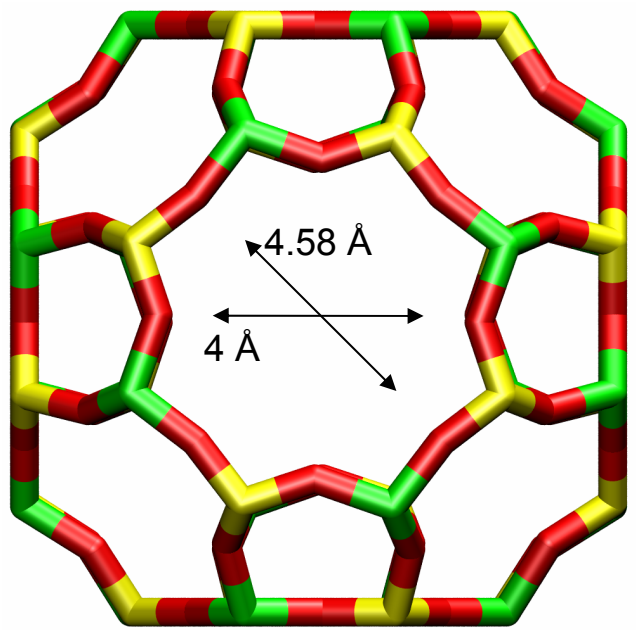


LTA-4A

| | LTA-4A |
|---|---|
| *a* /Å | 24.555 |
| *b* /Å | 24.555 |
| *c* /Å | 24.555 |
| Cell volume / Å$^3$ | 14805.39 |
| conversion factor for [molec/uc] to [mol per kg Framework] | 0.0733 |
| conversion factor for [molec/uc] to [kmol/m$^3$] | 0.2991 |
| $\rho$ [kg/m3] (with cations) | 1529.55 |
| MW unit cell [g/mol(framework+cations)] | 13637.27 |
| $\phi$, fractional pore volume | 0.375 |
| open space / Å$^3$/uc | 5552.0 |
| Pore volume / cm$^3$/g | 0.245 |
| Surface area /m$^2$/g | |
| DeLaunay diameter /Å | 4.00 |

The window dimension calculated using the van der Waals diameter of framework atoms = 2.7 Å is indicated above by the arrow.

Note that the $Na^+$ ions partially block the windows and therefore the diffusivities in LTA-4A are significantly lower than that for LTA Si. These cannot be determined from MD.

# MOFs and ZIFs (in alphabetical order, but MOF-74 with Co, Mg, Ni, and Zn are kept together)

# BeBTB pore landscapes

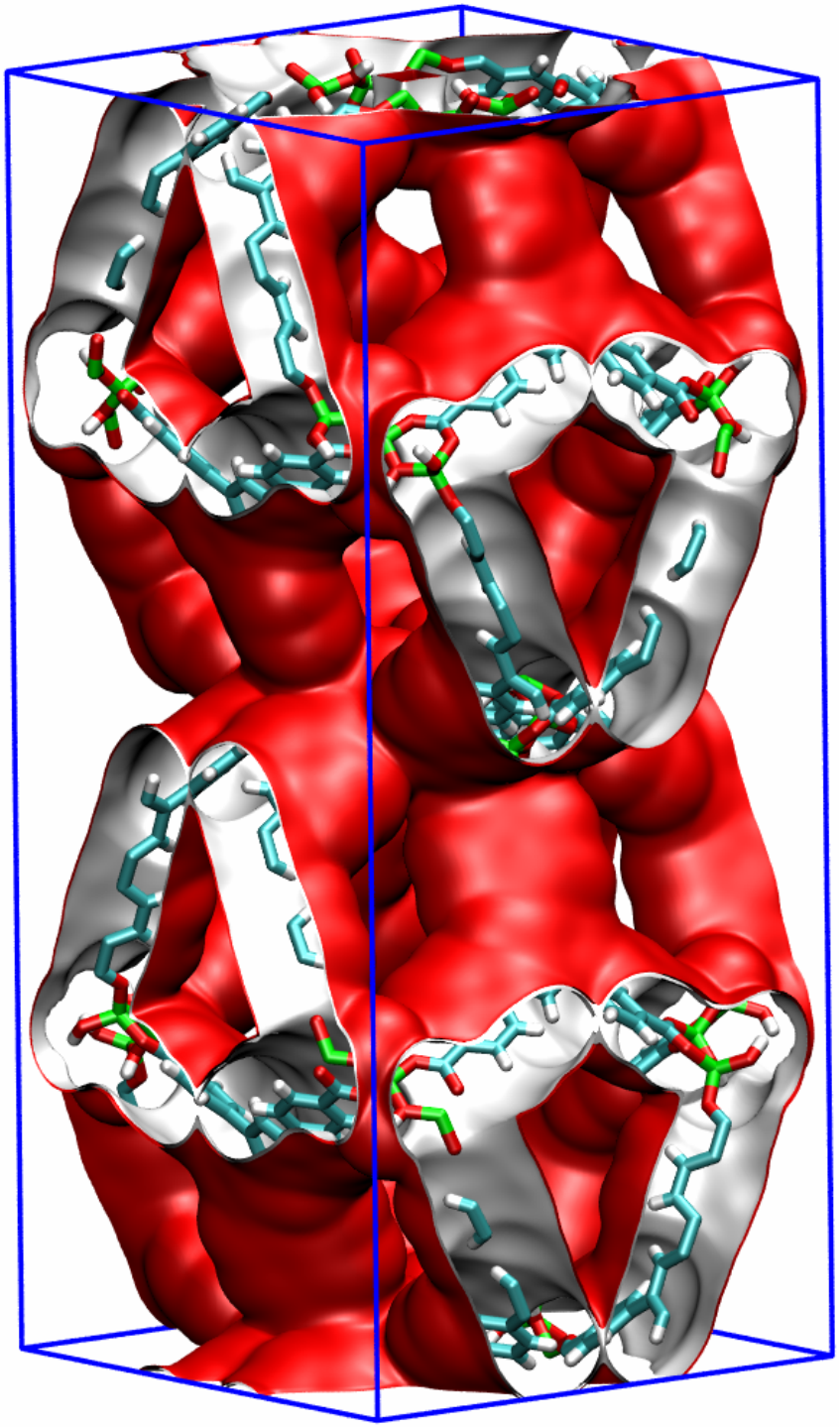

# BeBTB pore dimensions

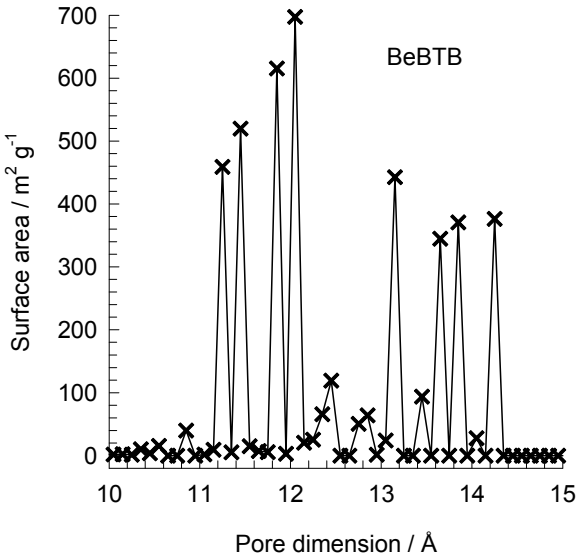


This plot of surface area versus pore dimension is determined using a combination of the DeLaunay triangulation method for pore dimension determination, and the procedure of Düren for determination of the surface area. The computational details will be described in detail in a forthcoming publication.

| | BeBTB |
|---|---|
| *a* /Å | 24.3013 |
| *b* /Å | 24.3013 |
| *c* /Å | 54.57 |
| Cell volume / $Å^3$ | 32226.49 |
| conversion factor for [molec/uc] to [mol per kg Framework] | 0.1218 |
| conversion factor for [molec/uc] to [kmol/$m^3$] | 0.0638 |
| $\rho$ [kg/m3] | 423.0851 |
| MW unit cell [g/mol(framework)] | 8210.785 |
| $\phi$, fractional pore volume | 0.807 |
| open space / $Å^3$/uc | 26013.8 |
| Pore volume / $cm^3$/g | 1.908 |
| Surface area /$m^2$/g | 4706.0 |
| DeLaunay diameter /Å | |

# Co(BDP) pore landscapes

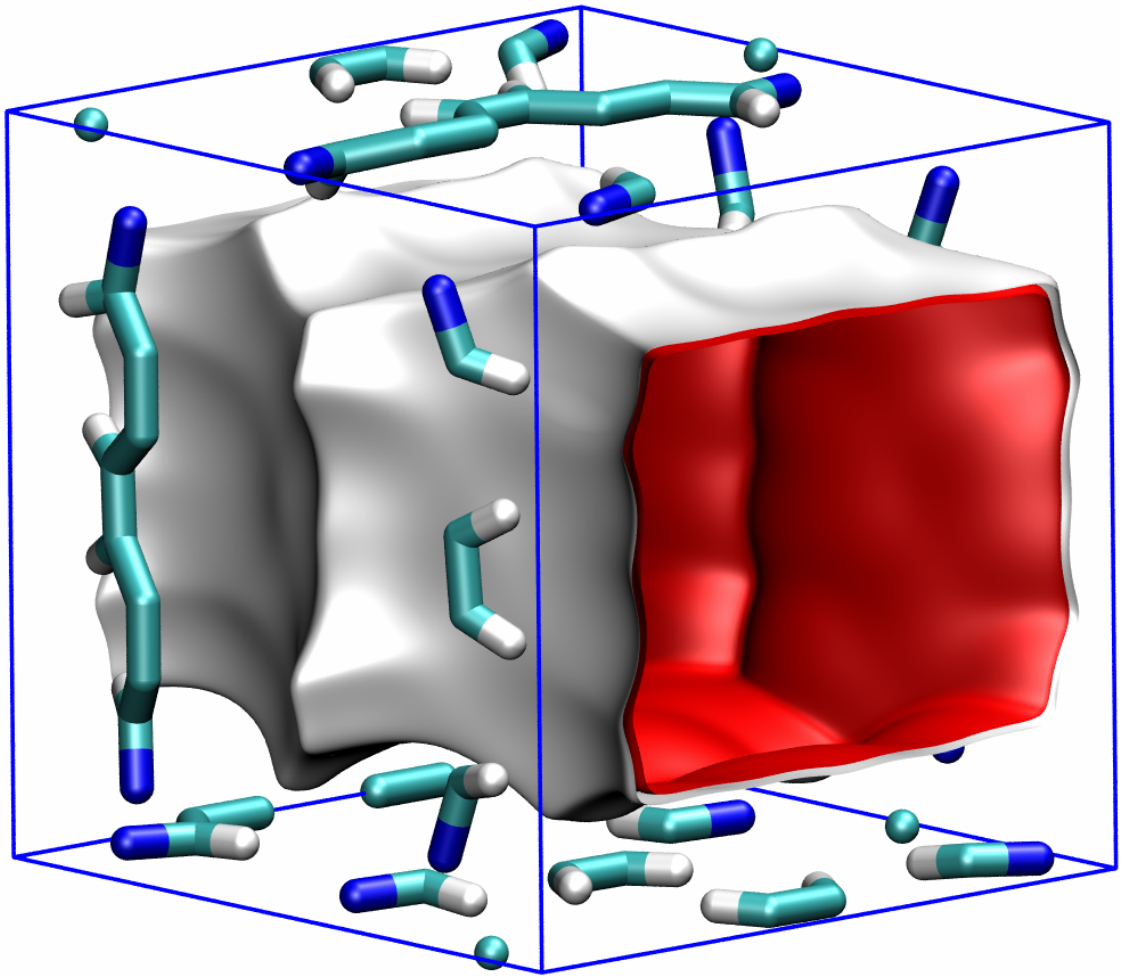

# Co(BDP) pore dimensions

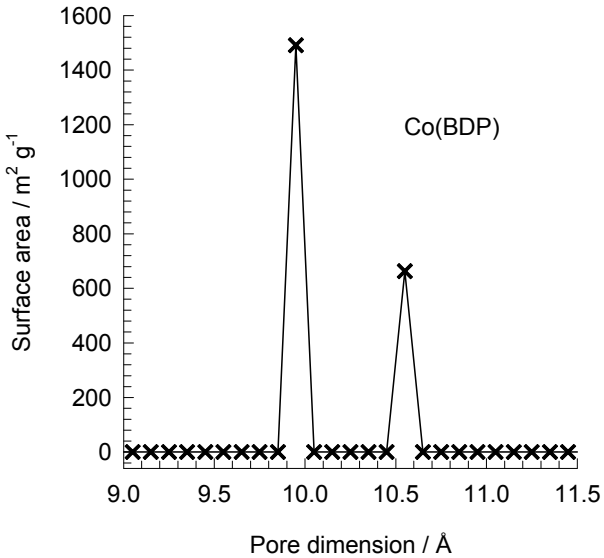


This plot of surface area versus pore dimension is determined using a combination of the DeLaunay triangulation method for pore dimension determination, and the procedure of Düren for determination of the surface area. The computational details will be described in detail in a forthcoming publication.

| | CoBDP |
|---|---|
| *a* /Å | 13.2529 |
| *b* /Å | 13.253 |
| *c* /Å | 13.995 |
| Cell volume / $Å^3$ | 2458.091 |
| conversion factor for [molec/uc] to [mol per kg Framework] | 0.9362 |
| conversion factor for [molec/uc] to [kmol/$m^3$] | 1.0102 |
| $\rho$ [kg/m3] | 721.5517 |
| MW unit cell [g/mol(framework)] | 1068.094 |
| $\phi$, fractional pore volume | 0.669 |
| open space / $Å^3$/uc | 1643.9 |
| Pore volume / $cm^3$/g | 0.927 |
| Surface area /$m^2$/g | 2148.8 |
| DeLaunay diameter /Å | 10 |

# CuBTC pore landscapes

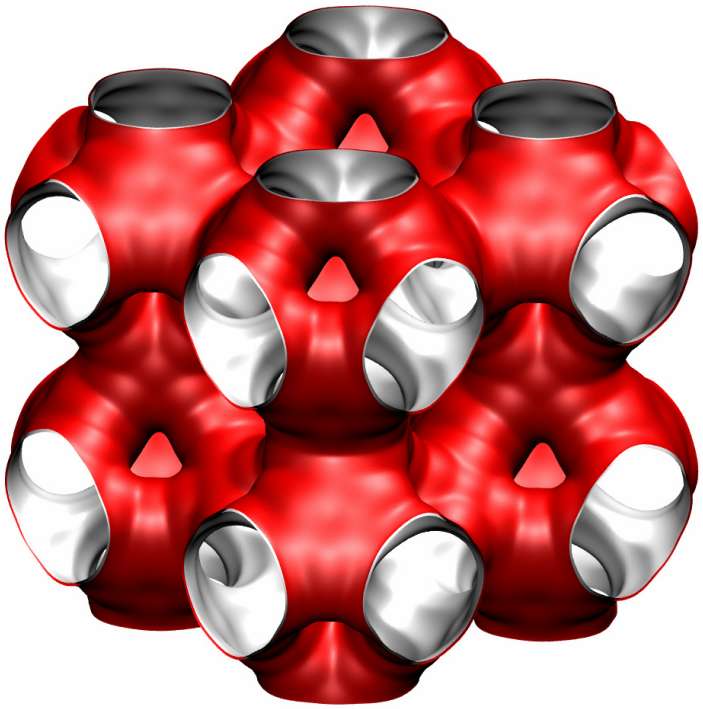

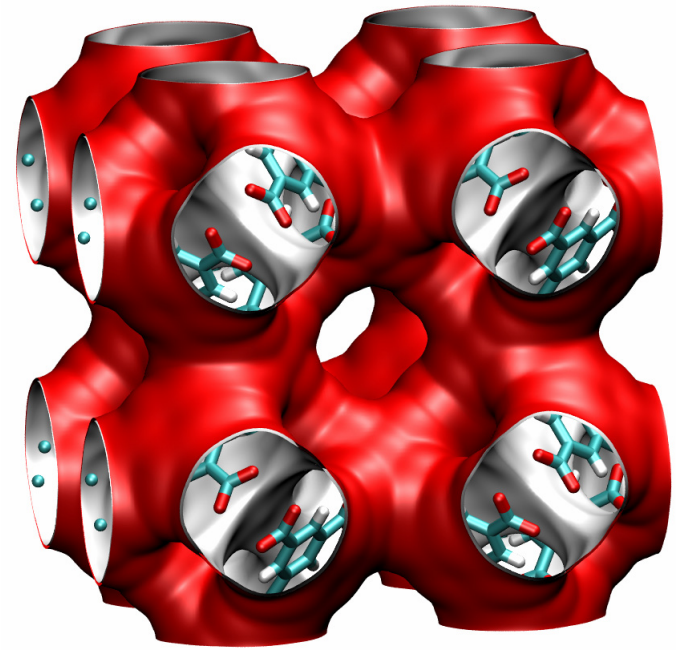

Snapshot of $CO_2/CH_4$ mixture

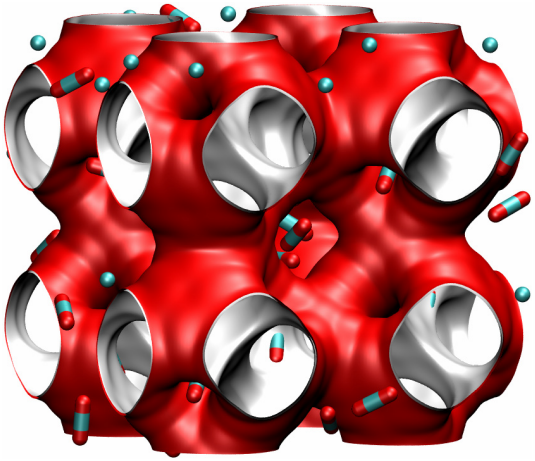

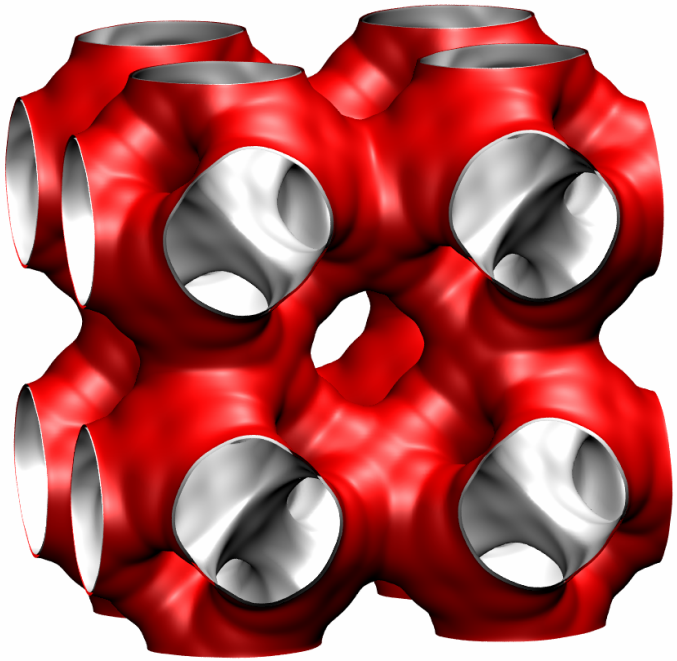

# CuBTC pore dimensions

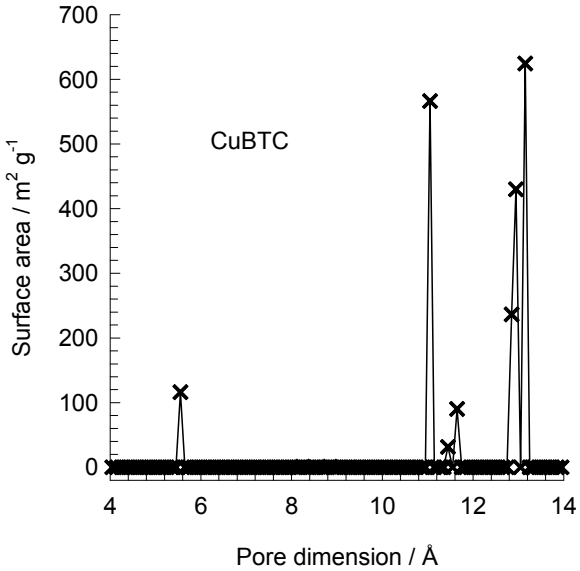


This plot of surface area versus pore dimension is determined using a combination of the DeLaunay triangulation method for pore dimension determination, and the procedure of Düren for determination of the surface area. The computational details will be described in detail in a forthcoming publication.

| | CuBTC |
|---|---|
| *a* /Å | 26.343 |
| *b* /Å | 26.343 |
| *c* /Å | 26.343 |
| Cell volume / Å$^3$ | 18280.82 |
| conversion factor for [molec/uc] to [mol per kg Framework] | 0.1034 |
| conversion factor for [molec/uc] to [kmol/m$^3$] | 0.1218 |
| $\rho$ [kg/m3] | 878.8298 |
| MW unit cell [g/mol(framework)] | 9674.855 |
| $\phi$, fractional pore volume | 0.746 |
| open space / Å$^3$/uc | 13628.4 |
| Pore volume / cm$^3$/g | 0.848 |
| Surface area /m$^2$/g | 2097.0 |
| DeLaunay diameter /Å | 6.23 |

# CuBTT pore landscapes

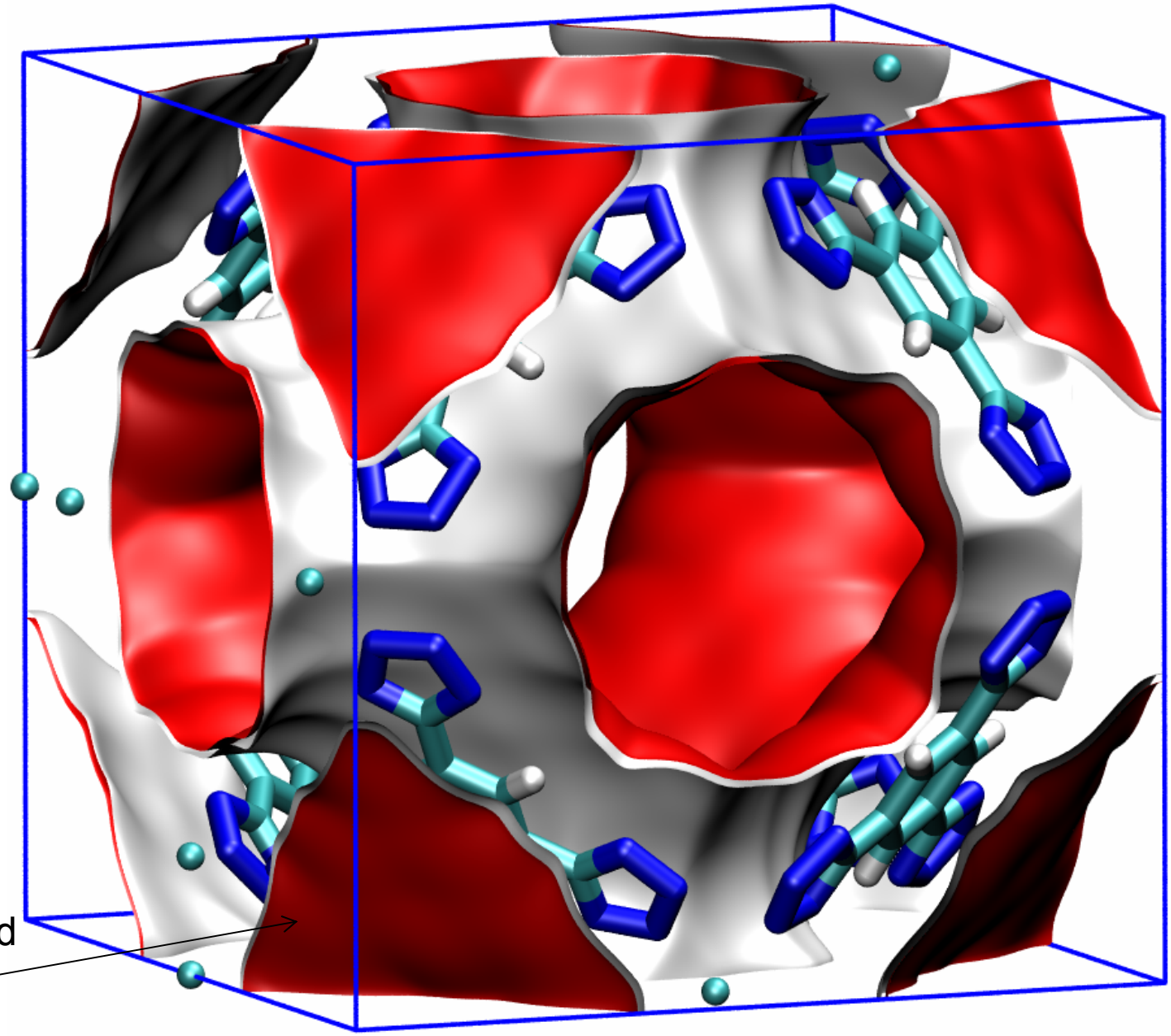

These inaccessible pockets were blocked in our simulations

# CuBTT pore dimensions

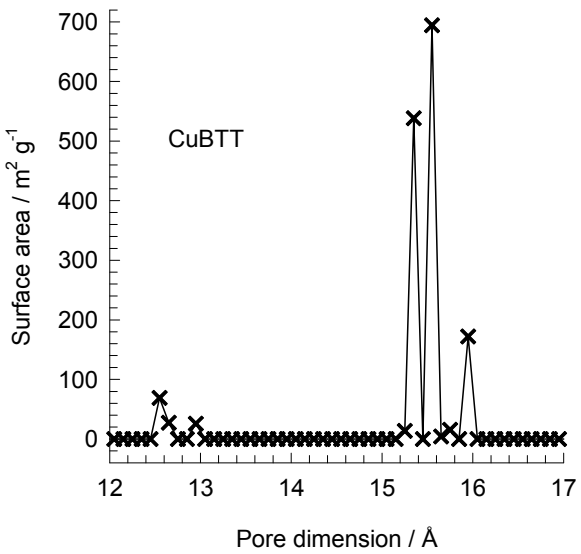


This plot of surface area versus pore dimension is determined using a combination of the DeLaunay triangulation method for pore dimension determination, and the procedure of Düren for determination of the surface area. The computational details will be described in detail in a forthcoming publication.

| | CuBTT (blocked) |
|---|---|
| *a* /Å | 18.595 |
| *b* /Å | 18.595 |
| *c* /Å | 18.595 |
| Cell volume / Å$^3$ | 6429.668 |
| conversion factor for [molec/uc] to [mol per kg Framework] | 0.3224 |
| conversion factor for [molec/uc] to [kmol/m$^3$] | 0.4547 |
| $\rho$ [kg/m3] | 801.0756 |
| MW unit cell [g/mol(framework)] | 3101.745 |
| $\phi$, fractional pore volume | 0.568 |
| open space / Å$^3$/uc | 3652.1 |
| Pore volume / cm$^3$/g | 0.709 |
| Surface area /m$^2$/g | 1564.6 |
| DeLaunay diameter /Å | 9.99 |

# IRMOF-1 pore landscape

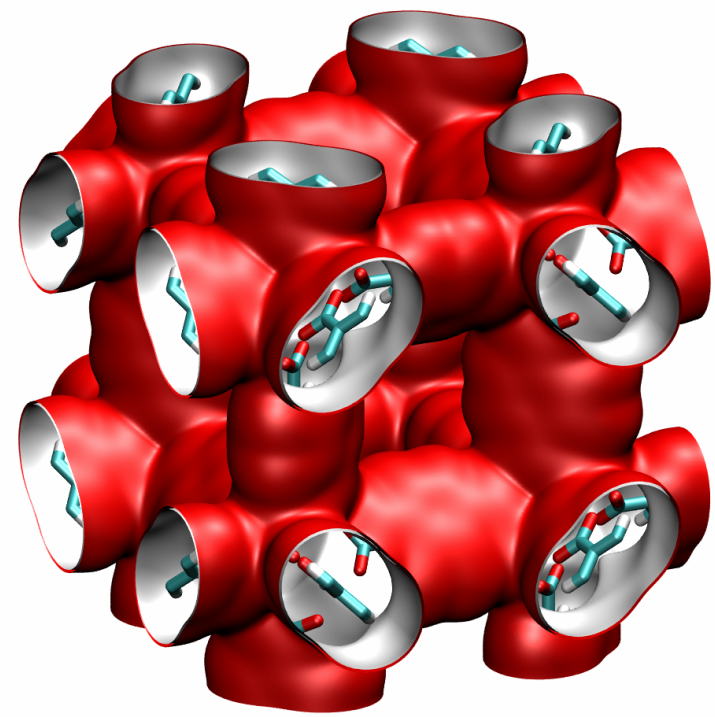

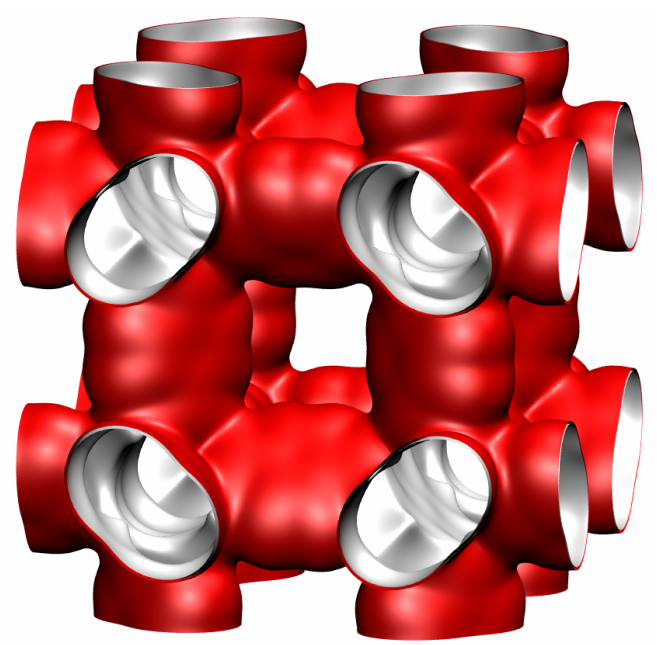

Snapshot of $CO_2/CH_4$ mixture

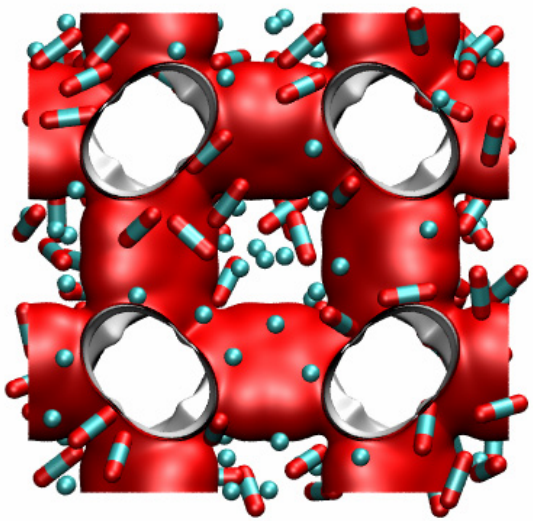

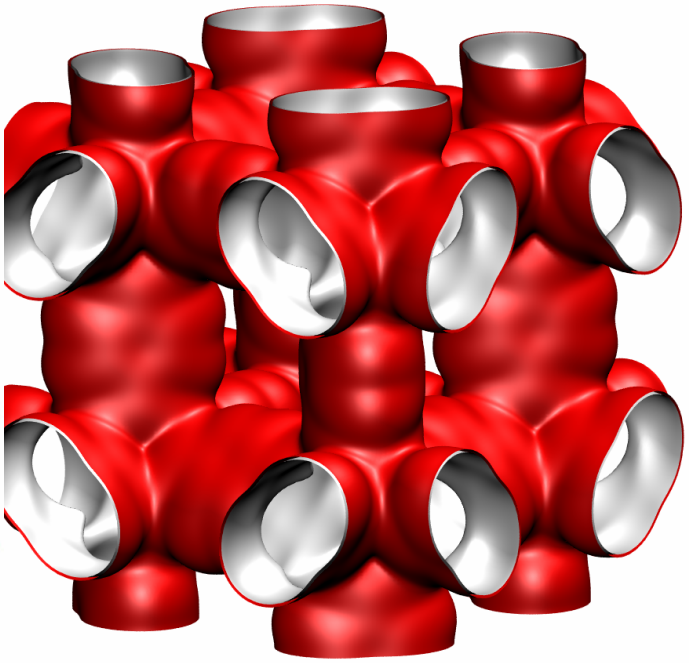

# IRMOF-1 pore dimensions

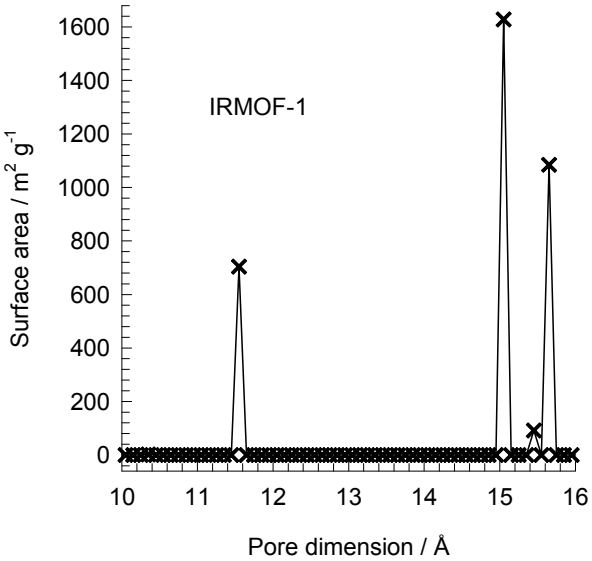


This plot of surface area versus pore dimension is determined using a combination of the DeLaunay triangulation method for pore dimension determination, and the procedure of Düren for determination of the surface area. The computational details will be described in detail in a forthcoming publication.

| | IRMOF-1 |
|---|---|
| *a* /Å | 25.832 |
| *b* /Å | 25.832 |
| *c* /Å | 25.832 |
| Cell volume / Å$^3$ | 17237.49 |
| conversion factor for [molec/uc] to [mol per kg Framework] | 0.1624 |
| conversion factor for [molec/uc] to [kmol/m$^3$] | 0.1186 |
| $\rho$ [kg/m3] | 593.2075 |
| MW unit cell [g/mol(framework)] | 6157.788 |
| $\phi$, fractional pore volume | 0.812 |
| open space / Å$^3$/uc | 13996.3 |
| Pore volume / cm$^3$/g | 1.369 |
| Surface area /m$^2$/g | 3522.2 |
| DeLaunay diameter /Å | 7.38 |

# MIL–47 pore landscape

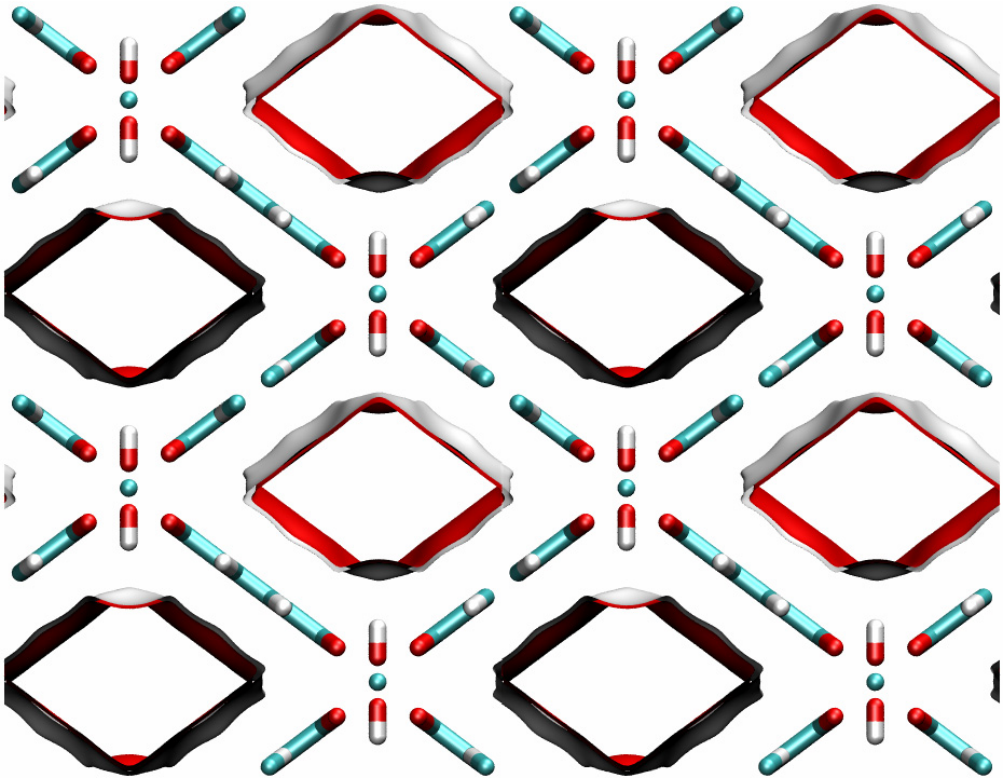

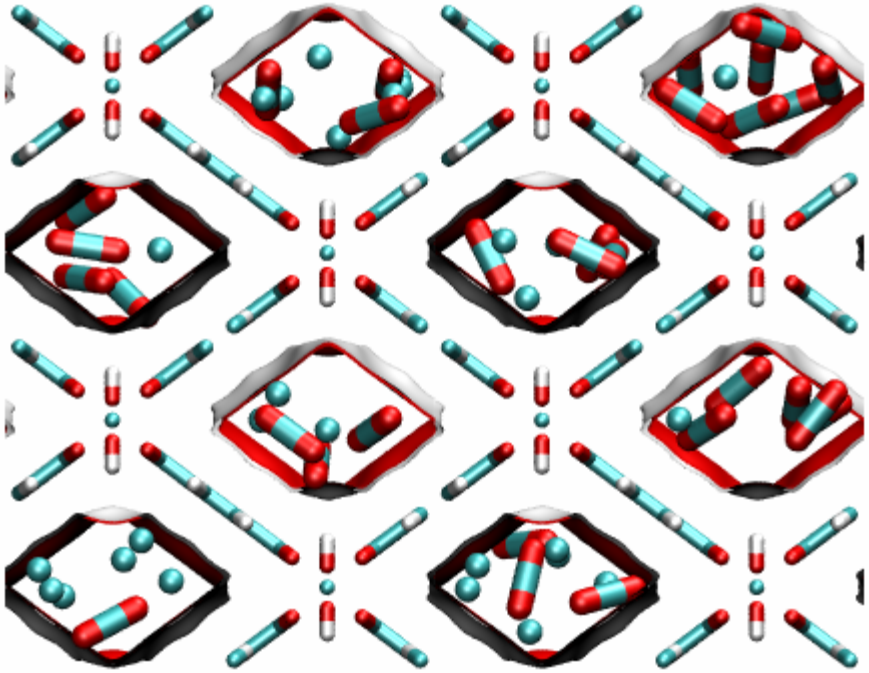

Snapshot of $CO_2/CH_4$ mixture

# MIL–47 dimensions

| | MIL-47 |
|---|---|
| *a* /Å | 6.808 |
| *b* /Å | 16.12 |
| *c* /Å | 13.917 |
| Cell volume / $Å^3$ | 1527.321 |
| conversion factor for [molec/uc] to [mol per kg Framework] | 1.0824 |
| conversion factor for [molec/uc] to [kmol/$m^3$] | 1.7868 |
| $\rho$ [kg/m3] | 1004.481 |
| MW unit cell [g/mol(framework)] | 923.881 |
| $\phi$, fractional pore volume | 0.608 |
| open space / $Å^3$/uc | 929.3 |
| Pore volume / $cm^3$/g | 0.606 |
| Surface area /$m^2$/g | 1472.8 |
| DeLaunay diameter /Å | 8.03 |

# MIL – 53 (Cr) pore landscape

**Simulation results**
**presented are for –lp structure, i.e. large pore**

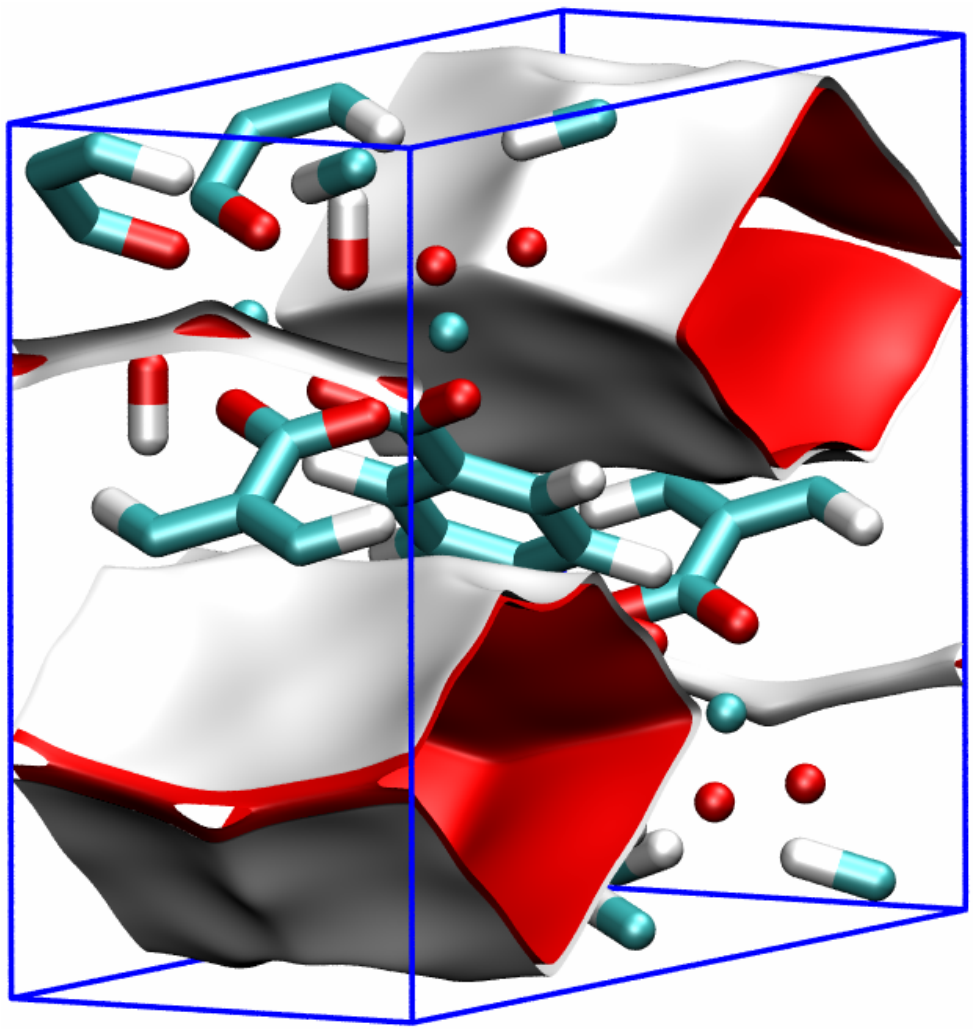

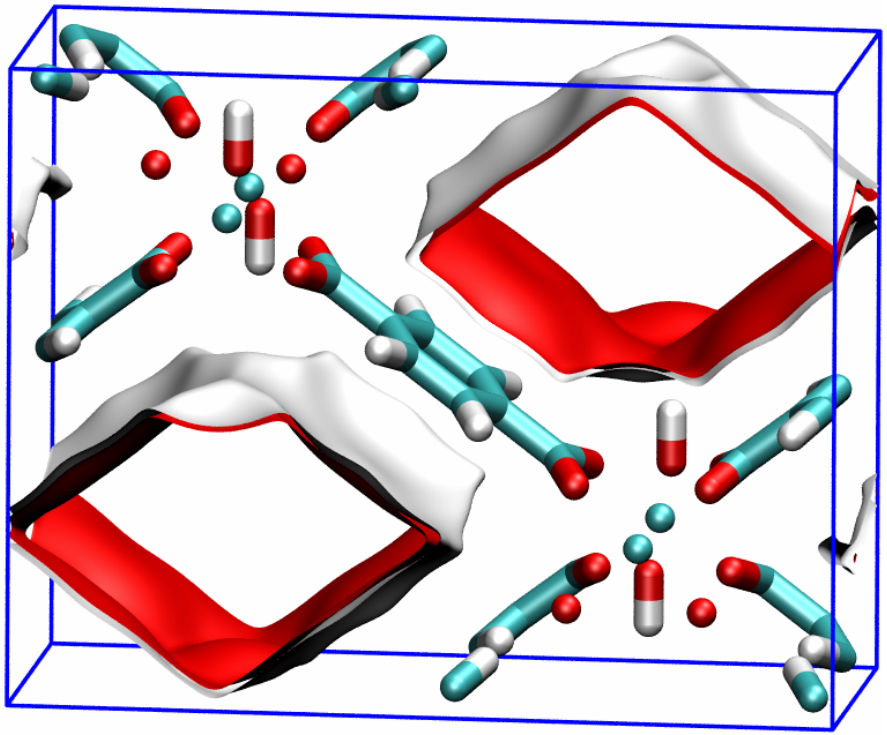

# MIL–53 (Cr) pore dimensions

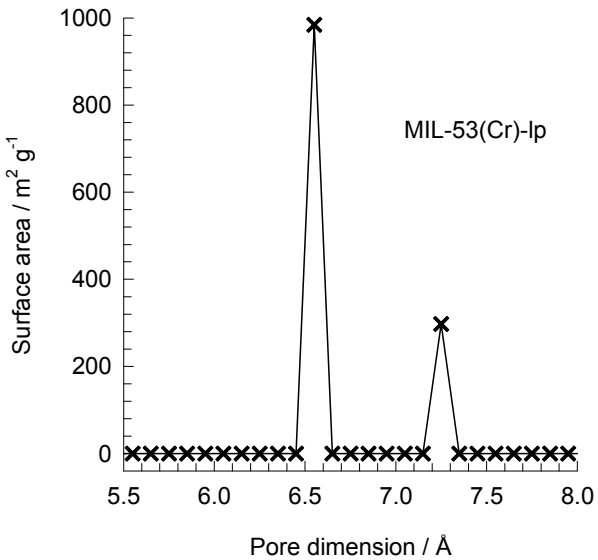


This plot of surface area versus pore dimension is determined using a combination of the DeLaunay triangulation method for pore dimension determination, and the procedure of Düren for determination of the surface area. The computational details will be described in detail in a forthcoming publication.

| | MIL53(Cr)-lp |
|---|---|
| *a* /Å | 16.733 |
| *b* /Å | 13.038 |
| *c* /Å | 6.812 |
| Cell volume / Å$^3$ | 1486.139 |
| conversion factor for [molec/uc] to [mol per kg Framework] | 1.0728 |
| conversion factor for [molec/uc] to [kmol/m$^3$] | 2.0716 |
| $\rho$ [kg/m3] | 1041.534 |
| MW unit cell [g/mol(framework)] | 932.1312 |
| $\phi$, fractional pore volume | 0.539 |
| open space / Å$^3$/uc | 801.6 |
| Pore volume / cm$^3$/g | 0.518 |
| Surface area /m$^2$/g | 1280.5 |
| DeLaunay diameter /Å | 7.40 |

# MgMOF-74 pore landscapes

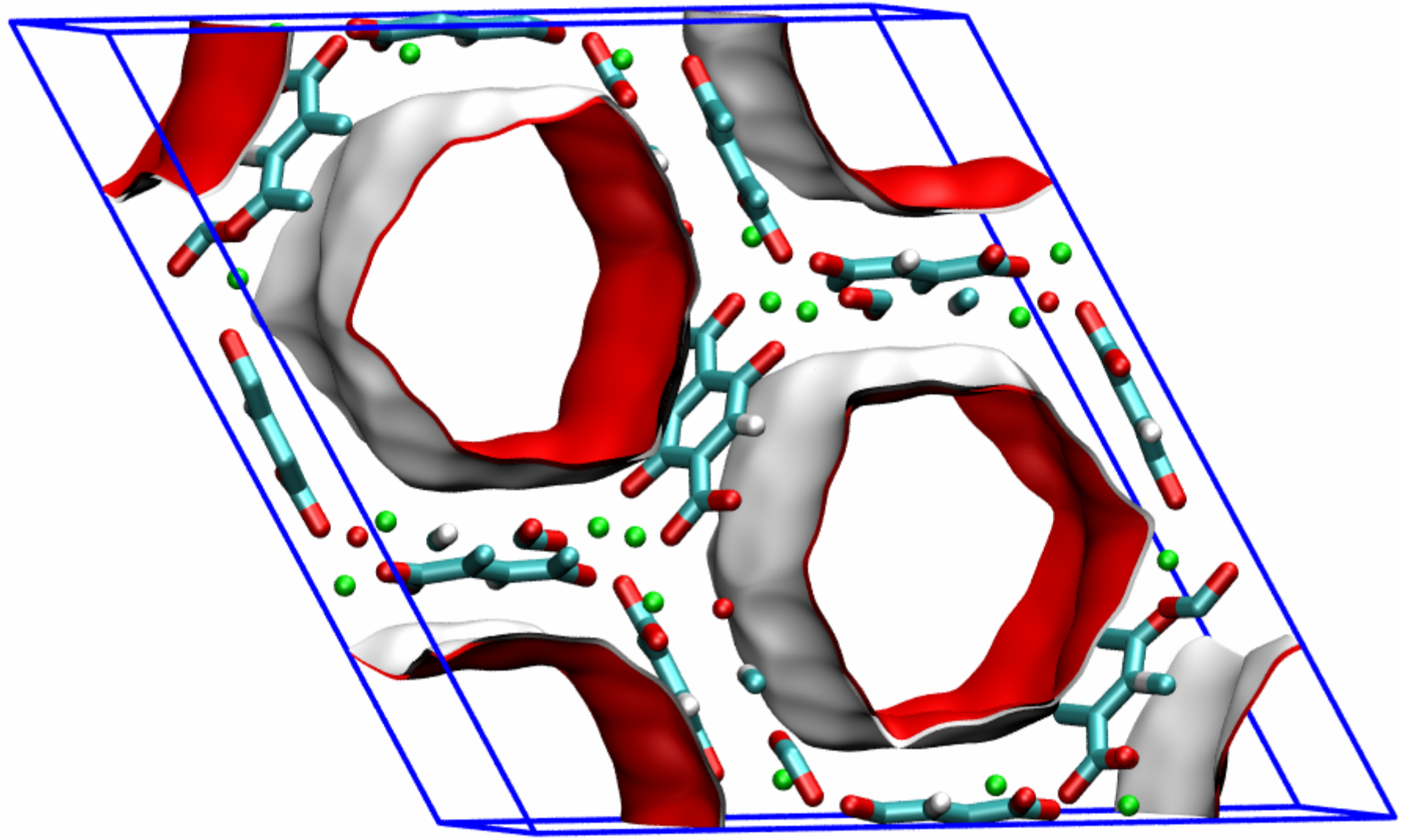

# MgMOF-74 pore dimensions

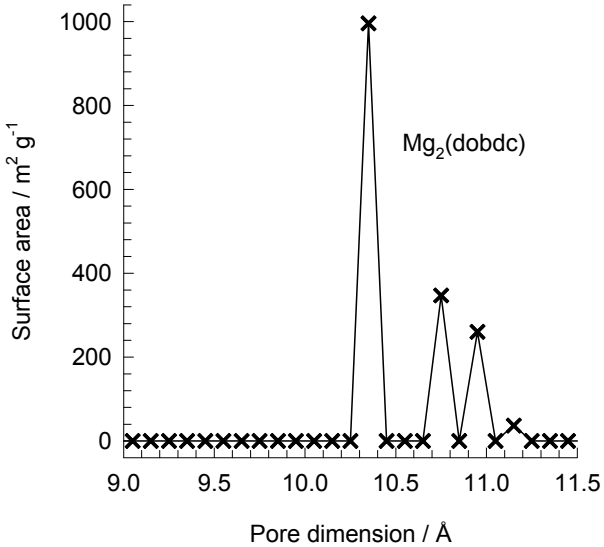


This plot of surface area versus pore dimension is determined using a combination of the DeLaunay triangulation method for pore dimension determination, and the procedure of Düren for determination of the surface area. The computational details will be described in detail in a forthcoming publication.

| | MgMOF-74 |
|---|---|
| *a* /Å | 25.8621 |
| *b* /Å | 25.8621 |
| *c* /Å | 6.91427 |
| Cell volume / $Å^3$ | 4005.019 |
| conversion factor for [molec/uc] to [mol per kg Framework] | 0.4580 |
| conversion factor for [molec/uc] to [kmol/$m^3$] | 0.5856 |
| $\rho$ [kg/m3] | 905.367 |
| MW unit cell [g/mol(framework)] | 2183.601 |
| $\phi$, fractional pore volume | 0.708 |
| open space / $Å^3$/uc | 2835.6 |
| Pore volume / $cm^3$/g | 0.782 |
| Surface area /$m^2$/g | 1640.0 |
| DeLaunay diameter /Å | 10.66 |

# ZnMOF-74 pore landscapes

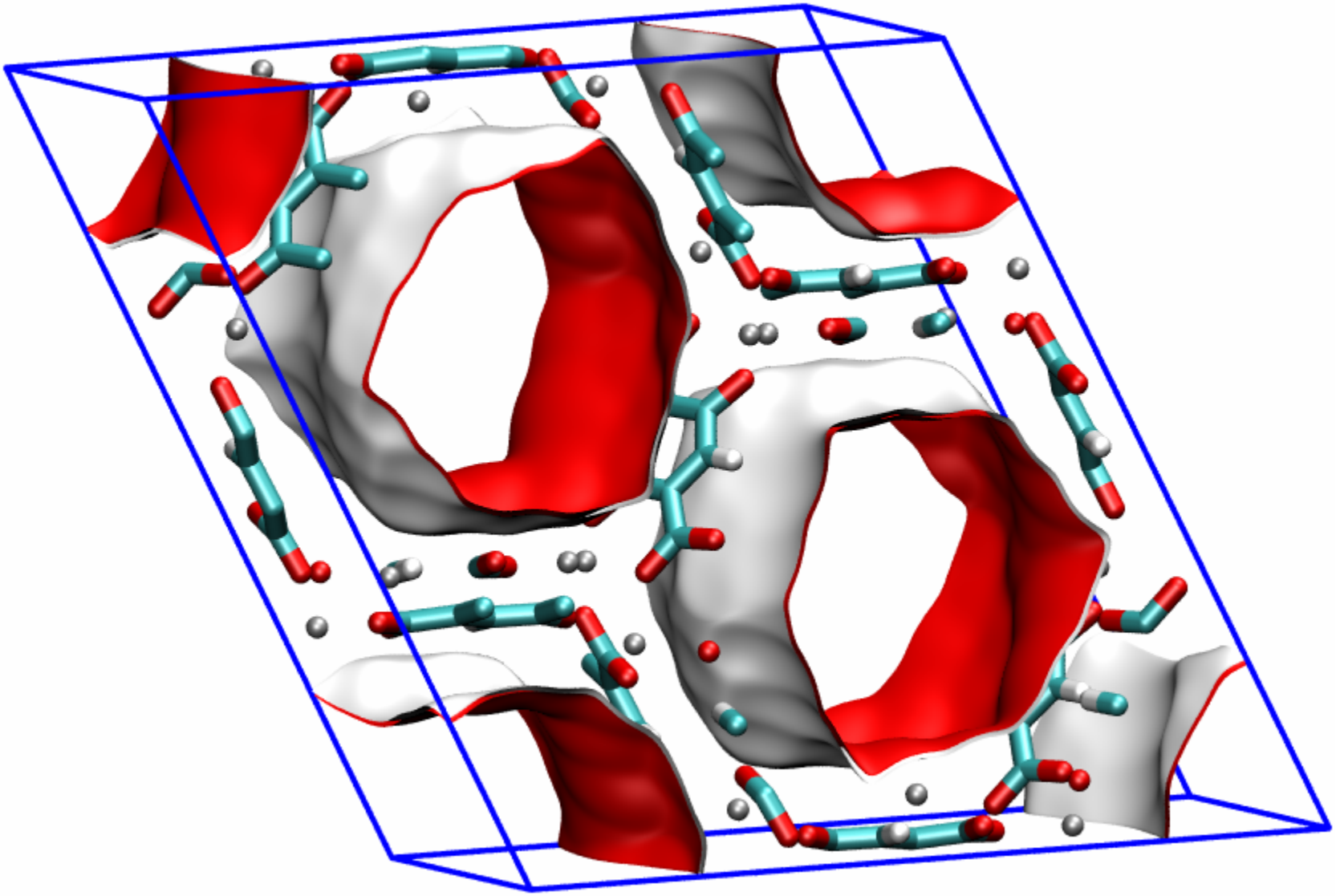

# ZnMOF-74 pore dimensions

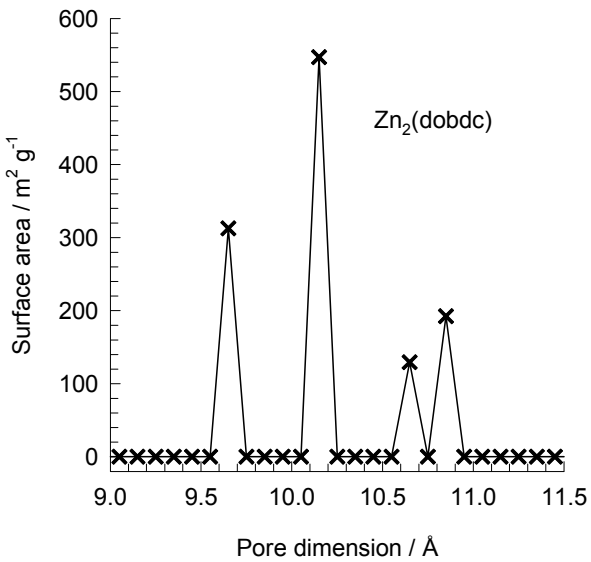


This plot of surface area versus pore dimension is determined using a combination of the DeLaunay triangulation method for pore dimension determination, and the procedure of Düren for determination of the surface area. The computational details will be described in detail in a forthcoming publication.

| | ZnMOF-74 |
|---|---|
| *a* /Å | 25.9322 |
| *b* /Å | 25.9322 |
| *c* /Å | 6.8365 |
| Cell volume / $Å^3$ | 3981.467 |
| conversion factor for [molec/uc] to [mol per kg Framework] | 0.3421 |
| conversion factor for [molec/uc] to [kmol/$m^3$] | 0.5881 |
| $\rho$ [kg/m3] | 1219.304 |
| MW unit cell [g/mol(framework)] | 2923.473 |
| $\phi$, fractional pore volume | 0.709 |
| open space / $Å^3$/uc | 2823.8 |
| Pore volume / $cm^3$/g | 0.582 |
| Surface area /$m^2$/g | 1176.0 |
| DeLaunay diameter /Å | 9.49 |

# CoMOF-74 pore landscapes

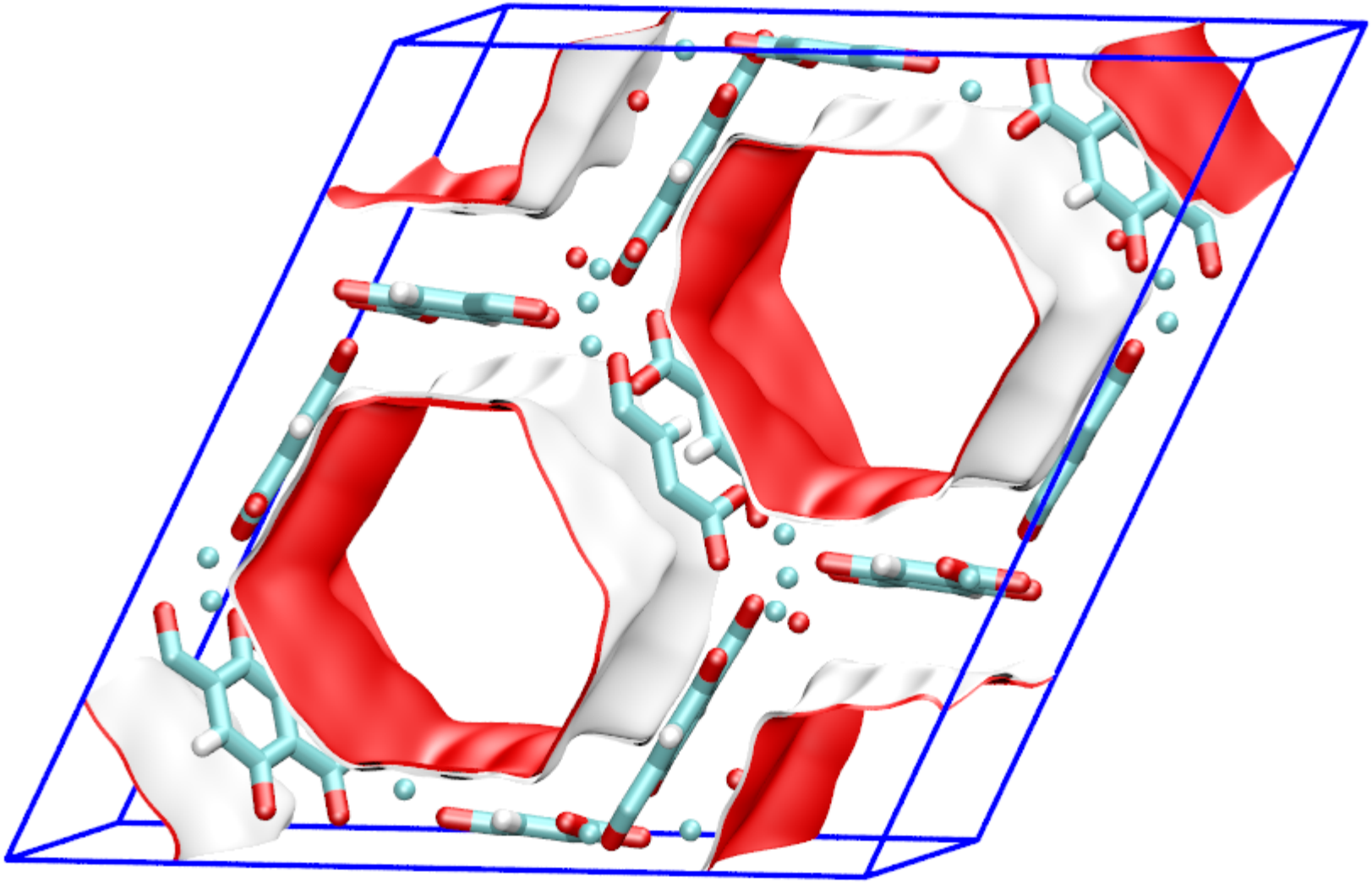

# CoMOF-74 pore dimensions

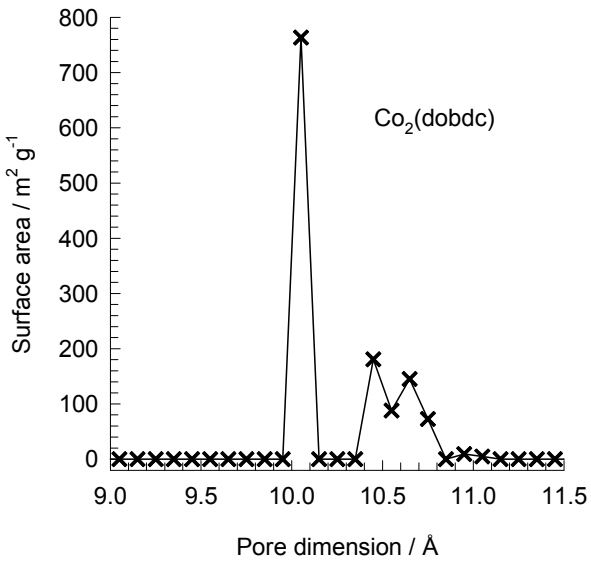


This plot of surface area versus pore dimension is determined using a combination of the DeLaunay triangulation method for pore dimension determination, and the procedure of Düren for determination of the surface area. The computational details will be described in detail in a forthcoming publication.

| | CoMOF-74 |
|---|---|
| *a* /Å | 25.885 |
| *b* /Å | 25.885 |
| *c* /Å | 6.8058 |
| Cell volume / $Å^3$ | 3949.173 |
| conversion factor for [molec/uc] to [mol per kg Framework] | 0.3563 |
| conversion factor for [molec/uc] to [kmol/$m^3$] | 0.5945 |
| $\rho$ [kg/m3] | 1180.261 |
| MW unit cell [g/mol(framework)] | 2806.908 |
| $\phi$, fractional pore volume | 0.707 |
| open space / $Å^3$/uc | 2793.1 |
| Pore volume / $cm^3$/g | 0.599 |
| Surface area /$m^2$/g | 1274.0 |
| DeLaunay diameter /Å | 9.52 |

# NiMOF-74 pore landscapes

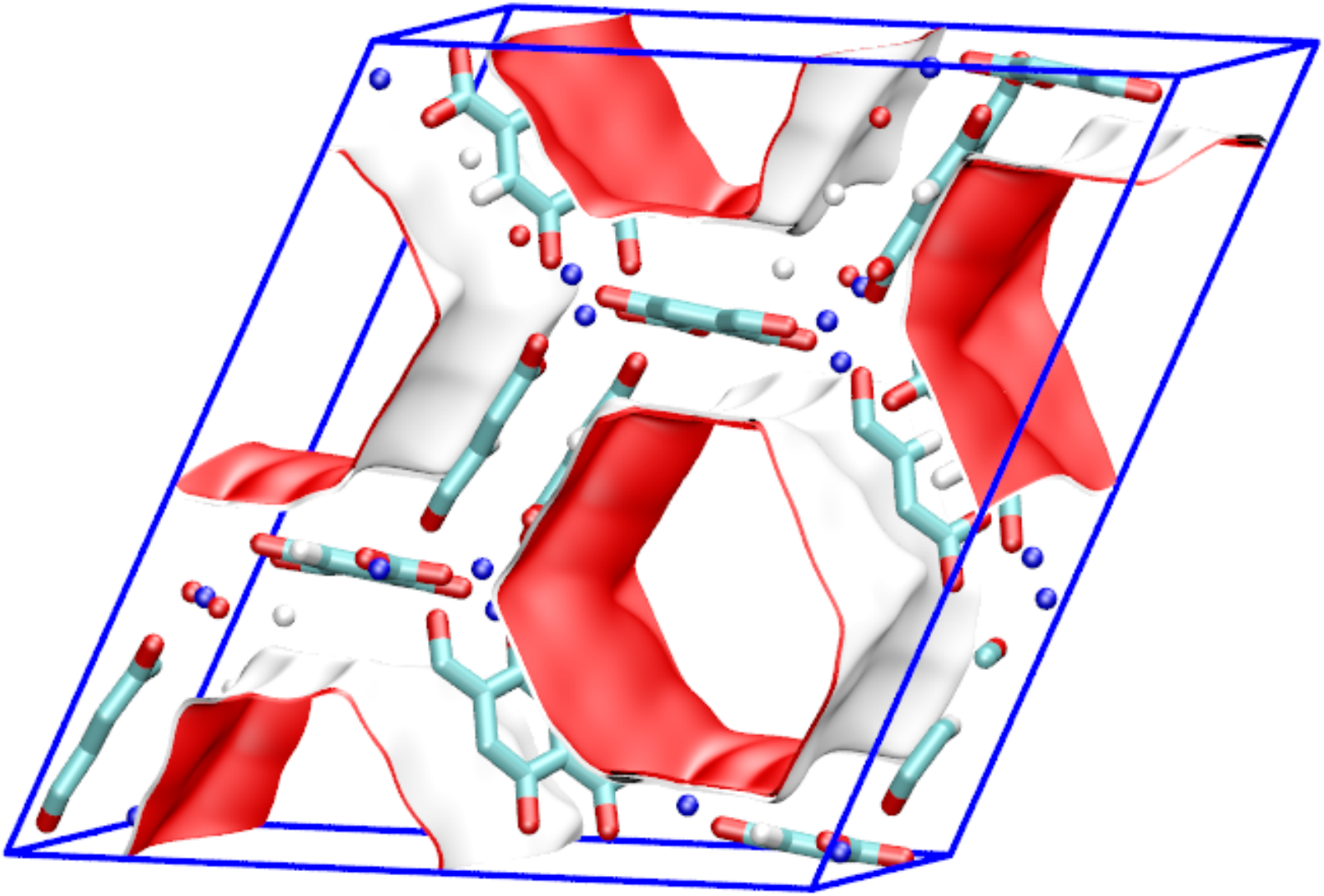

# NiMOF-74 pore dimensions

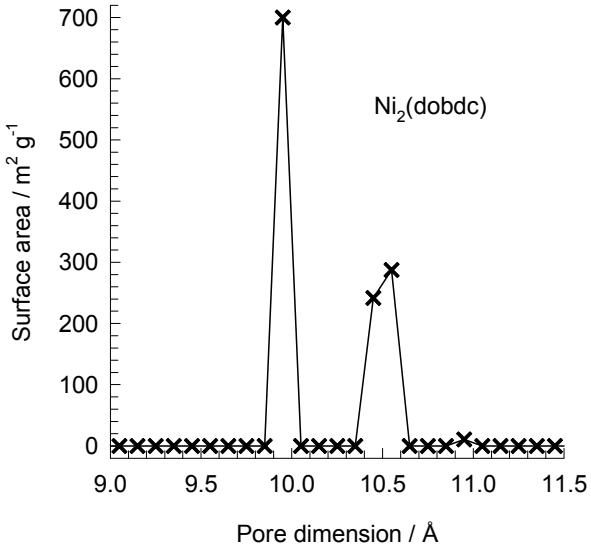


This plot of surface area versus pore dimension is determined using a combination of the DeLaunay triangulation method for pore dimension determination, and the procedure of Düren for determination of the surface area. The computational details will be described in detail in a forthcoming publication.

| | NiMOF-74 |
|---|---|
| *a* /Å | 25.7856 |
| *b* /Å | 25.7856 |
| *c* /Å | 6.7701 |
| Cell volume / Å$^3$ | 3898.344 |
| conversion factor for [molec/uc] to [mol per kg Framework] | 0.3568 |
| conversion factor for [molec/uc] to [kmol/m$^3$] | 0.6133 |
| $\rho$ [kg/m3] | 1193.811 |
| MW unit cell [g/mol(framework)] | 2802.592 |
| $\phi$, fractional pore volume | 0.695 |
| open space / Å$^3$/uc | 2707.6 |
| Pore volume / cm$^3$/g | 0.582 |
| Surface area /m$^2$/g | 1239.0 |
| DeLaunay diameter /Å | 9.80 |

# FeMOF-74 pore landscapes

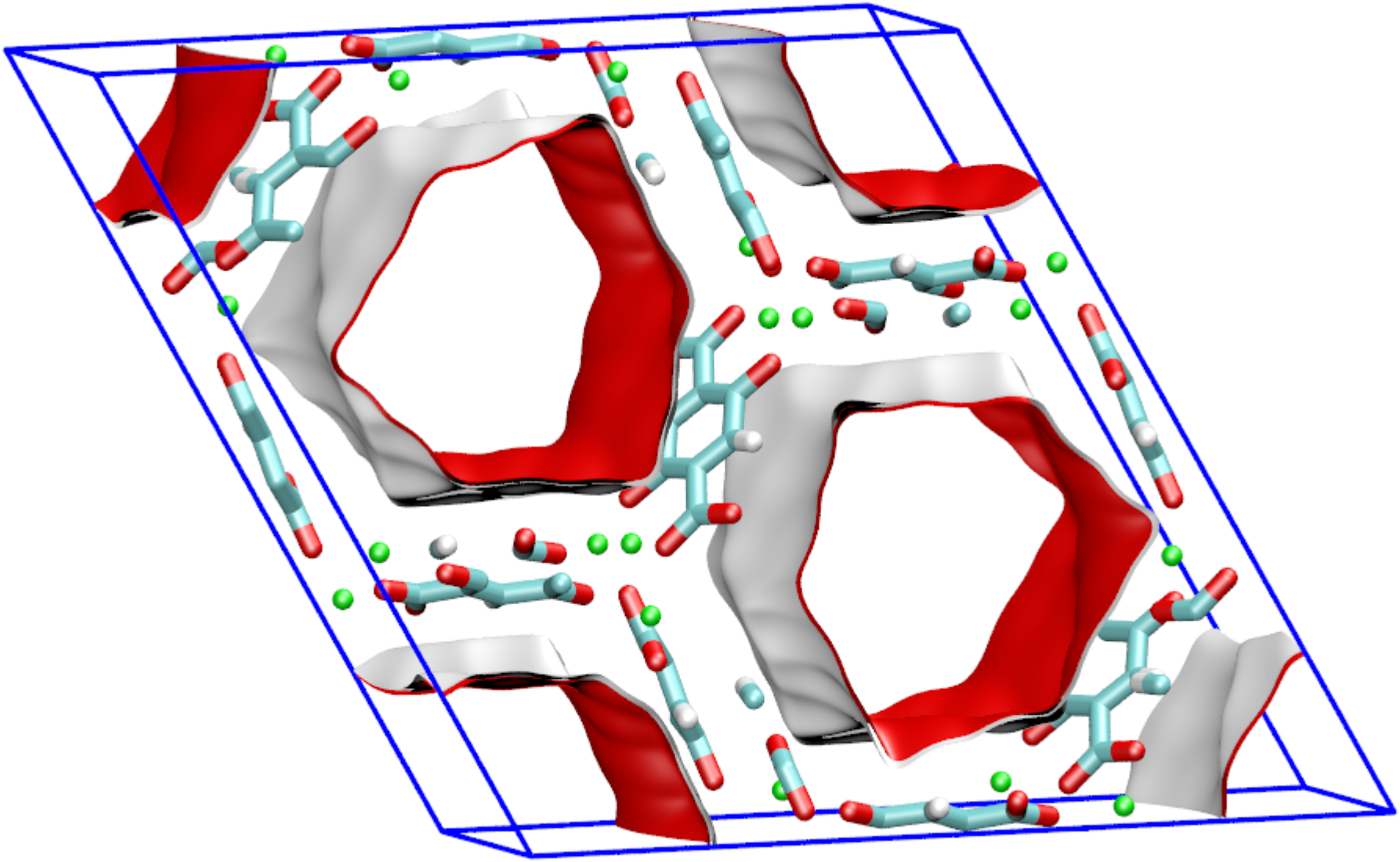

# FeMOF-74 pore dimensions

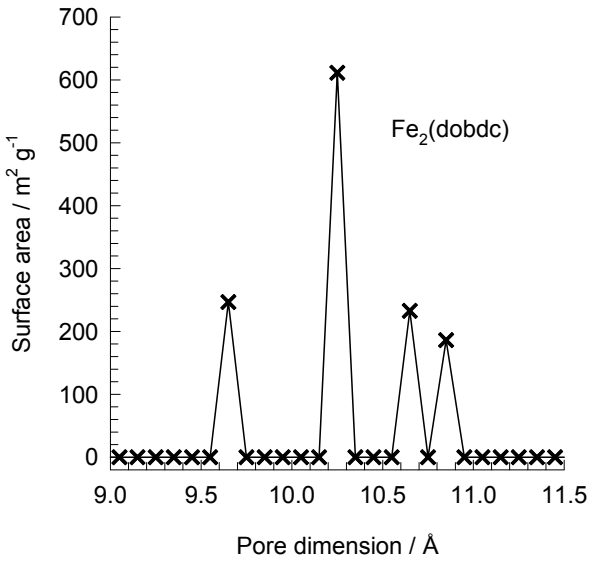


This plot of surface area versus pore dimension is determined using a combination of the DeLaunay triangulation method for pore dimension determination, and the procedure of Düren for determination of the surface area. The computational details will be described in detail in a forthcoming publication.

| | FeMOF-74 |
|---|---|
| *a* /Å | 26.1627 |
| *b* /Å | 26.1627 |
| *c* /Å | 6.8422 |
| Cell volume / $Å^3$ | 4055.94 |
| conversion factor for [molec/uc] to [mol per kg Framework] | 0.3635 |
| conversion factor for [molec/uc] to [kmol/$m^3$] | 0.5807 |
| $\rho$ [kg/m3] | 1126.434 |
| MW unit cell [g/mol (framework)] | 2751.321 |
| $\phi$, fractional pore volume | 0.705 |
| open space / $Å^3$/uc | 2859.7 |
| Pore volume / $cm^3$/g | 0.626 |
| Surface area /$m^2$/g | 1277.4 |
| DeLaunay diameter /Å | 11.12 |

# MOF-177 pore landscape

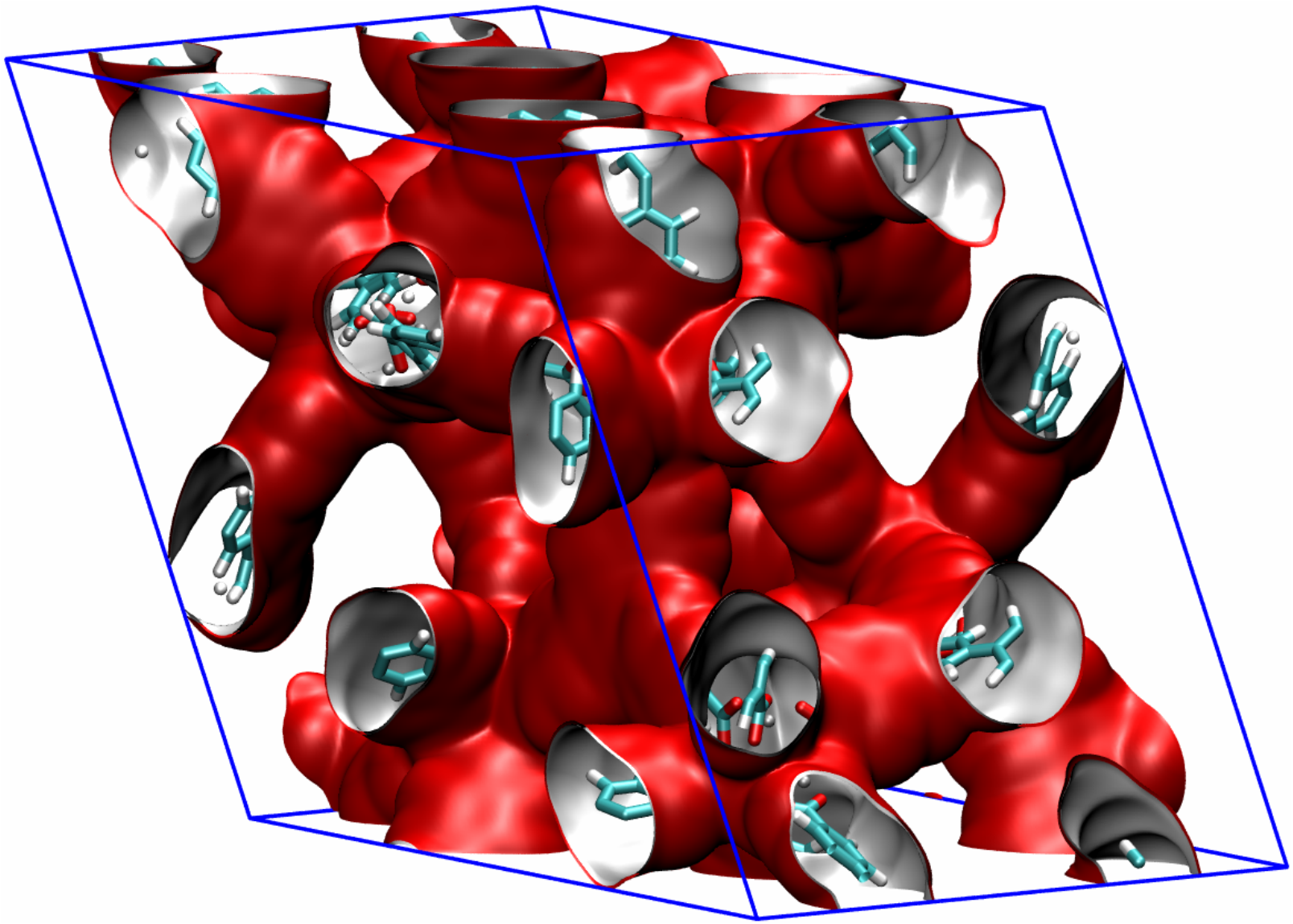

# MOF-177 pore dimensions

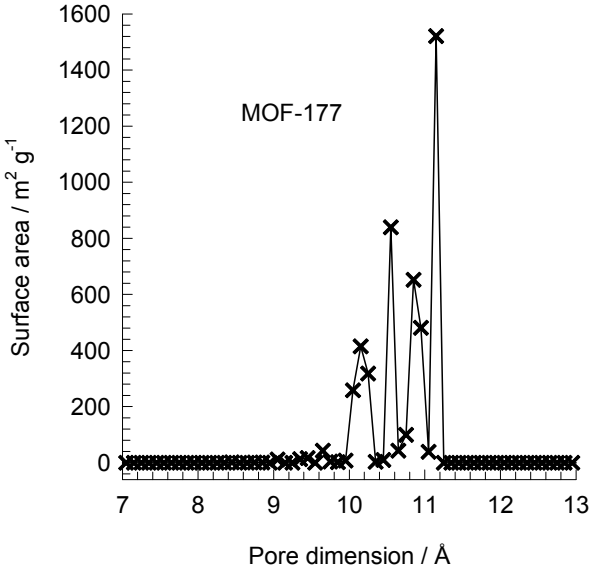


This plot of surface area versus pore dimension is determined using a combination of the DeLaunay triangulation method for pore dimension determination, and the procedure of Düren for determination of the surface area. The computational details will be described in detail in a forthcoming publication.

| | MOF-177 |
|---|---|
| *a* /Å | 37.072 |
| *b* /Å | 37.072 |
| *c* /Å | 30.033 |
| Cell volume / $Å^3$ | 35745.5 |
| conversion factor for [molec/uc] to [mol per kg Framework] | 0.1089 |
| conversion factor for [molec/uc] to [kmol/$m^3$] | 0.0553 |
| $\rho$ [kg/m3] | 426.5952 |
| MW unit cell [g/mol(framework)] | 9182.931 |
| $\phi$, fractional pore volume | 0.840 |
| open space / $Å^3$/uc | 30010.9 |
| Pore volume / $cm^3$/g | 1.968 |
| Surface area /$m^2$/g | 4781.0 |
| DeLaunay diameter /Å | 10.1 |

# Zn(bdc)dabco

## landscapes

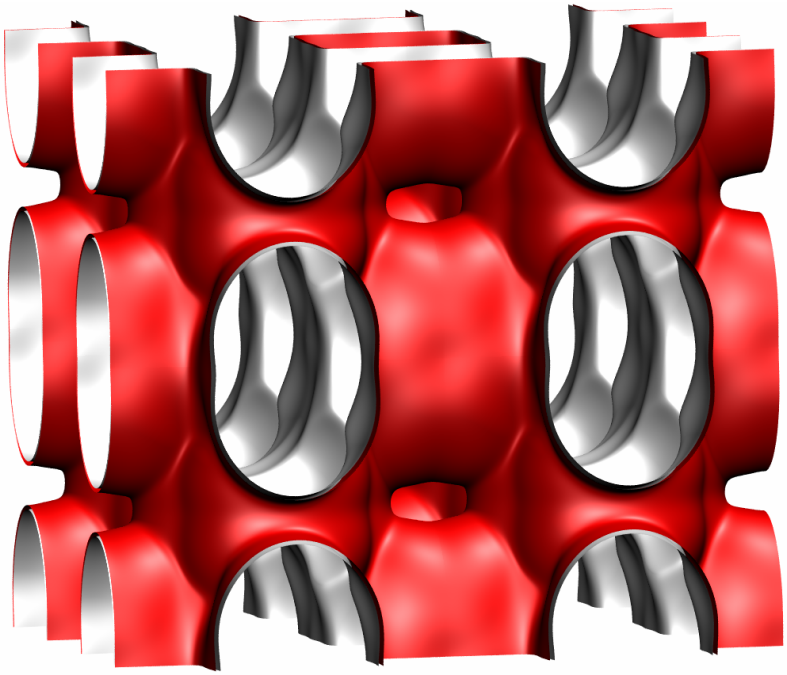

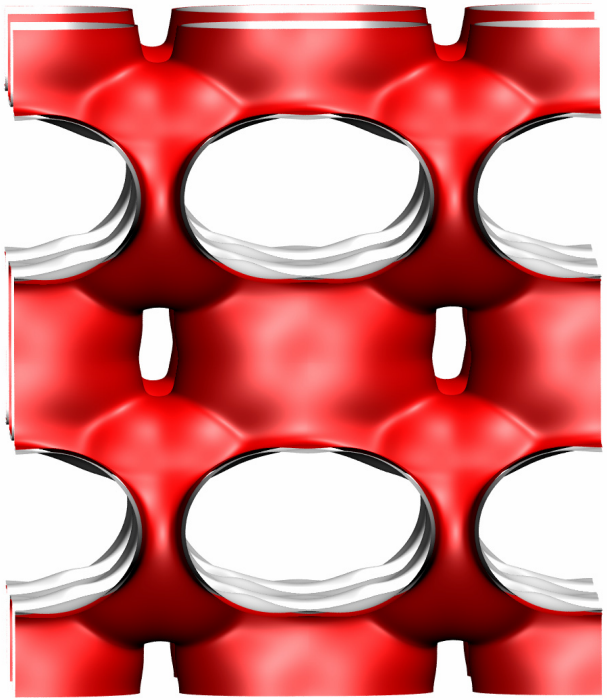

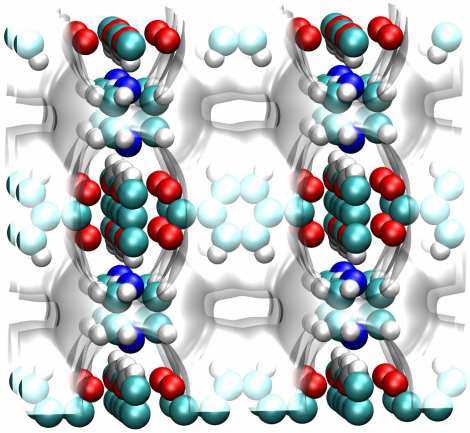

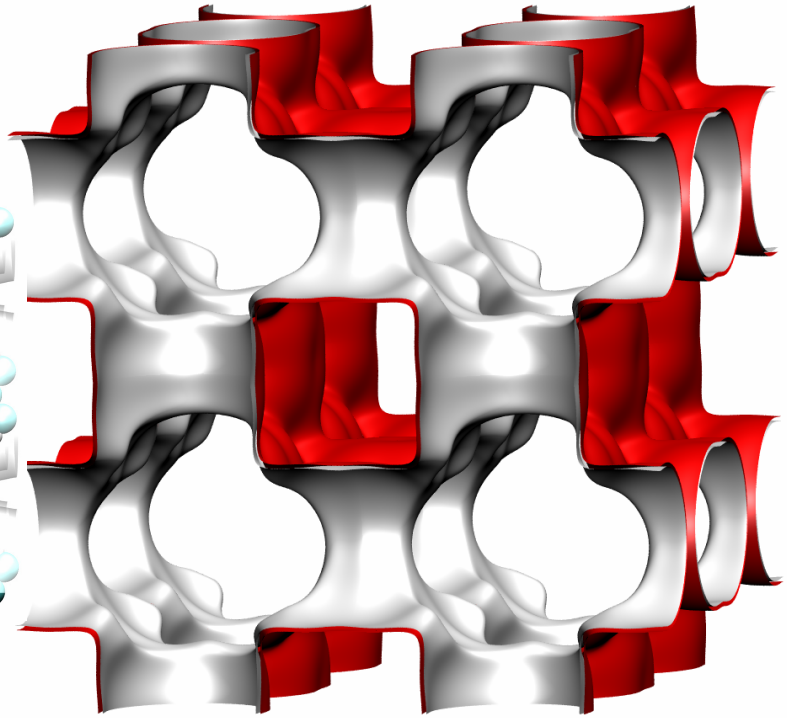

# Zn(bdc)dabco
## landscapes

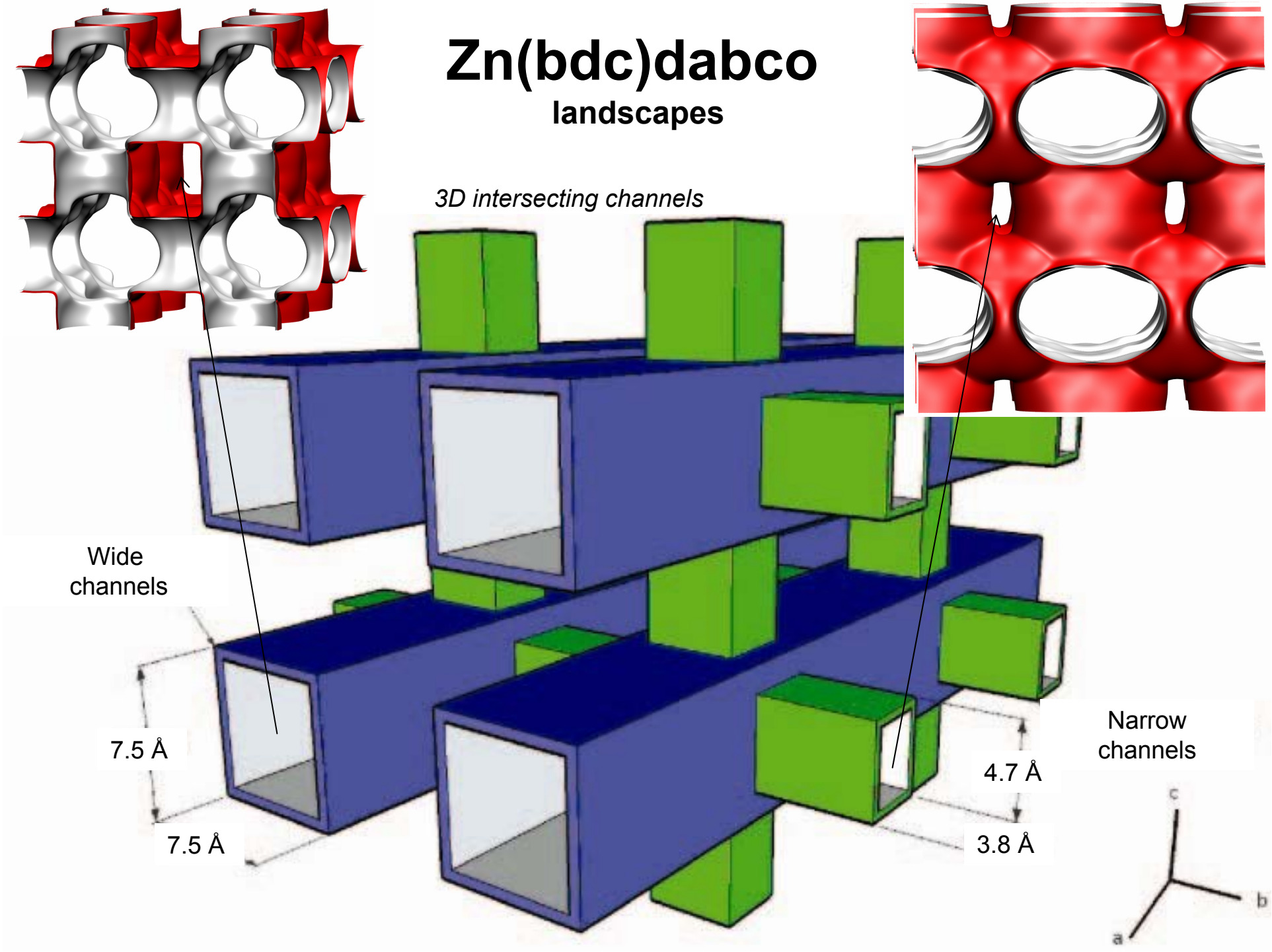

# Zn(bdc)dabco pore dimensions

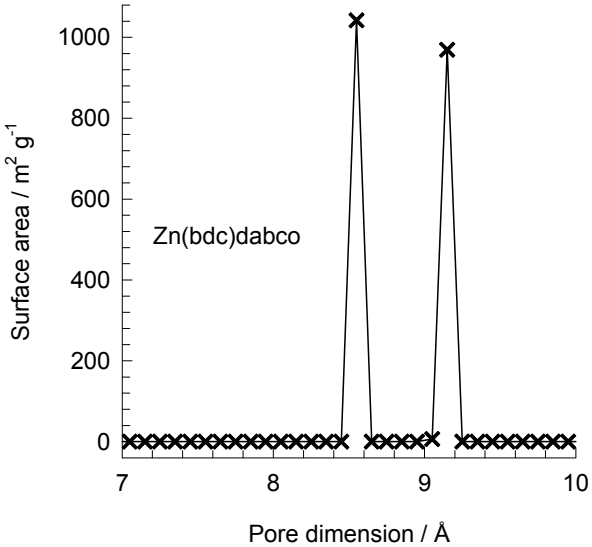


This plot of surface area versus pore dimension is determined using a combination of the DeLaunay triangulation method for pore dimension determination, and the procedure of Düren for determination of the surface area. The computational details will be described in detail in a forthcoming publication.

| | Zn(bdc)dabco |
|---|---|
| *a* /Å | 10.9288 |
| *b* /Å | 10.9288 |
| *c* /Å | 9.6084 |
| Cell volume / $Å^3$ | 1147.615 |
| conversion factor for [molec/uc] to [mol per kg Framework] | 1.7514 |
| conversion factor for [molec/uc] to [kmol/$m^3$] | 2.1867 |
| $\rho$ [kg/m3] | 826.1996 |
| MW unit cell [g/mol(framework)] | 570.9854 |
| $\phi$, fractional pore volume | 0.662 |
| open space / $Å^3$/uc | 759.4 |
| Pore volume / $cm^3$/g | 0.801 |
| Surface area /$m^2$/g | 2022.5 |
| DeLaunay diameter /Å | 8.32 |

# ZIF-8 pore landscapes

There are 2 cages per unit cell. To convert from molecules per cage to mol $kg^{-1}$, multiply by 0.7325.

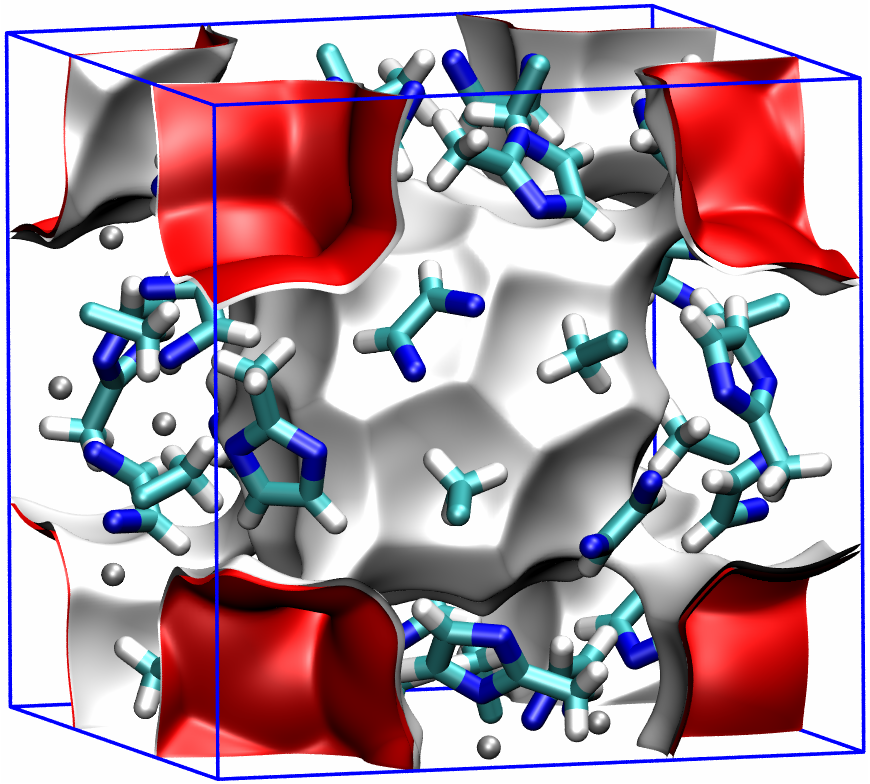

There are 2 cages per unit cell. The volume of one ZIF-8 cage is 1168 $Å^3$, significantly larger than that of a single cage of DDR (278 $Å^3$), or FAU (786 $Å^3$).

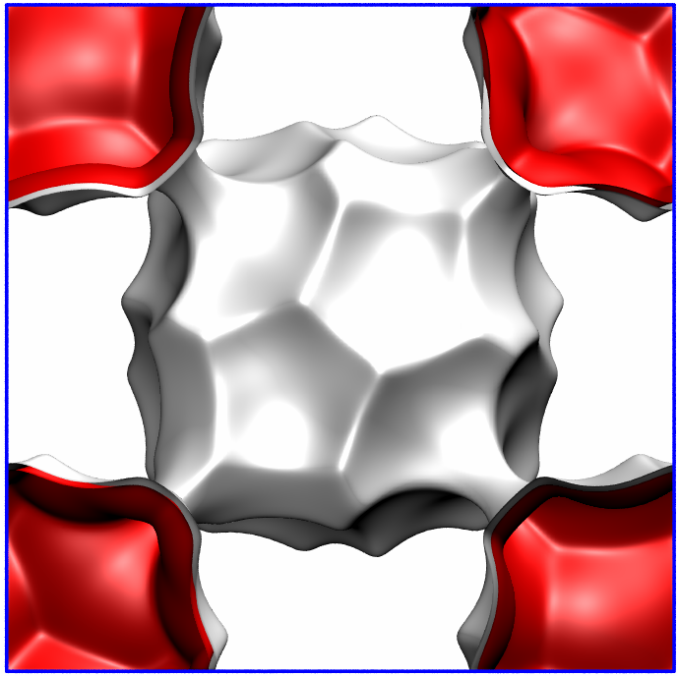

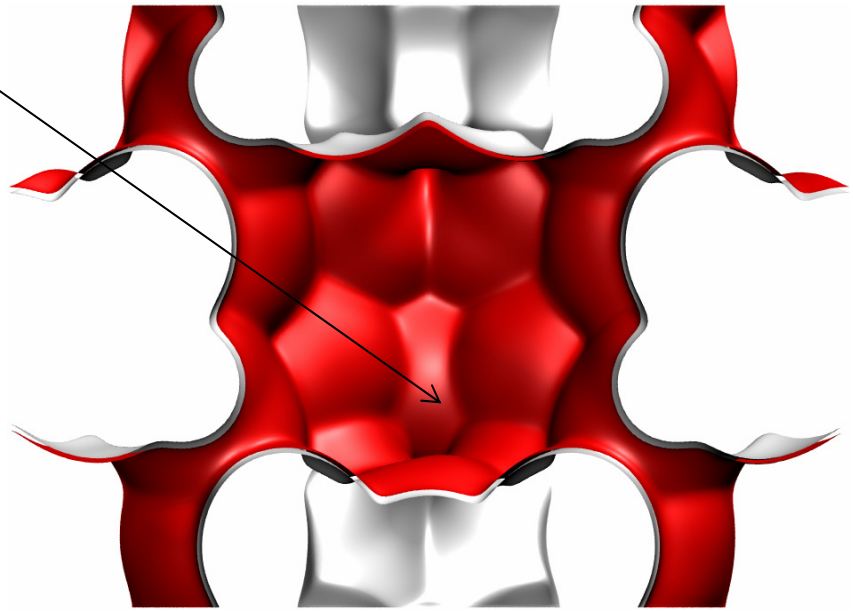

# ZIF-8 dimensions

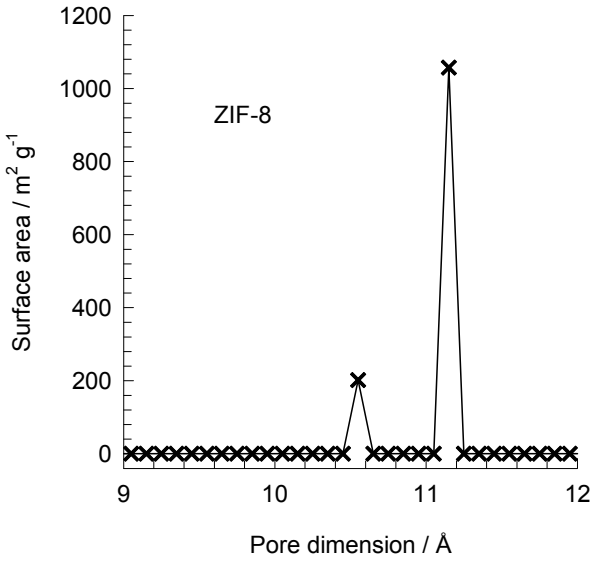


This plot of surface area versus pore dimension is determined using a combination of the DeLaunay triangulation method for pore dimension determination, and the procedure of Düren for determination of the surface area. The computational details will be described in detail in a forthcoming publication.

| | ZIF-8 |
|---|---|
| *a* /Å | 16.991 |
| *b* /Å | 16.991 |
| *c* /Å | 16.991 |
| Cell volume / Å$^3$ | 4905.201 |
| conversion factor for [molec/uc] to [mol per kg Framework] | 0.3663 |
| conversion factor for [molec/uc] to [kmol/m$^3$] | 0.7106 |
| $\rho$ [kg/m3] | 924.253 |
| MW unit cell [g/mol(framework)] | 2730.182 |
| $\phi$, fractional pore volume | 0.476 |
| open space / Å$^3$/uc | 2337.0 |
| Pore volume / cm$^3$/g | 0.515 |
| Surface area /m$^2$/g | 1164.7 |
| DeLaunay diameter /Å | 3.26 |

# ZIF-8 snapshot of $CO_2/CH_4$ mixture

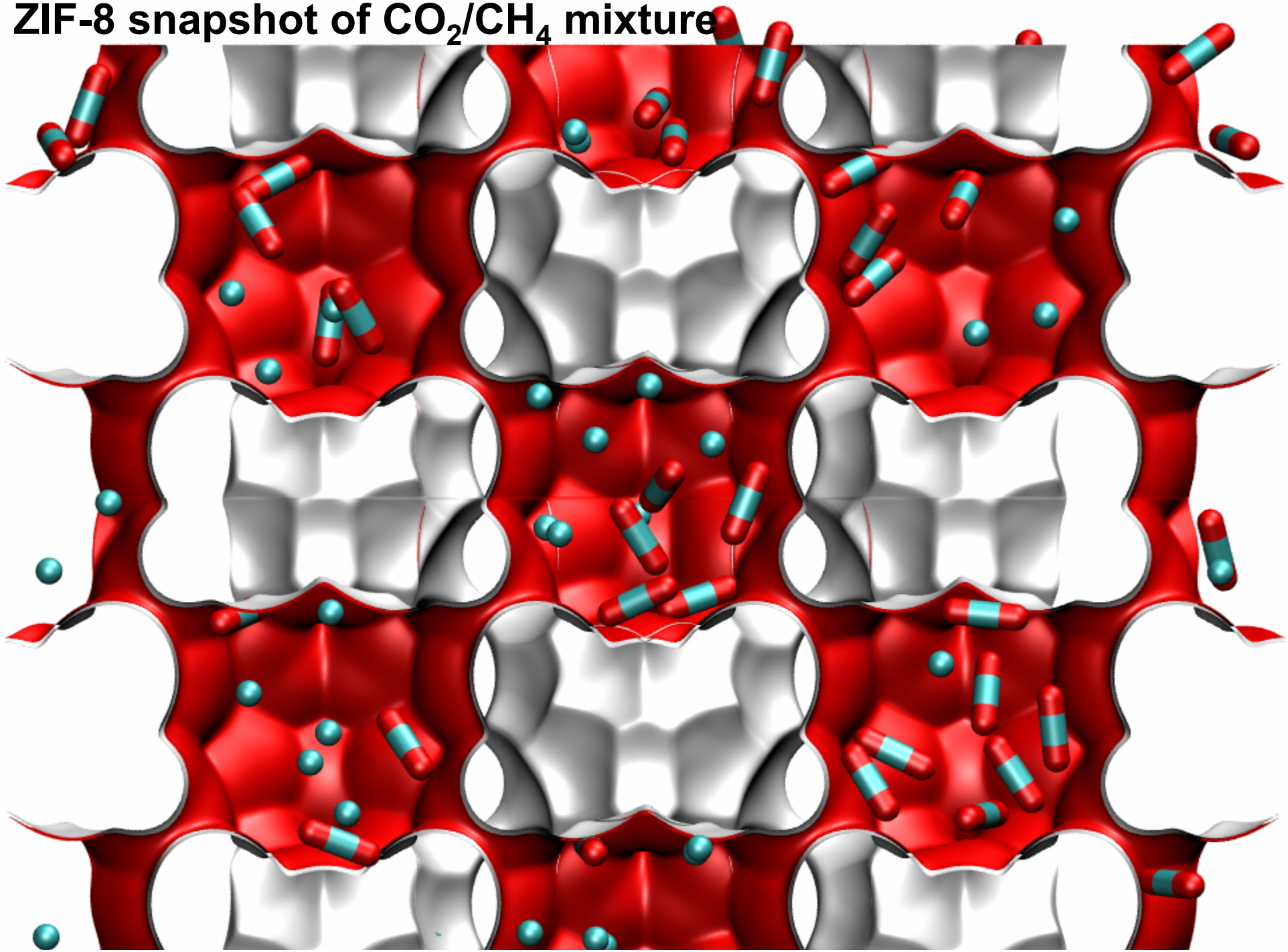

# BTP-COF with 3.4 nm hexagonal shaped pores

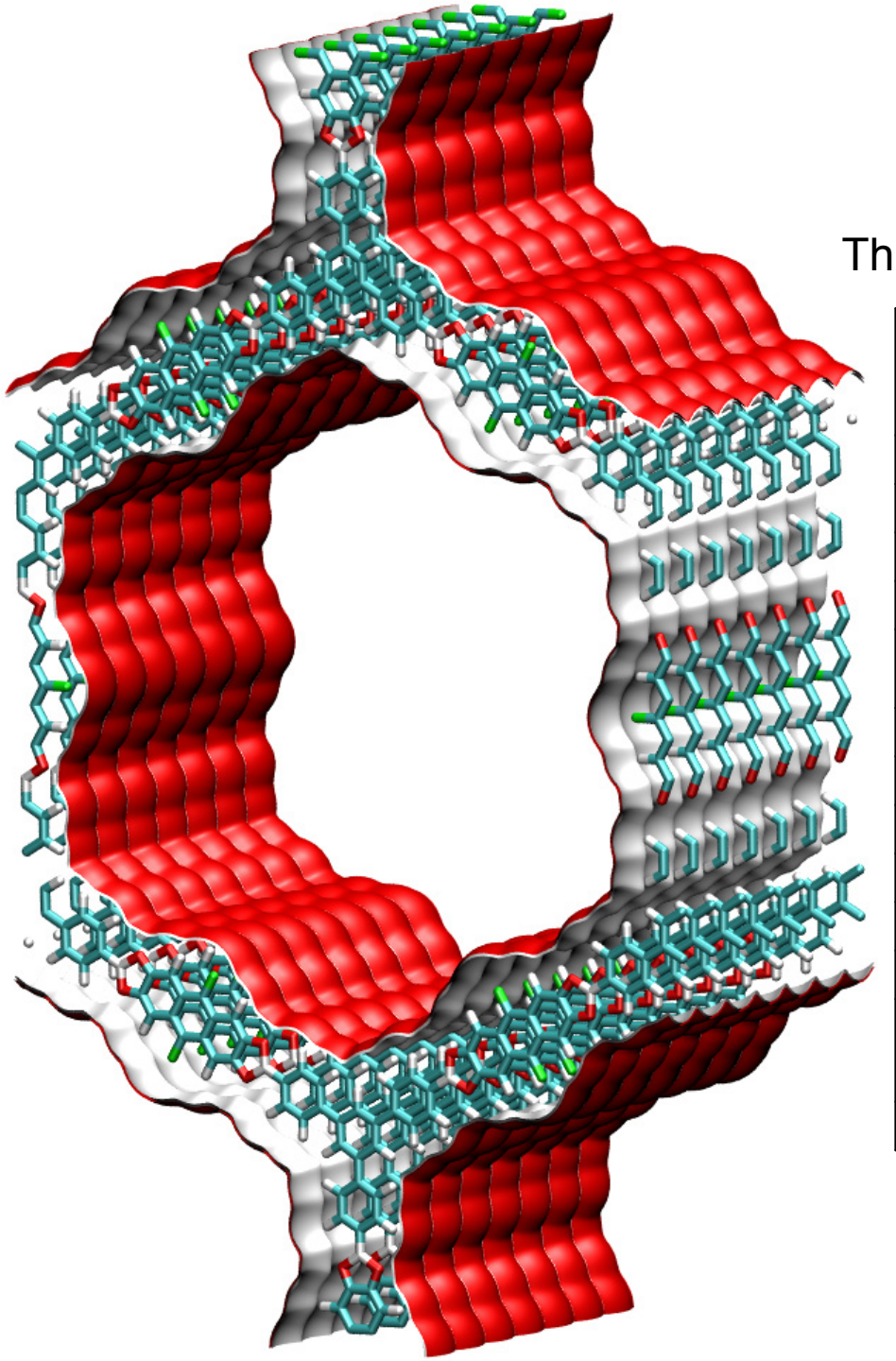

# BTP-COF landscape

This represents the 1x1x7 simulation box

| | BTP-COF |
|---|---|
| *a* /Å | 43.65 |
| *b* /Å | 75.604 |
| *c* /Å | 3.52 |
| Cell volume / Å$^3$ | 11616.4 |
| conversion factor for [molec/uc] to [mol per kg Framework] | 0.3403 |
| conversion factor for [molec/uc] to [kmol/m$^3$] | 0.1900 |
| $\rho$ [kg/m3] | 420.0831 |
| MW unit cell [g/mol(framework)] | 2938.67 |
| $\phi$, fractional pore volume | 0.752 |
| open space / Å$^3$/uc | 8738.7 |
| Pore volume / cm$^3$/g | 1.791 |
| Surface area /m$^2$/g | |
| DeLaunay diameter /Å | 34.26 |

# Carbon nanotubes

# CNTs have smooth surfaces